DISSERTATION

submitted to the
Combined Faculties for the Natural Sciences and for Mathematics
of the Ruperto - Carola University of Heidelberg, Germany
for the degree of
Doctor of Natural Sciences

presented by
Diplom - Biochemist Christiane Jost
born in Kempten, Germany

Oral examination:

Functional Aspects of Protein Kinase C
FRET Probe Performance

Referees: Dr. Elena Conti

Prof. Dr. Rainer Fink

INAUGURAL – DISSERTATION

zur

Erlangung der Doktorwürde

der

Naturwissenschaftlich-Mathematischen Gesamtfakultät

der

Ruprecht – Karls - Universität

Heidelberg

vorgelegt von

Diplom - Biochemikerin Christiane Jost

aus Kempten, Deutschland

Tag der mündlichen Prüfung:

Funktionelle Aspekte der Leistungsfähigkeit FRET basierender Protein Kinase C Sensoren

Gutachter: Dr. Elena Conti

Prof. Dr. Rainer Fink

Meiner Großmutter
und ELCH-TOURS

Acknowledgements

This work has been carried out in Carsten Schultz' laboratory at EMBL Heidelberg, Germany. I am very grateful to Carsten for giving me the opportunity to pursue my PhD under his supervision and introducing me to chemical biology. I also thank him for having been very fast in reading my thesis.

I thank the members of my TAC committee, Prof. Dr. Rainer Fink, Dr. Elena Conti and Dr. Andreas Ladurner for having been very helpful in many meetings. I especially thank Elena, who always had an open door and ear for me.

As my thesis mainly relied on microscopy, it would not have been possible without the help of the Advanced Light Microscopy Facility at EMBL. Jens Rietdorf, Stefan Terjung, Timo Zimmermann and Arne Seitz have always been there for late-night-last-minute help. Thank you very much!

My thank goes to Dr. Carsten Hoffmann in Würzburg, who taught me FlAsH labeling and welcomed me in Würzburg.

Michael Sattler, Bernd Simon and Gunter Stier were very helpful in discussing pleckstrin conformations over and over.

I would like to thank all past and present members of the Schultz lab for the last four years. I owe a huge thank you to Heike Stichnoth for patiently providing me with dozens of cell dishes a week and still being friendly and helpful in biggest chaos and stress! Gracias and thanks to Amanda and Adrian for relaxing lunch-breaks and lots of fun. Andrea, good luck with finishing your thesis!
Shannon and Antje have both been good colleagues but more importantly great friends as well. I thank Shannon for having read and corrected most of this thesis (and Antje, Markus and Adrian for having read the rest!).

My time would not have been as nice without my friends here in Heidelberg. I am very grateful for many coffee breaks, walks up the hill, chats in the corridors and, more important, fun outside the lab. As everyone enjoys reading their name, I will enumerate (in alphabetical order!). Please, if I forgot someone, account it to too little time and not purpose.
Thank you very much Antje, Atlanta, Birgit, Elad, Eli, Janus, JB, Johanna, Keren, Malcolm, Martin, Melina, Michal, Nga, Paulo, Patrick, Shannon, Thomas and Zoya!

I would like to seize this opportunity for thanking Kai Sicks and Melanie Boß, who have been my friends for a very long time, cheered me up and taken my mind of work. I enjoyed every minute of our long discussions and am happy to have you as my friends!

Besonderer Dank und merci beaucoup gilt meiner Familie, für Ihre Liebe und Unterstützung, in allem, was ich bisher unternommen habe.
Auch wenn es immer schwieriger wird, hoffe ich sehr, daß es bald wieder einen ELCH-TOURS Urlaub geben wird.

Markus danke ich für sehr Vieles und noch viel mehr! Ich freue mich darauf, wieder mit Dir in einer Stadt und in einem Land zu wohnen!

Summary

Understanding cellular signaling pathways and their cross talk increasingly depends on the visualization of their spatio-temporal dynamics.

This thesis investigates different factors influencing the performance of two FRET based protein kinase C (PKC) probes, KCP-1 and KCP-2. KCP-1 consists of the truncated PKC substrate pleckstrin, sandwiched between two fluorescent proteins, EYFP and GFP^2. KCP-2 is a shortened version of KCP-1, missing the last 18 amino acids of the pleckstrin insert (the acidic loop). The EYFP/GFP^2 emission ratio of KCP-1 increases upon phosphorylation, while it decreases in KCP-2. Both probes are reversible.

We examined the influence of linker length, charge distribution in particular domains of the probe, and fluorophore dimerization on probe performance. Different FRET pairs, including novel fluorescent proteins and novel labeling techniques, were tested in an effort to vary and optimize the spectral properties of KCP probes.

Both probes, KCP-1 and KCP-2, were shown to be sensitive to elongation in their N-terminal linker region. The signal amplitude of the probe was diminished with increasing linker length. Shortening of the same linker region reduced probe performance, although not to the same extent as elongation. This demonstrated the importance of linker length for proper orientation of the fluorophores in the probe molecule.

Any changes in the N-terminal PH domain of the pleckstrin insert, for example shortening or replacing basic amino acids with uncharged or acidic residues, had severe impact on probe performance. The direction of the KCP-1 signal was reversed, showing a decrease instead of an increase after phosphorylation. The reversal of signal in KCP-1 probes reflects that specific interactions between the PH domain and the acidic loop are crucial for probe performance. In KCP-2, the impact was less striking, although the signal was reduced.

Abolishing the fluorescent proteins' ability to dimerize, led to strongly reduced KCP-2-like signals in both probes. This is the first time that fluorophore

dimerization was shown to be essential for the mechanism of action of a genetically encoded sensor.

Based on this data, we propose the following models for the mechanism of these PKC probes:
In unphosphorylated KCP-2, dimerization of fluorophores serves as a clamp, pulling the two fluorophores together to a closed, quasi cyclized conformation. Phosphorylation of the probe leads to a more open conformation, increasing the average distance between the two fluorophores. This results in a decrease of FRET efficiency after phosphorylation.
Two interactions determine the mechanism in KCP-1. Again, the dimerization of the two fluorophores serves as a clamp, pulling the fluorophores to close proximity. An additional interaction between the PH domain and the acidic loop changes the relative orientation of the transition dipole moments in the probe, resulting in a decreased initial FRET efficiency, compared to KCP-2. Phosphorylation of the probe imposes a strain on the intramolecular architecture that rearranges the transition dipoles, leading to an increase in FRET efficiency.
The need for a molecular clamp, dimerization of fluorescent proteins in KCP-1 and KCP-2 probes, within the molecule explains why probes containing new monomeric fluorescent proteins or other labels based on full sized proteins did not yield functional sensors. Using the small fluorophore FlAsH, however, we were able to create a smaller sized PKC probe. This probe will allow NMR experiments and structural analysis of a FRET probe for the first time.

Zusammenfassung

Die Untersuchung zellulärer Signalwege und deren Wechselwirkungen bedient sich verstärkt Methoden zur Visualisierung räumlicher und zeitlicher Dynamik.

In dieser Dissertation werden verschiedenen Faktoren untersucht, die die Leistungsfähigkeit zweier auf FRET basierender Sensoren für Protein Kinase C beeinflussen (KCP-1 und KCP-2).

KCP-1 besteht aus einer verkürzten Form des PKC Substrats Pleckstrin und den fluoreszenten Proteinen, EYFP und GFP^2, die an den N- bzw. den C-Terminus von Pleckstrin gesetzt wurden. KCP-2 ist eine verkürzte Version von KCP-1, bei der die letzten 18 Aminosäuren des Pleckstrins („acidic loop“) entfernt wurden. Das Verhältnis der Emissionen von EYFP und GFP^2 nimmt zu, wenn KCP-1 phosphoryliert wird, während es bei KCP-2 abnimmt. Beide Sensoren sind komplett reversibel.

Wir haben den Einfluss der Länge von verbindenden Sequenzen, von Ladungsverteilungen in bestimmten Domänen des Sensors, und von der Dimerisierung der Fluorophore untersucht. Die Verwendung neuer fluoreszenter Proteine und Markierungstechniken wurde untersucht, um die spektralen Eigenschaften in KCP Proben zu optimieren und zu variieren.

Beide Sensoren, KCP-1 und KCP-2, zeigten veränderte Signalamplituden, wenn ihre N-terminale Verbindungsregion verlängert wurde. Mit zunehmender Länge der eingefügten Sequenz nahm die Amplitude des Signals ab. Eine Verkürzung der gleichen Region hatte einen ähnlichen Effekt, wenn auch weniger stark ausgeprägt.

Dies zeigt die Bedeutung der Länge von Verbindungssequenzen für die richtige Orientierung der Fluorophore im Sensor-Molekül.

Jede Veränderung in der N-terminalen PH-Domäne, z.B. Verkürzung der Domäne oder der Austausch basischer mit neutralen oder sauren Aminosäuren, hatte einen großen Einfluss auf das Verhalten der Sensoren. Die Richtung des KCP-1 Signals kehrte sich um. Anstelle eines ansteigenden Verhältnisses der EYFP/GFP2 Emissionen, wurde jetzt ein abnehmendes gemessen. Die Umkehrung des KCP-1 Signals verdeutlicht, daß durch die

Mutationen eine spezifische Bindung zwischen der PH-Domäne und dem „acidic loop“ zerstört wurde. In KCP-2 war der Effekt von Mutationen in der PH-Domäne weniger ausgeprägt, aber die Signalamplitude war deutlich herabgesetzt.
Wurde die Dimerisierung der fluoreszenten Proteine verhindert, führte dies zu einem stark reduzierten Signal mit KCP-2-ähnlichem Verlauf. Die ist das erste mal, dass gezeigt werden konnte, dass die Dimerisierng für die Funktion eines genetisch kodierten Sensors essentiell ist.

Ausgehend von diesen Daten, schlagen wir den folgenden Mechanismus für die Funktion der KCP Proben vor:
Im unphosphorylierten KCP-2 Molekül wirkt die Dimerisierung der fluoreszenten Proteine wie eine Klammer, die diese zusammenhält und zu einer quasi-zyklischen Struktur führt. Die Phosphorylierung erzeugt eine offene Konformation, mit einem vergösserten durchschnittlichen Abstand der Fluorophore. Dies verringert die FRET-Effizienz nach der Phosphorylierung.
In KCP-1 sind zwei Wechselwirkungen für den Mechanismus verantwortlich. Die Dimerisierung der beiden Fluorophore wirkt wieder als Klammer, die die Fluorophore näher zusammen zieht. Die zusätzliche Wechselwirkung zwischen der PH- und der DEP-Domäne sorgt allerdings für eine andere Orientierung der Übergangsdipolmomente der Fluorophore, welches die anfängliche FRET-Effizienz im Vergleich zu KCP-2 herabsetzt.
Durch die Phosporylierung wird eine zusätzliche Spannung in das Molekül eingeführt, die für eine Reorientierung der Übergangsdipolmomente und einer vergrößerten FRET-Effizienz führt.
Die Notwendigkeit einer molekularen Klammer innerhalb des Moleküls, wie zum Beispiel die Dimerisierung der Fluorophore, erklärt, weshalb Sensoren mit neuen monomeren Fluorophoren oder Markierungstechniken nicht funktionell waren.
Mit dem kleinen Fluorophor FlAsH gelang es, einen neuen PKC Sensor zu entwickeln, der klein genug ist, um zum ersten Mal NMR Strukturstudien an einer auf FRET basierenden Probe durchzuführen.

1 Aims of the Thesis

All processes in living organisms are governed by a complex signaling machinery. While it is possible to elucidate the interaction of individual components *in vitro*, their dynamics in time and space can only be studied *in vivo*. Fluorescence is ideally suited for investigation of biochemistry in living cells, as it is noninvasive and the necessary equipment is available in most laboratories. However, only a limited number of fluorescent sensors is available, probing protein-protein and protein-lipid interactions, changes in second messenger concentration or in local environment, e.g. PH or ion concentration.

The aim of this thesis is to gain a better understanding of the mechanism of action of two previously published PKC probes; to increase the range of fluorophores that can be used in the probe; and to reduce to the size of the probe, to enable structural analysis. Thorough understanding of the mechanisms will allow development of improved versions of the existing probes. The lessons learned can be applied to the development of new probes.

Specifically, the impact of linker length, the influence of inter-domain interactions and the importance of fluorophore dimerization, on probe performance is addressed.

In addition, we explore the potential of hybrid methods, combining genetically encoded tags with chemical fluorophores, for the design of new sensors based on novel FRET pairs. The reduced molecular size of some of these probes will for the first time allow following conformational changes of a FRET probe by NMR.

2 Introduction

2.1 Cell signaling

2.1.1 Overview

Understanding the complex networks underlying cell signaling increasingly relies on probes that visualize those processes *in vivo*. While *in vitro* experiments have provided a wealth of information, *in vivo* experiments provide a more realistic model of processes in the complex environment of a living cell. Cellular signaling networks are comprised of many different, interacting components. In order to understand the complex spatio-temporal dynamics of cell signaling, we need to follow as many components as possible at the same time. Fluorescent probes are useful tools for such an undertaking. There are a great variety of different colors, which are easily applied in many cell and tissue types and can be used to study cell biology and biochemistry in living cells.

In this thesis, we examine how existing probes function in order to understand the mechanism of action underlying these probes. Based on two existing protein kinase C (PKC) probes, KCP-1 and KCP-2[1,2], we study the effect of dimerization, charge distribution and linker length on these probes. We also examine the possibility of using different labeling systems for probes, increasing the applicability of the probe in wider areas of the optic spectrum.

We will first introduce protein kinase C and pleckstrin, followed by an overview of the physical basis of fluorescence and conclude with an overview about fluorescent labeling methods.

2.1.2 Protein kinase C

F. A. Lipmann and P. A. Levene at the Rockefeller University (New York) first identified the covalent attachment of a phosphate group to either serine or threonine residues of proteins in 1932 [3]. The first protein kinase to be found responsible for reversible phosphorylation was glycogen phosphorylase kinase in 1955 [4-6]. In the late 1960s, protein kinase A (PKA) was first

described[7], followed by protein kinase G (PKG) in the 1970s[8]. In 1977, Y. Nishizuka *et al* first identified a protein kinase that seemed to be constitutively active and did not require more than Mg^{2+} (it was therefore named PKM)[9-13]. They hypothesized that they had found an active proteolytic fragment, which had lost its auto-inhibitory element. In 1979, they identified the pro-enzyme and found that it was activated by membrane phospholipids, in particular phosphatidylserine (PS). They also observed that it was activated by the Ca^{2+}-dependant protease calpain and therefore named it protein kinase C (PKC)[14,15].

The PKC family is currently one of the most thoroughly studied group of enzymes with more than 43000 papers discussing different aspects of its function, structure, regulation and implications in diseases. PKCs belong to the superfamily of protein kinases A, G and C (AGC superfamily) and mediate many signals resulting from the generation of second messengers by lipid hydrolysis.

PKCs are involved in many key cellular processes. These include regulation of cell growth[16-19] and cell differentiation[18-22], gene expression[23], early development[24-26], apoptosis[27-30], regulation of cell-matrix contacts[31,32] or protection from cardiac ischaemia[33-38].

Seeing that PKCs are involved in all these pathways, it is not surprising that they have been implicated in many physiological functions and diseases. Examples include control of brain damage in stroke patients[39,40], ageing of the brain[41], neural plasticity and learning[42], drug addiction[43], hypertension[44], repair of intestinal injuries[45], type II diabetes[46,47], arteriosclerosis[38] and cancer[48,49].

PKCs are serine/threonine kinases and are represented in all eukaryotes. Twelve different isoenzymes have so far been described in the human genome. They can be classified in three groups: conventional PKC isoforms (cPKC), novel PKC isoforms (nPKC) and atypical isoforms (aPKC)[50]. Conventional PKCs, PKC-α[51,52], PKC-βI[51-53], PKC-βII[51-53] and PKC-γ[51,52], are activated by diacylglycerol (DAG) and Ca^{2+}. Novel PKCs, PKC-δ[54], PKC-ε[54],

PKC-η[55] and PKC-θ[56] are DAG sensitive but do not respond to calcium. Atypical PKCs, PKC-ζ[54] and PKC-ι[57], neither respond to DAG nor to calcium. PKC proteins consist of a single polypeptide chain subdivided into the regulatory N-terminal region and the catalytic C-terminal region. Four conserved domains can be identified, C1 and C2 and the kinase domain, which is subdivided into C3 and C4, representing the ATP-binding and substrate binding lobes of the kinase (Fig. 2.1)[58].

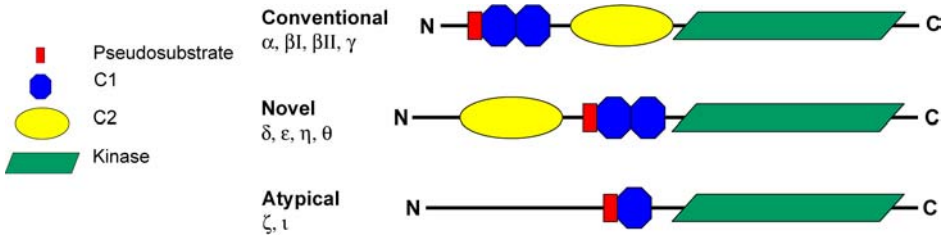

Fig. 2.1 Schematic representation of the conserved domains in PKCs

The C-terminal catalytic domain is conserved in all PKC subfamily members and is inhibited by the pseudosubstrate domain (red). The N-terminal regulatory domain differs structurally and functionally. Conventional isoenzymes contain a tandem C1 domain that binds DAG or phorbol esters and a C2 domain that binds to PS (Ca^{2+} dependent). Novel isoenzymes contain a C2-like domain that is not able to bind Ca^{2+}. Atypical isoenzymes contain neither functional C1 nor C2 domains. Adapted from[59,60].

The pseudosubstrate (red in Fig. 2.1) domain binds to the kinase region and auto-inhibits the enzyme[60,61]. The pseudosubstrate sequence retains the hallmarks of a PKC phosphorylation site (several basic residues around the phosphorylation site[62]), but has an alanine at the predicted serine/threonine phosphorylation site:

N'-K^{108}-F^{109}-A^{110}-R^{111}-K^{112}-S^{113}-T^{114}-R^{115}-R^{116}-S^{117}-R^{118}-L^{119}-C'

(pleckstrin phosphorylation site[63])

N'-R^{19}-F^{20}-A^{21}-R^{22}-K^{23}-G^{24}-A^{25}-L^{26}-R^{27}-Q^{28}-K^{29}-N^{30}-C'

(PKC pseudosubstrate[60])

Within the pseudosubstrate region, Ala^{25} is crucial. Mutation of Ala^{25} to serine converts the pseudosubstrate region into a potent substrate. The pseudosubstrate has to be removed from the kinase core for activation of PKC[64,65].

The C1 domain (blue in Fig. 2.1) binds DAG through a Cys-rich motif, which is duplicated in most enzymes[58,66,67]. This domain is responsible for strong over-

activation of PKC by phorbol esters. It binds phorbol ester over two orders of magnitude tighter than DAG[68]. Phorbol esters can replace DAG for strong PKC stimulation: not only do they bind tighter to the C1 domain, but they are also metabolized slowly, prolonging their effect[69,70]. DAG and phorbol esters serve as hydrophobic anchors, recruiting PKC to the plasma membrane.

The C2 domain (yellow in Fig. 2.1) contains, in conventional isoenzymes, the Ca^{2+} binding site. It contains a recognition site for acidic lipids and is responsible for Ca^{2+} dependent membrane targeting[71]. In nPKCs the Ca^{2+} binding site is inactive, but there is evidence for the C2 domain of PKC-δ being a protein interaction site[72]. However, in all PKCs the C2 domain of is responsible for lipid binding[73,74]. C1 and C2 domains can also be found in proteins other than PKC[75-77]. Some C1 domain containing proteins, which are not PKCs, are phorbol ester responsive as well. This has to be considered when observing effects after phorbol ester stimulation, especially when observing proteins that might be regulated by PKC themselves, such as the C1-containing protein families of chimaerin[78] and Munc[79].
Domains C3 and C4 form the kinase region (green in Fig. 2.1), where C3 binds ATP and C4 the substrate[80]. PKC typically phosphorylates serine and threonine residues in a basic sequence, but it has less sequence specificity than PKA, for example[81].
The regulatory and catalytic regions are connected by a hinge that becomes proteolytically labile when the enzyme is membrane bound[82]. Cleavage of the hinge results in the constitutively active kinase PKM[9-13].

PKC is activated by many signals in cells, an increased amount of DAG in the membrane being the best described one. The inital pathway for DAG production is the cleavage of phosphatidylinositol 4,5-bisphosphate (PIP_2) by phospholipase C (PLC), resulting in formation of soluble inositol 1,4,5-trisphosphate (IP_3) and membrane-bound DAG. Soluble IP_3 leads to an increased Ca^{2+} level, which in turn drives localization of cPKCs to the membrane, where interact with DAG now present at elevated levels[83,84]. PLC itself is activated by many effectors, for example by binding to a G protein-coupled, serpentine or tyrosine-kinase receptor (Fig. 2.2).

The hydrolysis of other phospholipids, namely phosphatidylcholine (PC), is also known to produce DAG (Fig. 2.2), although at a slower rate than in the pathway through PLC and PIP_2 breakdown[85,86]. Phospholipase D (PLD) degrades PC to phosphatidic acid (PA), which is then de-phosphorylated to DAG by phosphohydrolase (PAP). This appears to be responsible for sustained activation of PKC, which is important for the longer responses, for example required during cell proliferation and differentiation[61,70,87,88].

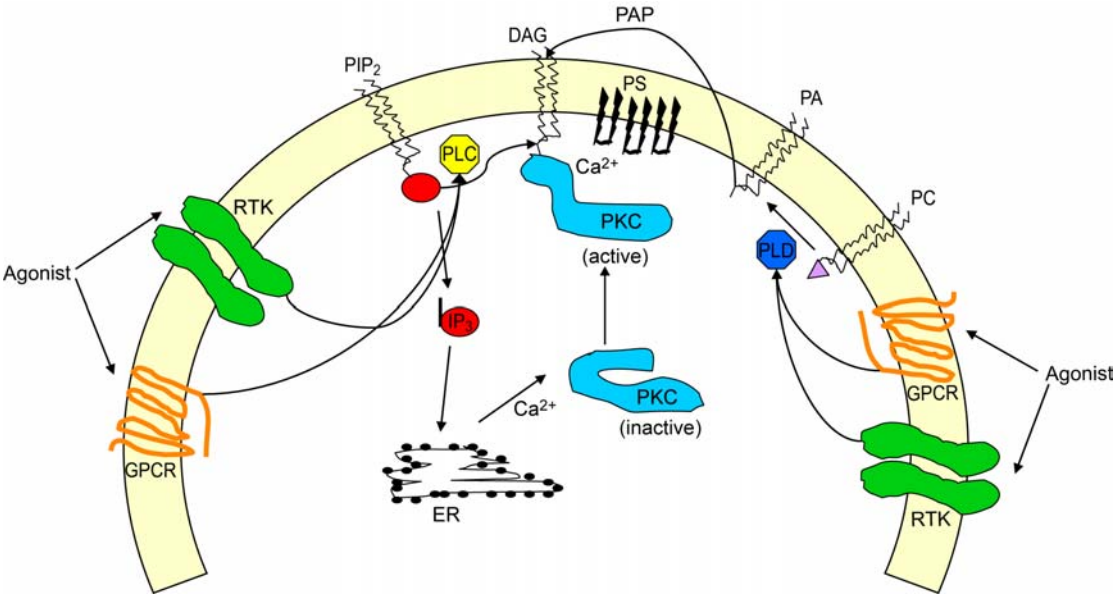

Fig. 2.2 Schematic illustration of PKC activating signals

Agonist-binding to G protein-coupled receptors (GPCR) or receptor tyrosine kinases (RTK) activates phospholipase C (PLC), which hydrolyses phosphatidylinositol 4,5-bisphosphate (PIP_2) to inositol 1,4,5-trisphosphate (IP_3) and diacylglycerol (DAG). IP_3 elevates intracellular calcium levels, protein kinase C is recruited to the membrane, where it binds to phosphatidylserine (PS) and DAG and is activated. Stimulation of GPCRs or RTKs can also lead to activation of phospholipase D (PLD), which hydrolyses phosphatidylcholine (PC) to phosphatidic acid (PA). PA is subsequently de-phosphorylated by phosphohydrolase (PAP) to DAG. *Modified from*[61,70]

The activation of cPKCs and nPKCs is regulated by two mechanisms: phosphorylation of the enzyme itself and allosteric binding of cofactors that remove the pseudosubstrate from the substrate-binding site.

Inital phosphorylation of PKCs is regulated by the phosphoinositide-dependent kinase PDK-1[89-92]. PDK-1 is generally involved in phosphorylating AGC superfamily protein kinases in their catalytical loop[93,94]. It consists of a kinase domain and a phosphatidylinositol 3,4,5 triphosphate-binding pleckstrin homology domain[95,96]. In PKA, this phosphorylation has been shown to be important for aligning the catalytic site of the enzyme properly[97]. According to

structural modeling, phosphorylation serves the same function in PKC-α and PKC-β[98]. The PDK-1-dependent phosphorylation of the activation loop in cPKCs, nPKCs and aPKCs is followed by rapid additional phosphorylation events, partly autophosphorylations in C-terminal regions[99-102]. These phosphorylations help lock the enzyme in its active conformation, although the exact order and requirement for PDK-1 independent phosphorylations remains to be established[103]. Phosphorylation does not activate the enzyme itself, but it is required for catalytic competence in cPKCs and nPKCs. Activation without previous phosphorylation is impossible. In contrast, phosphorylation directly activates aPKCs.

Membrane localization and interaction with DAG are crucial for full activation of cPKCs and nPKCs. cPKCs are recruited to the membrane by interaction of the C2 domain with Ca^{2+} and anionic phospholipids. This interaction enhances binding to DAG at the membrane[104-108].

The active, membrane-bound enzyme efficiently phosphorylates its substrates. Additional regulatory mechanisms include interaction with PKC binding proteins[109]. These proteins can be subdivided into those that are also substrates (STICKs: *s*ubstrates *t*hat *i*nteract with *C*-*k*inase)[110,111]; scaffolding proteins (RICKs: *r*eceptors for *i*nactive *C*-*k*inases)[112] that can restrict membrane and substrate access prior to PKC activation; and complexes, that can control substrate access after PKC activation (RACKs: for *a*ctive *C*-*k*inases)[113-116]. Localization of the PKC through targeting sequences (NLS/NES) is also important for isoenzymes specificity[117].

2.1.3 Pleckstrin

Several PKC probes have been developed based on different PKC substrates in cells[118-121]. The probe used in this thesis is based on pleckstrin, the major substrate of PKC in platelets and leukocytes[122-129]. Pleckstrin (*p*latelet and *l*eukocyte *C* *k*inase *s*ubstrate) is a rational template for a PKC probe, as it is absent from all other cells and is therefore not likely to interfere with signaling in other cells. In addition, it has been shown in NMR experiments to undergo

conformational changes upon phosphorylation (Sattler group, EMBL Heidelberg, unpublished results).

Pleckstrin is phosphorylated at three phosphorylation sites by PKC. The phosphorylation sites lie between a PH and a DEP domain (Fig. 2.3) and consists of two serines and a threonine (N'-KFARK**ST**RR**S**IRL-C', phosphorylation sites in bold)[63,130-133].

Phosphorylation leads to translocation from the cytosol to the membrane in about 50% of pleckstrin molecules, which also depends on guanosinetriphosphate (GTP) binding proteins in platelets[134]. A clear function, however, has not been determined for pleckstrin in platelets. Activation of pleckstrin triggers cytoskeleton/membrane association[134]. There is evidence that pleckstrin interacts with $G_{\beta\gamma}$ and phosphatidylinositol kinases after activation[135,136] and its activation correlates with secretion of granule contents of platelets[124].

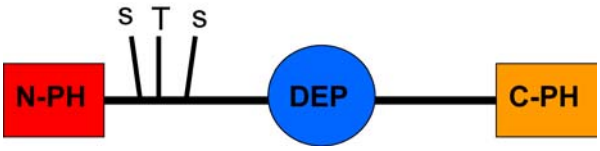

Fig. 2.3 Domain architecture of pleckstrin

Pleckstrin consists of two PH domains, one N-terminal and one C-terminal, than enclose the PKC phosphorylation site and a DEP domain.

In possessing two PH and the DEP domains, pleckstrin contains two modules that are found in many signaling molecules[137-139]. The PH (Pleckstrin homology domain) was first discovered in pleckstrin and is particularly common in kinases and GTPases. They are diverse in sequence, but have a conserved three dimensional fold. It consists of a 7-stranded β sandwich capped by an α-helix[140]. The N-terminal PH domain of pleckstrin was one of the first PH domain structures solved[141]. It was shown to bind liposomes containing phosphatidylinositol-4,5-bisphosphate (PIP_2)[142,143], suggesting a membrane targeting function of PH domains. The binding for PIP_2 was shown to be mediated by a positively charged face of the PH domain that consists of three "variable loops". These loops are the most variable part in length and sequence within the family of PH domains[137,144]. These variable loops and their positively charged face bind to the polyphosphorylated inositol rings of

different phosphoinositides with weak or high affinity. Other examples include, the PH domain at the N-terminus of phospholipase C-δ, which binds PIP_2 and inositol 1,4,5-trisphosphate (IP_3)[145,146] or the PH domain of protein kinase B (PKB), which binds equally well to phosphatidylinositol 3,4,5-triphosphate (PIP_3) or to phosphatidylinositol 3,4-diphosphate[147,148]. A large number of PH domains, however, bind phosphoinositides or inositol phosphates only with low affinity and poor specificity[149]. In a qualitative filter binding assay, comparing binding of different PH domains to multiple phosphoinositides (PI), Kavran *et al.* demonstrated that PH domains from *β*-adrenergic receptor kinase *β*1, spectrin, Ras-GAP, pleckstrin (N-PH) and diacylglycerol kinase- *β* bound to every PI tested in the assay. Both PH domains of pleckstrin, N-PH and C-PH, are able to bind the G-protein heterodimer $G_{\alpha\beta}$ in vitro[150]. Mutational analysis of this interaction showed that the protein binding site of N-PH and C-PH are located within the first 30 amino acids of the PH domain.

The DEP domain was first discovered in signaling proteins like disheveled, Egl-10 and pleckstrin (hence the name DEP domain), but it is also present in certain kinases and regulators of G-protein signaling[151]. DEP domains are usually present as a single copy, only few proteins contain more than one DEP domain[152,153]. Little is known about its function, but it has been suggested to be involved in targeting of signaling molecules to the plasma membrane[154,155].

2.2 Fluorescence and fluorescent in vivo labeling

2.2.1 Fluorescence and Fluorescence Resonance Energy Transfer

Fluorescence phenomena are caused by changes of the electronic distribution in molecules after irradiation with electromagnetic waves. An electron is excited to a higher energy level by absorption of a photon, and relaxes back to the ground state by emission of a photon with a longer wavelength. The energies needed for this are about 100 kJ/mol, which corresponds to wavelengths in the visible and ultra violet region of the spectrum[156,157].

In the quantum model, electrons in a molecule can occupy only discrete energetic states. The electron does not have access to a continuous energy landscape, but only to certain energetic states [156,157].

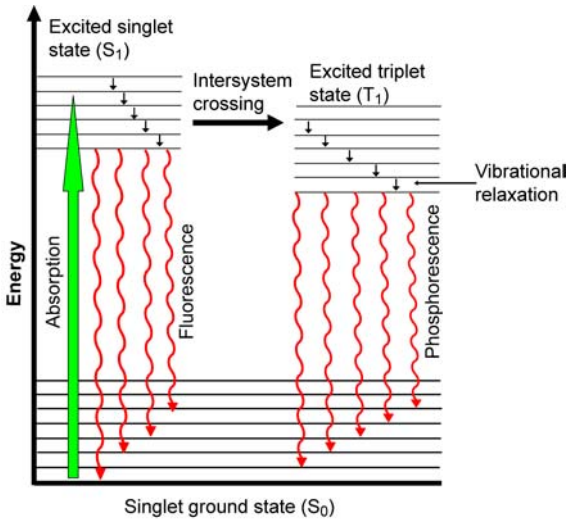

Fig. 2.4 Jablonski diagram

A Jablonski diagram is a simple schematic illustration of energy levels involved in absorption, fluorescence and phosphorescence. Electrons can be excited from ground state to higher electronic states by absorption of photons. Energy can be lost in a non-radiative way through vibrational relaxation or be emitted as photons of a lower wavelength (fluorescence). *Modified from*[156].

Transitions between energy states with different principal quantum numbers are allowed in fluorescence, but those with a change of the angular momentum are forbidden. As the ground state is devoid of an angular momentum, only transitions to other singlet states are allowed. Transitions with changes of angular momentum (intersystem crossing) have a very low

probability and give rise to the phenomenon of phosphorescence. The different energy levels are usually depicted in a Jablonski diagram (Fig. 2.4).
Transitions only occur when light with the wavelength λ, corresponding to the energy difference of the exited and the ground state, is used. This is given by the Planck equation:

$$E_{exited} - E_{ground} = h\nu = \frac{hc}{\lambda} \quad (Eq.\ 1),$$

where *h* is the Planck constant and *v* the frequency.

In atomic spectra, electronic transitions give rise to very sharp bands in the spectrum. In larger molecules, the energy levels of the excited electronic states are modulated by the vibrational levels of the nuclei. Large molecules have a large number of different vibrational states, which leads to a broad, almost continuous distribution of energy levels and a smooth spectrum with no resolved bands that can be attributed to individual transitions.
Typically, the fluorescent molecule sits at the lowest energy vibrational state before it is excited. From there, it can absorb light to reach one of the vibrational states of the first excited electronic energy level. The molecule subsequently decays to the lowest vibrational level of the excited state without emission of photons. The relaxation to one of the vibrational levels of the ground state is coupled to the emission of a photon. Since part of the energy is already dispersed in non-radiative processes, the emission wavelength is usually higher then the excitation wavelength (the difference between excitation and emission wavelength is called Stokes-Shift)[156,157].
The electron stays in the excited state for some time before it relaxes back to the ground state. During this fluorescence lifetime τ_0, the excited molecule can transfer its energy to a neighboring molecule. This so called fluorescence resonance energy transfer was first described by V. T. Förster in 1948[158]. The transfer is based on a long range dipole-dipole interaction. The typical range of those interactions is 2-10 nm, which makes it ideally suited for distance measurements at the scale of biological macromolecules and complexes[159].

The rate of energy transfer can be derived as follows:

$$k_t(r) = \frac{1}{\tau_D}\left(\frac{R_0}{r}\right)^6 \quad (\textit{Eq. 2}),$$

where τ_D is the lifetime of the excited state of the donor in the absence of the acceptor and r is the distance between the fluorophores. As expected, the distance has a strong influence on the transfer rate. As the transfer rate scales with $1/r^6$, a doubling of the distance reduces the transfer rate 64 times.
The Förster Radius, R_0, summarizes other factors influencing the transfer rate: $R_0 = 0.221\left(\frac{\kappa^2 Q_D}{n^4}\int_0^\infty F_D(\lambda)\varepsilon_A(\lambda)\lambda^4 d\lambda\right)^{1/6}$ (*Eq. 3*)

The refractive index n is a measure for the shielding of transition dipole interactions by the solvent. κ is a factor that describes the relative orientations of the transition dipoles for the excitation. It is maximal for collinear transition dipoles κ=4 and minimal for perpendicular transition dipoles κ=0. For a mixture of molecules with random relative orientations due to rotation diffusion one can assume κ=*2/3*. The integral describes the spectral overlap of the acceptor absorbance spectrum ε(λ) and the donor fluoresce intensity $F_D(\lambda)$. A large overlap between the two spectra is essential for an efficient FRET.
Since the transfer rate itself is difficult to measure directly, it is convenient to calculate which percentage of photons will be transferred to the acceptor for a given rate $k_{t,}$. This property is called FRET efficiency *E*:

$$E = \frac{k_t}{\tau_D^{-1} + k_t} \text{ (Eq. 4)}$$

This can be rearranged to:

$$E = \frac{R_0^6}{R_0^6 + r^6} \text{ (Eq. 5)}$$

The Förster radius is therefore the distance, at which half of the energy is transferred to the donor.

Several methods are commonly employed to measure FRET efficiency. They can be combined with conventional and confocal microscopes to measure spatially resolved FRET efficiencies in cells or other biological sample[159,160].

The first way of detecting FRET is measuring an increase in the acceptor fluorescence upon donor excitation (sensitized emission)[161]. This seems to be the most straightforward method of measuring FRET but has drawbacks in practice. The emission spectra of most fluorophores have long tails towards longer wavelengths, which makes it difficult to separate donor and acceptor emission completely (bleed-through). The overlap of the emission spectra has to be experimentally determined and corrected for in the evaluation of the data (unmixing).

Measuring the increase in donor fluorescence after photo-bleaching of the acceptor is another method of detecting FRET (acceptor photo-bleaching)[161,162].

The difference between donor emission before (F_{DA}) and after (F_D) selective bleaching of the acceptor is a direct measure for the percentage of excitation energy transferred to the acceptor:

$$E = 1 - \frac{F_{DA}}{F_D} \quad \text{(Eq. 6)}$$

The emission spectrum of the acceptor usually does not extend to shorter wavelengths of the donor spectrum, spectral overlap is therefore a lesser problem in this method. The main disadvantage is that the method is difficult to apply quantitatively in living cells, because of the long times required for the complete bleaching of the acceptor. It is a reliable method, if cells can be fixed without damaging the structures to be observed. It has to be considered, however, that even though bleaching destroys acceptor fluorescence, the acceptor might still quench some donor fluorescence as the chromophore itself remains intact.

A third method of measuring FRET efficiencies is observing the decrease of donor fluorescence lifetime in the presence of the acceptor[163,164].

The fluorescence lifetime τ_D depends on the rate of decay due to radiative (k_r) and non-radiative ($\mathbf{k_{nr}}$) processes:

$k_t = \tau_D^{-1} = k_r + k_{nr}$ *(Eq. 7)*

k_t is the total decay rate.

In the absence of an acceptor the fluorescence will decay with a characteristic rate. FRET adds another non-radiative decay rate to the total rate. The

fluorescence lifetime of the donor in the presence of the acceptor τ_{DA} is therefore smaller than in its absence (τ_D).
This is related to the FRET efficiency:

$$E = 1 - \frac{\tau_{DA}}{\tau_D} \quad \text{(Eq. 8)}$$

Life time measurements can be performed in several ways. The most straightforward is to use a pulsed laser source for excitation and measure the decay of fluorescence intensity directly. Since typical lifetimes are well below 5 ns, this method has high demands on both, the pulsing laser and the time resolution of the detector.
The lifetime can also be measured in the frequency domain. The sample is illuminated with a continuous wave laser and the intensity of the laser beam is modulated with a high frequency. The lifetime of the excited state leads to a phase shift between the modulation of the excited state and emission light.
The main advantage of lifetime imaging is that it can be applied in living cells, since it has a high time resolution and does not require the long bleaching periods of the acceptor photo-bleaching method. Lifetimes are sensitive to other environmental factors like ionic strength, pH or hydrophobicity of the solvent. Those influences have to be considered when interpreting life time data. An additional caveat of life time imaging is that it provides no information about sensor concentrations.
Another widely used approach, does not determine absolute FRET effciencies, but a relative change by following donor-acceptor ratios[165-170]. We used this approach to measure PKC activity in living cells in this.

The applications of FRET in biology are wide spread[171]. Two main applications have emerged over the last decade.
The first is the determination of protein-protein interactions in living cells. The resolution of a light microscope is normally limited to around 200 nm. This is enough to visualize co-localization of fluorescently labeled proteins in the same cellular substructure, but not to determine whether proteins bind to each other or not. FRET, on the other hand, is limited to distances smaller than 10 nm, which corresponds to the distance of directly interacting or bound proteins. This has been used extensively in numerous biological systems to

verify the protein-protein interactions *in vivo*. Examples include elements of the COPI vesicle machinery[172], glycosyltransferases[173], G-protein-coupled receptors[174], the EGFP receptor[175] or cholera toxin[176].

A second area, in which the FRET principle is extensively used, is the development of probes to visualize biochemistry in living cells. Any change, binding of co-factors, de-/phosphorylation[168], protease activity[167,177] or receptor activation[178] that changes the distance or orientation between two fluorophores might be detected by FRET. Classic examples are the so called cameleon probes[165,166,179,180], developed to visualize the beginning, termination and spatial distribution of Ca^{2+} signaling events. They consist of ECFP and EYFP connected by calmodulin (CAM) and the calmodulin binding peptide of myosin light chain kinase (MLCKp). When the Ca^{2+} concentration rises, it binds to the CAM domain, which in turn binds to MLCKp. This change decreases the distance between CFP and YFP and leads to an increased FRET efficiency[181-183]. In principle the Ca^{2+} concentration could be determined inside living cells by comparing the FRET efficiency with those obtained from control experiments *in vitro*[184,185].

2.2.2 Fluorescent *in vivo* labeling of proteins

Few different methods are available for fluorescent labeling of proteins in living cells. Attaching fluorophores to antibodies for specific labeling of proteins has been used for a long time on permeabilized cells. This method has profited from the development of Quantum Dots (QD). QDs are inorganic nanocrystals with very distinct fluorescence properties that can be attached to antibodies or streptavidin. Their size (10 to 30 nm when coated) prevents them from passing the membrane, their use is therefore restricted to permeabilized membranes or extracellular proteins[186-188]. A recent commercial development (Promega), is the so-called HaloTag®[189,190]. It is based on a modified prokaryotic hydrolase. The 33kD monomeric protein can be used for N- and C-terminal fusions. Ligands can be constructed that specifically react with active cysteine, amine or carboxy-groups in the Halo protein. They contain a linker region that ensures specificity of the covalent attachment to

the Halo protein. The functional region can be attached to a large number of molecules ranging from fluorophores to biotin and other affinity labels.
Far more common for in-vivo labeling is the use of genetically encoded fluorescent proteins. Hybrid methods, combining a genetically encoded tag with small chemical dyes are becoming more widely used, combining the advantage of a genetic tag with the large variability of fluorescent dyes.

The following paragraphs describe the methods for *in vivo* labeling of proteins used in this thesis.

2.2.3 Fluorescent proteins

The first fluorescent protein, the green fluorescent protein (GFP) from the jellyfish *Aequorea Victoria*, was purified in 1962 by Shimomura *et al*[191]. It took 30 more years until the gene encoding GFP was cloned[192] and it could be shown that expression in other organisms than *Aequorea*[193,194] was possible.

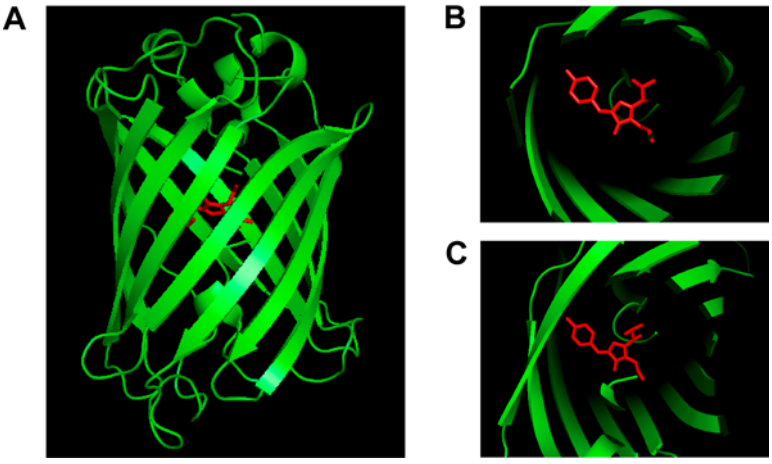

Fig. 2.5 Crystal structure of GFP

A Crystal structure of wild-type GFP. The chromophore at the center of the β-barrel is shown in red. PDB no 1GFL.

B Enlarged view of the fluorophore of GFP (red). The fluorophore consists of amino acids S^{65}-Tyr^{66}-Gly^{67}.

C Enlarged view of the fluorophore of EGFP (red). In EGFP, Ser65 has been mutated to Thr. PDB no 1Q4A.

The 27kD GFP protein folds into an 11-stranded β-barrel with an α-helix running along the axis (see Fig. 2.5 A) [195,196]. The chromophore is formed by Ser^{65}-Tyr^{66}-Gly^{67} located in the central α-helix (see Fig. 2.5 B).

It forms post-translationally in a two stage oxygen-dependent cyclization reaction. No other cellular factors are needed for the maturation reaction. The half time of the maturation of wild type GFP (wtGFP) is 25-85 min. The chromophore is buried and well protected by the β-barrel structure of the protein. β-barrel folding occurs prior to the maturation of the chromophore and has a half time of about 10 min[197].

The spectrum of wtGFP is complex and broad. The excitation spectrum has a major peak at 395 nm and a minor peak at 475 nm. The emission maxima are at 508 and 503 nm, depending on the excitation[198]. The spectral properties of wtGFP are pH sensitive.

The wtGFP sequence has been extensively mutated to reduce the limitations of wtGFP. The first widely used GFP variant was enhanced GFP (EGFP). In EGFP Ser^{65} was mutated to threonine (see Fig. 2.5 C)[199]. The mutation leads to an ionization of the phenol of the chromophore shifting the excitation maximum to a single peak at 490 nm with a 4-6 times increased intensity. The maturation is accelerated four times in the S65T mutant[198]. An additional F64L mutation in EGFP further increases the brightness of GFP and reduces the maturation time[200]. EGFP was codon optimized for a more efficient expression in higher eukaryotes, like mammals[201].

Many applications in biology require the use of multiple colors. A large number of spectral variants of GFP have been developed by different groups. Significantly red shifted variants can be produced by stacking an aromatic ring next to the phenolate ion of the chromophore. The most commonly used variant is EYFP, which contains the mutation T203Y. The excitation peak is shifted to 512 nm and the emission to 525 nm. Additional mutations in the periphery of the fluorophore increase the extinction coefficient (V68L) and accelerate folding (S72A)[195]. EYFP was shown to be sensitive to environmental influences like pH or chlorine ions, which was overcome by introducing an additional mutation (Q69M). The new variant, called Citrine has increased photostability and decreased pH and chlorine sensitivity[202]. Further mutations at the fluorophore or surrounding region have created several more colors based on the wtGFP from *A. victoria*. Examples include a cyan fluorescent protein (ECFP), which has an excitation maximum at 434 nm and

an emission maximum at 475 nm[203] or an even more blue-shifted protein, the blue fluorescent protein (BFP). Although it has interesting spectral properties (excitation at 380 nm and emission at 442 nm), its poor photostability and dim fluorescence make it rarely used[198]. Monomeric versions of EYFP and ECFP have recently been improved for faster folding and improved brightness[204].

Another desirable property in fluorescent proteins is a large Stokes shift for better separation of excitation and emission wavelength. Sapphire and GFP^2 are proteins that have this quality. Sapphire and GFP^2 have an excitation and emission peak at 399 and 511 nm, respectively[205,206].

Despite the efforts of several groups, no protein further red shifted than YFP has been developed based on the *A. victoria* GFP. Work has therefore concentrated on finding new fluorescent proteins from other organisms that have are red shifted compared to GFP. DsRed, cloned from coral *Discosoma* species[207], has been developed into a number of variants with desirable photo- and biochemical properties. The original DsRed has a strong tendency for tetramerization and matures very slowly ($t_{1/2}$ ~10h)[208], which renders it difficult to use for most applications. A monomeric version with an improved maturation time was developed by the Tsien laboratory, but it was five times dimer than the original DsRed and less photostable[209]. Extensive mutational screens have yielded a large number of improved variants with diverse spectral characteristics[210,211]. Promising variants found in this screens include the monomeric red shifted variants mPlum (590/649), mCherry (587/610) and mOrange (548/562)[210]. Several more FPs of other species were also described, including a monomeric orange FP (mKO) from the coral *Acropara* species[212], MonsterGreen™ (Promega) from *Montastraea cavernosa* and AcGFP1 cloned from *Aequorea corulescens* (BD Bioscience).

A whole family of proteins has been cloned from *Anthozoa* reef corals. Currently efforts are underway to produce monomeric variants and to increase maturation speed and brightness[213].

A number of photoactivatable (pa) and photoswitchable (ps) fluorescent proteins have been developed in the last few years. pa-GFP is essentially non fluorescent in its ground state, but can be irreversibly activated with a short pulse of 413 nm light[214,215]. pa-mRFP1 can be activated with a 380 nm light. ps-CFP and ps-CFP2 change their fluorescence maxima from 468 to 511 nm

upon UV-irradiation (The proteins are derived from *A. corulescens* not from *A. Victoria)*[216,217].

A fascinating development is the FP Dronpa, which can be switched from a non-fluorescent state to a green fluorescent state with 400 nm, but also switched off again with intense blue light (470-500 nm). Both processes are entirely reversible and repeatable[218]. The Kaede family of fluorescent proteins shows promising results for the development of efficient photoswitchable FPs, but have so far been hampered by tetramerization and low stability above 30°C[217,219,220].

For FRET applications, the donor-acceptor pair should ideally fulfill several criteria in order to have a large Förster radius: The donor should have a large quantum yield, the spectral overlap should be as large as possible and the donor should have a large stokes shift to allow a selective excitation of the donor. For applications in tissues or living animals, FRET pairs should have long excitation and emission wavelengths and should be stable in two-photon excitation. For labeling of other proteins the FPs should be monomeric, although a weak dimerization can enhance the observed signal without changing the behavior of the tagged proteins (see this thesis).

The donor/acceptor pairs with the best spectral properties at the moment are CyPet-YPet[221] and GFP^2-EYFP[206]. For applications, where an acceptor emission further red is desirable, the best pair currently seems to be cyan MiCy with orange mKO. Both were cloned from *Acropara* species. MiCy forms dimers, which makes it difficult to use in most application[212]. Experiments with other donors for mKO have not been reported so far.

In the red region of the spectrum no satisfying donor/acceptor combination has been reported so far. GFP and DsRed form a good donor/acceptor pair with an R_0 comparable to the common CFP/YFP pair[222,223], but the strong tetramerization of DsRed is of disadvantage. Experiments using the new mRFP1 variants have not been reported so far[210,211]. Clearly the development of improved long wavelength FRET pairs is important for the application of FRET in tissue.

Table 2.1 summarizes the spectral properties of several fluorescent proteins mentioned in this thesis.

Name	Excitation [nm] (ε)	Emission [nm] (QY)	Brightness	Photostability [sec]	Oligomer-ization
BFP	382 (21)	448 (0.24)	5	ND	weak dimer
wt-GFP	395 (27.5) 472 (7.5)	504 (0.79)	21	ND	weak dimer
GFP[2]	396 (84)	510 (0.61)	51	ND	weak dimer
T-Sapphire	399 (44)	511 (0.6)	26	25	weak dimer
ECFP	433 (28)	475 (0.45)	13	64	weak dimer
CyPEt	435 (35)	477 (0.51)	18	59	weak dimer
EGFP	488 (55)	508 (0.6)	34	174	weak dimer
MiCy	472 (27)	495 (0.90)	24	ND	dimer
AcGFP1	475 (32)	505 (0.82)	27	ND	monomer
EYFP	514 (83)	527 (0.61)	50	60	weak dimer
YPet	514 (43)	527 (0.62)	51	60	weak dimer
Citrine	516 (77)	529 (0.76)	59	50	weak dimer
mKO	548 (52)	559 (0.6)	31	122	monomer
mOrange	548 (71)	562 (0.69)	49	9	monomer
DsRed	558 (75)	583 (0.79)	60	ND	tetramer
mRFP1	584 (50)	607 (0.25)	12.5	6.2	monomer
mCherry	587 (72)	610 (0.22)	16	96	monomer
mPlum	590 (41)	649 (0.1)	4.1	53	monomer

Table 2.1 Spectral properties of some fluorescent proteins

ε is the absorption coefficient in $mM^{-1}cm^{-1}$, QY is the quantum yield. The brightness is the product of ε and QY in $mM^{-1}cm^{-1}$. The photostability is the time in seconds to go from en initial emission of 1000 photons/s to 500 with constant excitation intensity. This does not necessarily reflect the photostability under other conditions. ND = not determined. Source:[210,212,224-226] and http://www.clontech.com/

2.2.4 Fluorescent labeling of proteins in living cells with AGT

Specifically attaching small, chemically synthesized molecules is another way of efficiently labeling proteins in living cells. These methods have certain requirements to meet. The dye has to specifically recognize a tag and bind to it with high affinity. The tag should neither be too big, nor disturb the tagged proteins function and should not occur naturally in cells. In addition, the dyes should not be toxic for cells and pass the membrane easily.

AGT labeling is based on the DNA repair enzyme human O^6-alkylguanine-DNA alkyltransferase (AGT)[227,228]. AGT plays an important role in cellular defense against alkylating agents by removing alkyl adducts at the O^6-position

of guanine and covalently binding it to one of its cysteines. This prevents one of the most harmful lesions as it leads to GC→AT transition mutations, which are associated with mutagenic, toxic and carcinogenic effects[229]. The substrate specificity of AGT is relatively low since it readily reacts with O^6-benzylguanine (BG) derivatives. This property can be used for the labeling of proteins that are tagged with AGT. By synthesizing BG derivatives of fluorophores, these fluorophores can be irreversibly transferred to AGT and hence the protein of interest (Fig. 2.6). AGT labeling can be very specific and fast, but technically challenging. This enables labeling of a single AGT fusion protein with a wide range of different dyes[230,231]. AGT has been used for protein labeling as an alternative to GFP in anaerobic organisms[232].

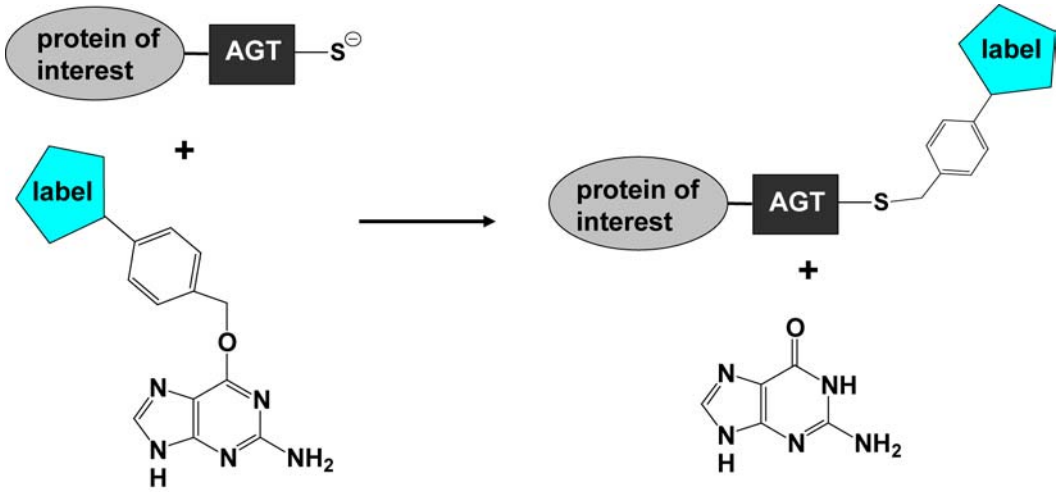

Fig. 2.6 Covalent labeling of a protein of interest fused to AGT

An O^6-benzylguanine (BG) fluorophore derivative is recognized by AGT and readily transferred to a cysteine residue of the protein. The label is covalently bound and the reaction irreversible.

2.2.5 Fluorescent labeling of proteins in living cells with FlAsH

Arsenoxides are known to have a high affinity for thiols, including closely spaced cysteines. FlAsH, containing two arsenoxides, has a high affinity for four appropriately spaced cysteines. The rigid spacing of the two arsenoxides enables FlAsH to bind with high specificity to the small tetracysteine motif (TCM) introduced into proteins (Fig. 2.7 A). This approach was first introduced by Tsien *et al.* in 1998[233]. The tetracysteine motif has since been optimized for selective binding of FlAsH, higher fluorescence quantum yield and better

dithiol resistance, thereby reducing background labeling[234]. The best motif found so far consists of 12 amino acids with the sequence FLNCCPGCCMEP.

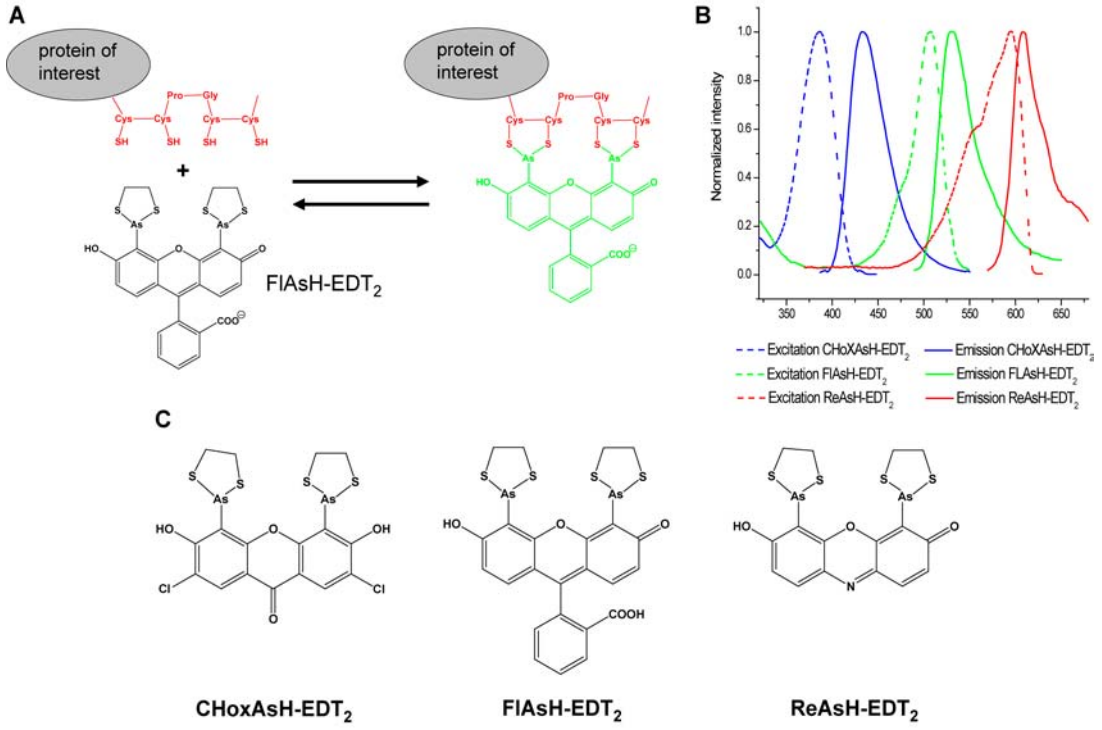

Fig. 2.7 Fluorescent labeling of proteins in living cells with FlAsH

A A protein encoding the tetracysteine motif (TCM) is labeled with FlAsH-EDT_2. When binding to the TCM, the FlAsH becomes fluorescent.

B Normalized spectra of the excitation (dashed line) and emission (solid line) of CHoxAsH-EDT_2, FlAsH-EDT_2 and ReAsH-EDT_2.

C chemical structures of CHoxAsH-EDT_2, FlAsH-EDT_2 and ReAsH-EDT_2.

This labeling method, however, still has relatively high background[235], especially when compared to genetically encoded fluorescent proteins or AGT.

FlAsH is best isolated as a FlAsH-EDT_2 adduct, which enters cells easily. FlAsH-EDT_2 is practically non-fluorescent, but FlAsH bound to the TCM has a quantum yield of 0.4 (≥$5x10^4$ times more fluorescent as FlAsH-EDT_2). The standard FlAsH has excitation and emission peaks at 508 and 528 nm, respectively. Other colors include ReAsH (excitation and emission maxima at 593 and 608 nm, respectively) and CHoxAsH-EDT_2 (excitation and emission maxima at 380 and 430 nm, respectively)[236] (Fig. 2.7 B and C).

FlAsH and ReAsH have been used in many applications, e. g. in FRET based assays to determine G protein-coupled receptor activation[178], in correlative

fluorescence and electron microscopy[237], for determination of protein age by multicolor fluorescence pulse-chase[237,238] or in chromophore-assisted light inactivation (CALI)[239,240]. CHoxAsH has been used to a lesser extend as it is less bright and has lower photostability than the other two dyes.

The key advantage of the FlAsH labeling method, compared to other labels such as FPs or AGT, is the small size of the tag. It has previously been shown, that the size of the tag used for the labeling of proteins, can influence the functionality of the tagged protein. S. Jacobs *et al.* showed that C-terminal tagging of the microtubule protein β-tubulin (*Tub2*) in *S. cerevisiae* resulted in nonviable haploid cells, while labeling with FlAsH did not affect protein function[241].

2.3 Fluorescent probes

In recent years, an increasing number of probes, utilizing fluorescence as a detection marker, have been developed [160,242-244]. In basic applications, the fluorophore is used as a marker for the tagged protein, monitoring appearance, localization or degradation of the protein. Inherent properties of fluorescent proteins or fluorophores can be used to detect changes in the concentration of PH or halides. SNARF is a red fluorescent fluorophore, whose emission depends on PH, that has been used for measuring local changes in PH inside cells[245]. Fluorescent proteins have also been employed for PH measurements[246-248] and the yellow emission variant (YFP) is useful to follow Cl^- flux in epithelial cells[249].

A simple way to follow dynamics in the cell, based on fluorescent tagging of a protein, is to observe domains that translocates upon activation. An example for this kind of biosensor is a GFP-tagged C1 domain of protein kinase C (PKC), which translocates to the plasma membrane upon increase of diacylglycerol (DAG) in the membrane[250]. Other examples include the PA binding domain of Raf[251] or the pleckstrin homology domain (PH domain) of several proteins[252-254], which all translocate to the plasma membrane upon their specific cue.

Many probes have been developed that are based on fluorescence resonance energy transfer (FRET, see 2.2.1) between a donor and an acceptor fluorophore. Some measure interactions between proteins, others detect changes in the intracellular concentration of second messengers. Changes in cGMP concentration were measured by change in FRET from ECFP to EYFP. The donor and acceptor fluorophores were fused to two different cGMP receptors (truncated cGMP-dependent protein kinase or cGMP-dependent protein kinase Iα) which both change their conformation upon cGMP binding[255,256].

Interactions between two proteins can be detected by fusing donor and acceptor fluorophores to the interaction partners. Transcription factor homo- and heterodimerization[257], G-protein dissociation[258] and other interactions[170,259-264] have been visualized this way. Other probes are based on a substrates peptide , e.g. for kinases, sandwiched between a donor and acceptor fluorophore, that undergo conformational change upon phosphorylation by their respective kinase[2,118-121,265].

Understanding of how existing probes are working is essential for the improvement and development of new probes. Two PKC probes and a dual PKC/PKA probe have been developed in our lab[1,2]. This thesis intends to understand the mechanism of action of two of these probes, KCP-1 and KCP-2, in order to improve existing probes and develop new sensors.

3 Materials and Methods

3.1 Materials and equipment

3.1.1 Chemicals and kits

Standard chemicals were purchased from Sigma-Aldrich AG (Steinheim, Germany), Serva (Heidelberg, Germany) or Merck (Darmstadt, Germany) at the highest purity available.
Bradykinin, 2-[1-(3-Dimethylaminopropyl)-5-methoxyindol-3-yl]-3-(1H-indol-3-yl) maleimide (Gö6983) and Phorbol-12-myristate-13-acetate (PMA or 13-acetate 4α-TPA, TPA) were purchased from CalBioChem (Eggenheim, Germany).
Kits for DNA purification were purchased from Qiagen GmbH (Hilden, Germany).
Competent cells (XL1-Blue Subcloning Grade Competent Cell) were bought from Stratagene (La Jolla, USA).

3.1.2 Enzymes

Enzymes for recombinant DNA work were purchased from New England Biolabs (Ipswich, USA), Stratagene (La Jolla, USA) or Fermentas (St. Leon-Roth, Germany).

3.1.3 Reagents and buffers

Reagents and buffers were prepared according to standard protocols unless otherwise mentioned [266,267].

3.1.4 DNA primers and oligonucleotides

DNA primers and oligonucleotides were purchased from MWG Biotech GmbH (Ebersberg, Germany).

3.1.5 Plasmids

The following standard plasmids were purchased from Clontech (Carlsbad, USA): pEGFP, pEYFP and pECFP. The vector containing pGFP2 was purchased from PerkinElmer Life and Analytical Sciences, Inc. (Boston, USA).

The following plasmids were kind donations by the following people:

GEhAGT-B-CaaX	A. Keppler, EMBL, Heidelberg, Germany
pNuc-GEhAGT-B	A. Keppler, EMBL, Heidelberg, Germany
AGT177	A. Keppler, EMBL, Heidelberg, Germany
pET9d-Pleckstrin(1-221)	M. Sattler, EMBL Heidelberg, Germany
pET9d-Pleckstrin(1-239)	M. Sattler, EMBL Heidelberg, Germany
mCherry	R. Y. Tsien, UCSD, San Diego, USA
mOrange	R. Y. Tsien, UCSD, San Diego, USA

3.1.6 Bacteria

E. Coli BL21 (DE) for protein expression
E. Coli XL1blue for DNA amplification

3.1.7 Cell lines

HeLa CCL-2 (human)	LGC Promochem GmbH, Wesel, Germany
N1E-115 (murine)	LGC Promochem GmbH, Wesel, Germany
HEK-293 (human)	LGC Promochem GmbH, Wesel, Germany

3.1.8 Cell culture and imaging

Chemicals and solutions for cell culture were purchased from Gibco (Eggenstein, Germany).
Transfection reagent, Fugene6, was purchased from Roche (Mannheim, Germany.

Cell dishes with glass bottoms were purchased from MatTek (Ashland, USA) and welled cover slides (LabTek) from Nunc (Wiesbaden, Germany).

3.1.9 Microscopes and other equipment

Leica AOBS SP2	Leica Microsystems (Heidelberg, Germany)
Visitron System	
Zeiss Axiovert	Carl Zeiss Mikroskopiesysteme (Jena, Germany)
CCD camera Coolsnap	HQ Photometrics, Roper Scientific, Inc. (Trenton, USA)
Filter wheel system	Visitron Systems GmbH (Puchheim, Germany)
FlAsH microscope set-up	
Zeiss Axiovert 135	Carl Zeiss Mikroskopiesysteme (Jena, Germany)
Filters and dichroics	Till Photonics GmbH (Gräfelfing, Germany)
Fluorimeter	Photon Technology International Quantamaster QM4/2000SE (PhotoMed GmbH, Seefeld, Germany)
DNA spotter	
Virtek Chipwriter Compact	Eurogentec (Seraing, Belgium)
Pins: PTS/ PTLS 600	Point Technologies, Inc (Boulder, USA)
Microinjection	
InjectMan NI2 micromanipulator	Eppendorf (Hamburg, Germany)
Femtotips II	Eppendorf (Hamburg, Germany)

3.1.10 Software

ImageJ	(http://rsb.info.nih.gov/ij/) W. Rasband, NIH, Bethesda, USA
Metamorph v6.2r4	Universal Imaging Corp., 2004
Origin v6.1	OriginLab Corporation, Northampton, USA
Fluorimeter	Felix v1.41.

3.2 Methods

3.2.1 General methods

DNA cloning was performed according to standard procedures[266,267].
Kits for purification of plasmid DNA, as well as for purification of PCR and restriction products, were used according to the protocol of the supplier.
DNA sequencing was performed by EMBL genomics core facility.

3.2.1.1 PCR

PCR was performed in thin-walled 0.2 ml tubes. A standard PCR usually contained:

- 50 to 100 ng of template DNA
- 100 ng primer, 5' and 3', each
- 250 µM dNTPs

10x *PfuTurbo* DNA polymerase buffer
2-3 U *PfuTurbo* DNA polymerase

- H_2O up to a total of 50 µl

Some PCRs contained a mix of 1-2 U *Pfu* polymerase and 1-2 U *TAQ* polymerase to increase amplification efficiency while ensuring proof-reading activity.

A typical PCR consisted of the following cycles:

95 °C – 5 min	denaturing	
95 °C – 30 s	denaturing	5 cycles
50 °C – 45 s	annealing	
72 °C – 1 min	extension	
95 °C – 30 s	denaturing	25 cycles
55 °C – 45 s	annealing	
72 °C – 1 min	extension	
72 °C – 10 min	extension	

Annealing temperature was varied according to the melting temperature of the primers. Extension time was varied according to the expected size of the product. The last extension step was added for increased proof-reading.
PCR products were analyzed on a 0.8-1.5% agarose gel, according to the length of the expected fragment.

3.2.1.2 Introduction of point mutations

a) Site-directed mutagenesis

A single mutation can easily be introduced into an existing vector by using site-directed mutagenesis (see Fig. 3.1 A). Two primers, containing the desired mutation, and flanked by the correct and matching sequence, have to be designed. In a PCR, the plasmid is denatured to facilitate annealing of the primers. *PfuTurbo* DNA polymerase extends the mutagenic primers, resulting in nicked circular strands. The only difference compared to a regular PCR is the much longer extension time, as the whole plasmid has to be synthesized (calculate 2 min per kb DNA).

After the PCR, the restriction enzyme DpnI is added to the reaction mix for 1 h at 37°C. This enzyme digests the methylated, non-mutated parent DNA, while leaving the newly synthesized one intact. A small amount (usually 2 µl) of the circular, nicked dsDNA can be transformed into competent bacteria, where the nick will be repaired and the plasmid multiplied.

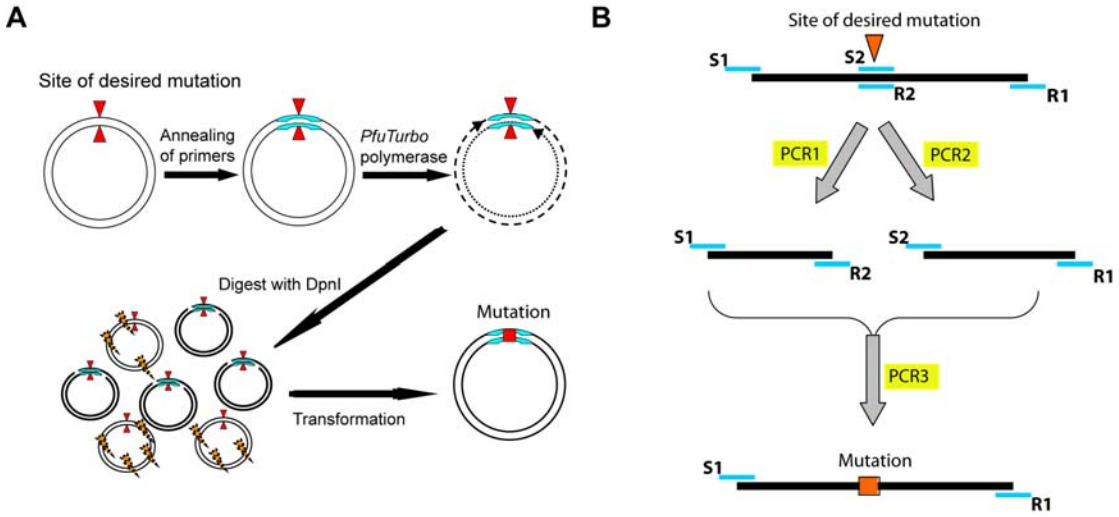

Fig. 3.1 Introduction of point mutations

Schematic representation of two methods to introduce point mutations into DNA

A Site-directed mutagenesis: the mutation is introduced into a plasmid using two mutagenic primers and a PCR of the whole plasmid.

B Introduction of mutations via three independent PCRs: the mutation is introduced by performing three PCRs with two mutagenic primers and two primers containing restriction sites for cloning.

For a detailed description of the two methods, see 3.2.1.2.

b) Introduction of mutations via three PCR steps

Site directed mutagenesis should not be used if the primers introducing the mutation can anneal on several sites on the vector, introducing the mutation more than once. If this is the case, mutations can be introduced via three different PCRs (Fig. 3.1 B). This method is also recommended if restriction sites have to be introduced at the ends of the desired PCR product for further cloning.

Four different primers have to be designed for this method. The first two are a sense primer at the 5'-end (S1) and a reverse primer at the 3'-end (R1) of the target DNA. These primers usually contain the restriction site, which is going to be used to clone the PCR product into the destination vector.

The second set of primers consists of a sense (S2) and a reverse (R2) primer that are complementary to each other and contain the single mutation. More than one point mutation can be introduced using this method; however with an increasing number of mutations, the risk of incorrect or no annealing increases.
In two separate PCRs, two parts of the molecule are created, each containing the mutation. The PCRs use the same template, but PCR1 is performed with primers S1 and R2, while in PCR2 primers S2 and R1 are used. In PCR 3, the products of the previous two reactions are mixed with primers S1 and R1. This connects the two parts, yielding the full construct (see Fig. 3.1).

3.2.1.3 Oligonucleotide ligation

The easiest way to introduce short stretches of DNA is oligonucleotide ligation. Two complementary primers, coding for the desired insert and with sticky ends matching the appropriate restriction site(s), have to be designed.
The primers are first dimerized by mixing 500 pmol of sense and reverse primer and heating them to 95°C for 5 min. The mixture is allowed to cool to room temperature. For the kinase reaction, 10 pmol DNA is mixed with 10 U of T4-Polynucleotide Kinase (T4-PNK) in a buffered solution containing 10 µM ATP. This mixture is incubated at 37°C for 40 min. T4-PNK is subsequently inactivated by heating to 60°C for 20 min.
In order to ligate the dimerized DNA oligos into the target plasmid, 0.4 pmol DNA is mixed with 1 µl (usually between 0.3-0.6 µg DNA) of the previously digested plasmid DNA. T4-DNA ligase is added and the mixture left at room temperature for 30 min. Primers for oligonucleotide ligation have to be designed with sticky ends complementary to the appropriate target DNA sequence. The ligation can then be transformed into chemically competent bacteria.
Chemically competent bacteria were prepared according to standard protocol[266,267] or bought from Stratagene (La Jolla, USA).

3.2.1.4 Cell culture

Cell cultures were maintained by Heike Stichnoth and cultured at 37°C and 5% CO_2. HeLa CCL-2 cells were cultured in DMEM with 10% FCS and Primocin; N1E-115 cells were cultured in high-glucose DMEM with 10% FCS and Primocin. HeLa CCL-2 and HEK-293 were subcultured twice a week; N1E-115 three times a week.

3.2.1.5 Transient transfection of mammalian cells

Cells were transfected at 40-60% confluency with 1 µg of total DNA using Fugene6 in Optimem, according to the protocol of the manufacturer. Cells were incubated at 37°C and 5% CO_2 to allow for protein expression. Expression time was usually between 15 and 48 h.

3.2.1.6 DNA spotting

For parallel experiments with several different constructs on one microscope slide, small amounts of DNA were spotted on welled glass slides (LabTek chambers) together with transfection reagent. Cells could be seeded on these slides and imaged after attachment and protein expression.
The spotting was performed by Holger Erfle (Mitocheck, EMBL Heidelberg).
Lipofectamine (3.5 µl) was added to 4 µl Optimem with 0.4 M sucrose and left standing at room temperature for 5 min. DNA (1 µg) was added to the mix and incubated for another 15 min. Subsequently, 7.5 µl of an aqueous solution with 0.2% gelatin and 0.001% Fibronectin was added to the mix and, after an incubation of 15 min, spotted onto the slides with pins of diameter 600 µm. The arrays could be kept at 4°C for several weeks.
For experiments, the slides were covered with a HeLa cell suspension in Optimem. Cells were imaged 20-24 h later allowing enough time for cell attachment and protein expression.

3.2.1.7 AGT labeling

HeLa CCL2 cells were transiently transfected with DNA coding for one of the listed AGT-PKC probes (see 3.2.2.5 a). The AGT labelling dyes were prepared as 0.8 µM stock solutions in DMSO. Cells were incubated in HEPES buffer (115 mM NaCl, 1.2 mM $CaCl_2$, 1.2 mM $MgCl_2$, 2.4 mM $K_2HPO_4 \cdot 3\ H_2O$, 10 mM Glucose·1 H_2O, 20 mM HEPES, pH 7.4) or Optimem containing 5 µM of the respective labelling dye for 5-15 min, washed with PBS buffer three times and kept at 37°C in medium until imaging.

The non-cell permeable dye O^6-benzylguanine-Cy3 (BG-Cy3) had to be microinjected for AGT labelling. These microinjections were performed by Antje Keppler (EMBL Heidelberg). BG-Cy3 was diluted in water to a final concentration of 30 µM and microinjected into cells. Cells were injected with 50 hPa injection pressure for 0.8 sec by penetrating the cell surface with an injection capillary micropipette. For all dyes, imaging was only started 30 min after washing or microinjection, respectively.

The BG-2-OH-nile red was synthesized by Shannon Black (EMBL Heidelberg), with the O^6-benzylguanine-Cl precursor kindly provided by Maik Kindermann (EPFL, Lausanne, Switzerland).

All other BG-dyes were kindly provided by Kai Johnsson (EPFL, Lausanne, Switzerland).

3.2.1.8 FlAsH labeling

HEK-293 cells were transiently transfected with DNA coding for one of the listed CFP/ FlAsH PKC probes (see 3.2.2.5 b). The cells were labeled with FlAsH 24-48 h after transfection, according to the following procedure[237]. FlAsH was synthesized by Andreas Schleifenbaum (EMBL, Heidelberg).

FlAsH was first incubated with 12.5 µM EDT, giving FlAsH-EDT_2. FlAsH-EDT_2 was then used at a final concentration of 1 µM in a (microscope) dish and cells were incubated for 1 h at 37°C in Hank's Balanced Salt Solution (HBSS: 10 mM HEPES, 140 mM NaCl, 5.4 mM KCl, 1 mM $MgCl_2$, 2 mM $CaCl_2$ and 1 g/L Glucose at pH 7.3). After incubation, unbound and non-specifically bound FlAsH was removed by a 10 min washing step with 200 µM EDT in HBSS.

Labeled cells were kept at 37°C in medium until imaging.
FlAsH binding to the tetracysteine motif was destroyed by adding 5 mM British-Anti-Lewisite, (BAL, 2,3-dimercaptopropanol). BAL competes for FlAsH binding and removes FlAsH from the tetracysteine target sequence, rendering it non-fluorescent. Addition of BAL is necessary for calculation of FRET efficiency. The FRET efficiency is calculated by dividing the difference in ECFP (mCFP) fluorescence at its maximum (after BAL addition) and its minimum (start value ECFP) with the maximum value: $FRET_{eff} = \frac{ECFP_{\max} - ECFP_{start}}{ECFP_{\max}}$.

3.2.1.9 Live cell imaging with wide field microscopy

a) Wide field microscopy for PKC probes using GFP^2 and EYFP

Wide field microscopy was performed on a Zeiss Axiovert microscope with automatic stage and fast emission and excitation filter wheels. Images were recorded with a CCD camera using Metamorph software. Cell medium was replaced by HEPES buffer one hour before the experiments and. Cells were kept starving at 37°C and 5% CO_2. The experiments were performed at 37°C in a heating chamber.
Compounds for addition were prepared as 1000x stock solutions in DMSO or water according to the protocol of the supplier. The compounds were pre-dissolved in 100 µl buffer before addition to the experiment.
GFP^2 in all KCP-1 and KCP-2 samples was excited through a DAPI filter (405/20 nm). Excitation and emission light were separated through a 425 dclp beam splitter. GFP^2 fluorescence was detected through a 500/20 nm filter; EYFP fluorescence through a 535/30 nm filter. As expression levels and fluorescence intensities were usually high, a 90% neutral grey filter was used to dim the excitation light. Camera sensitivity was increased by 4X4 binning. Exposure times were adjusted for each experiment, but were usually not higher than 200 ms. Five to six different stage positions were usually recorded in one experiment using a 63x oil objective.

b) Wide field microscopy for PKC probes using ECFP and FlAsH

Fluorescence imaging of FlAsH labeled probes was performed on a Zeiss Axiovert 135 inverted microscope with a 63x oil immersion objective. Cells labeled as described in 3.2.1.8, were mounted in an appropriate holder and placed on the microscope at room temperature. Samples were excited at 420/20 nm (dichroic 450 nm) with light from a polychrome IV (Till Photonics). Pictures were taken every 1.5 s with different illumination times (usually less than 50 ms). Fluorescence was measured in an area inside the cell to minimize artifacts caused by background. The emission ratio, FlAsH to ECFP, was measured with emission filters 475/40 nm (ECFP) and 535/25 nm (FlAsH), beam splitter dclp 505 nm. The emission ratio was corrected for bleed-through of ECFP into the FlAsH channel to give a corrected emission ratio (bleed-through of FlAsH into the ECFP channel is negligible). FlAsH emission at 490 nm was determined in order to subtract the direct excitation of FlAsH.

3.2.1.10 Live cell imaging with confocal microscopy

Confocal imaging was performed on a Leica SP2 AOBS system.
Cell medium was replaced by HEPES buffer one hour before the experiments. Cells were kept at 37°C and 5% CO_2. The experiments were performed at room temperature. Cell dishes were taken out of the incubator 10 min prior to the experiments, to equilibrate to room temperature.
Compounds for addition were prepared as 1000x stock solutions in DMSO or water according to the protocol of the supplier. The compounds were pre-dissolved in 50 µl buffer before addition to the experiment.
GFP^2 in all KCP-1 and KCP-2 samples was excited with a 405 nm laser. Emission for GFP^2 was measured between 490 to 510 nm; for EYFP between 520 to 540 nm. EYFP was directly excited using a 514 nm laser.
The FRET pair mOrange/ mCherry was imaged using a 532 nm laser for excitation. Emission of mOrange was measured from 560 to 600 nm; mCherry from 610 to 650 nm.

Laser and PMT power were adjusted for each FRET experiment, but PMT values were set the same for both channels.
Pictures were taken every 15 s with two line averages for each image.

3.2.1.11 Data analysis

If not otherwise mentioned, live cell FRET experiments were analyzed as follows: the fluorescence intensities of both channels (donor and acceptor) were directly taken from the unprocessed original microscope data set. Regions of interest (ROI) were defined in the cytosol of the cell and in the background not overgrown with cells. Mean fluorescence intensities were calculated using ImageJ[268]. The background was subtracted for each time point and the ratio of acceptor/ donor mean intensities in the chosen ROI were calculated. The result was normalized to the value one, using the scientific analysis program Origin[269].
Cells chosen for analysis usually expressed the probes to a medium level. The nucleus was excluded from data analysis, as it does not show a change in emission ratio, thereby lowering the cytosolic signal. The nucleus data were usually taken as a reference, but not shown in the figures for clarity.

3.2.1.12 Acceptor photo-bleaching experiments

FRET efficiencies were determined by acceptor photo-bleaching experiments (2.2.1).
Experiments were performed on a Leica AOBS SP2 equipped with strong lasers for photo-bleaching and making use of the FRET acceptor photo-bleaching module provided by the Leica software.
First, pictures of the two fluorophores were taken at their excitation maximum. Subsequently, the acceptor was bleached at its excitation maximum. Finally, images of both fluorophores were taken again at their excitation maximum. A picture always consisted of an average of four scans. See Table 3.1 for laser settings.

	GFP^2	EYFP	mOrange	mCherry
Donor excitation	405 nm		532 nm	
Acceptor excitation		514 nm		594 nm
Donor emission	490-510 nm		550-585 nm	
Acceptor emission		525-545 nm		610-645
Bleach λ		514 nm		594 nm

Table 3.1 Laser settings for acceptor photo bleaching experiments

Data were analyzed using an ImageJ plugin originally written by Alen Piljić (EMBL, Heidelberg) and modified to suit these experiments.
The plugin takes pre- and post-bleaching pictures of the donor, first subtracts the background and then runs a median filter with two iterations over it, to remove noise. The images are then thresholded and the pre-bleach picture is subtracted from the post-bleach picture. A median filter (single iteration) was applied to the resultant picture. Finally, the percent FRET efficiency was calculated by dividing the subtracted picture by the post-bleach picture.

3.2.1.13 Cell lysates and trypsination experiments

Trypsination experiments are another method to study FRET efficiencies. Trypsin proteolytically cleaves the probe, leaving the fluorophores intact, so that they diffuse and FRET cannot be observed any more.
HeLa cells were transfected in round dishes (Ø 40 mm) with the constructs of interest. Cells were harvested 20-48 h after transfection, washed with PBS and detached with Trypsin. Trypsination was stopped by addition of 5 ml medium or Optimem. Cells were spun down in a centrifuge at 4°C and 300 g for 10 min. Cells were washed with PBS after the first centrifuge run and spun again. PBS was discarded and the cell pellet resuspended in RIPA buffer (100 mM NaCl, 50 mM HEPES, 1% NP-40, pH 7.4). The mixture was left rocking in the cold room for 15 min and then centrifuged for 15 min at 4°C and 14000 rpm (Eppendorf table centrifuge). Finally, the supernatant was transferred to a clean tube. The lysates were kept in the dark at 4°C.
Emission ratios of the samples were measured on the same day in 10 µl cuvettes in the fluorimeter. EYFP/GFP^2 FRET pairs were excited with 405 nm

and the emission measured between 485 and 545 nm (2 nm step size, integration time 1 s). The FRET pair mOrange/mCherry was excited at 532 nm and the emission was measured from 550 to 650 nm (2 nm step size, integration time 1 s). In order to destroy the FRET between both fluorophores in a FRET pair, trypsin (4 µl of PBS with 0.5% trypsin) was added to the cuvette and the emission wasrecorded 5 min after addition. Finally, the percent FRET efficiency was calculated by dividing the difference in average fluorescence intensity between 490-510 nm (550-585 nm for mOrange) before and after trypsin by the average fluorescence intensity between 490-510 nm after trypsin cleavage(550-585 nm for mOrange).

3.2.2 Cloning of Constructs

3.2.2.1 Introduction

Plasmids of the so called dummy construct, KCP-1[1] and KCP-2[2], were obtained from Andreas Schleifenbaum (EMBL, Heidelberg).

The dummy construct consists of a vector which encodes an N-terminal EYFP and a C-terminal GFP[2], linked by a dummy sequence. The dummy sequence (717 bp) does not code for anything specific, it only serves as placeholder. Cutting with BbsI releases this dummy sequence and opens NcoI and BamHI sites into which any sequence can be inserted. The sequence will then be placed between the two fluorophores (see Fig. 3.2 A).

The original KCP-1 probe has an insert of 239 amino acids instead of the dummy sequence. This insert is derived from pleckstrin and contains three phosphorylation sites that are recognized by PKC. The phosphorylation sites are flanked by a PH domain on the N-terminal side and a DEP domain on the C-terminal side (see Fig. 3.2 B).

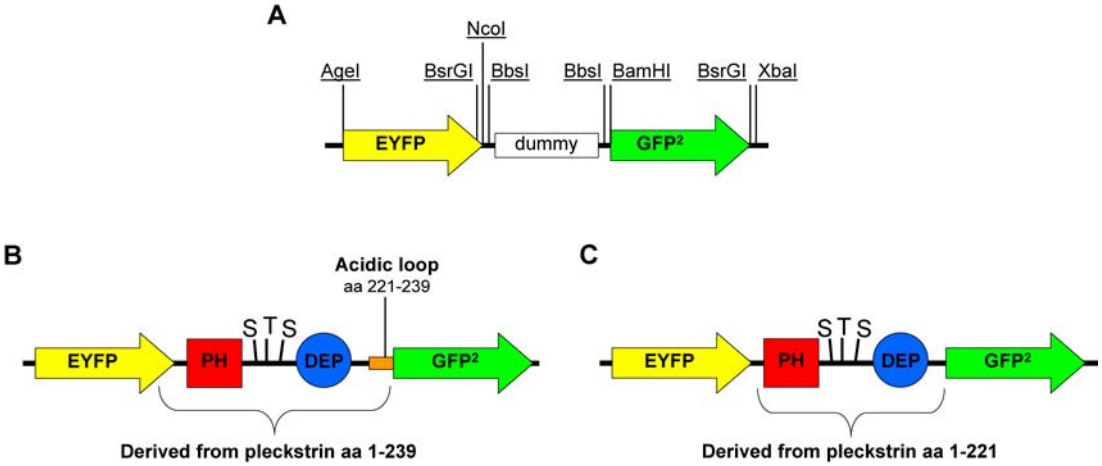

Fig. 3.2 Schematic representation of vectors and restriction sites used for cloning of constructs

A Representation of the dummy construct, which contains both fluorophores, but no pleckstrin insert.

B Representation of KCP-1, which contains both fluorophores and the long pleckstrin insert with the acidic loop (amino acids 1-239).

C Representation of KCP-2, which contains both fluorophores and the short pleckstrin insert lacking the acidic loop (amino acids 1-221).

For a detailed description of these constructs, see 3.2.2.1.

KCP-2 is a truncated version of KCP-1 (see Fig. 3.2 C), missing the last 18 C-terminal amino acids of pleckstrin (between the DEP domain and the second fluorophore). Within these 18 amino acids are five acidic ones. We therefore named this stretch the "acidic loop".
The respective pleckstrin sequences, yielding the KCP-1 and KCP-2 constructs, were obtained by digestion of pET9d-Pleckstrin (1-221) or pET9d-Pleckstrin (1-239) with BamHI and NcoI, and subsequent ligation into the digested dummy construct.
Changes to the fluorophores of the construct were either performed on the dummy construct, with the respective sequences for KCP-1 or KCP-2 inserted afterwards, or on the probes themselves.
KCP-1 and KCP-2 always refer to the original clones from Andreas Schleifenbaum. They are the references to which all other clones are compared. If KCP-1 or KCP-2 is part of a construct's name (as suffix or prefix), this shows from where the clone has been derived. It also indicates the existence (KCP-1) or absence (KCP-2) of the acidic loop. As this thesis studies the effect of fluorophores on probe performance, the fluorophores are changed quite often, while the pleckstrin derived sequence remains the same as in KCP-1 and KCP-2, respectively.

3.2.2.2 Variations in the N-terminal linker region

a) Additional amino acids in the N-terminal linker region

Additional amino acids were introduced into KCP-1 and KCP-2 using oligonucleotide ligation. For this, a unique BspEI restriction site in the N-terminal linker region was used (see Fig. 3.3). DNA oligonucleotides coding for 3, 6, 10 or 12 amino acids and sticky ends complementing the BspEI site were designed. These DNA oligonucleotides were cloned into the vector plasmid according to the protocol for oligonucleotide ligation (3.2.1.3).

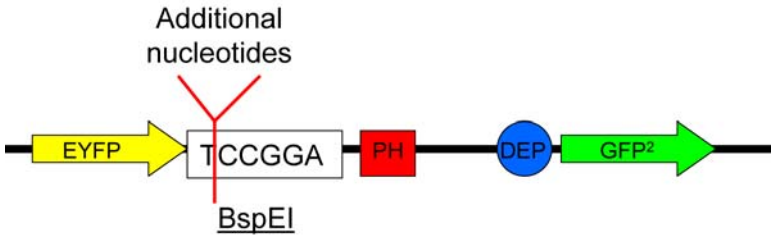

Fig. 3.3 Introduction of additional amino acids into KCP-1 and KCP-2

Three, six, ten or twelve additional amino acids were introduced into a unique BspEI restriction site in KCP-1 and KCP-2.

For a detailed description of cloning, see 3.2.2.2 a.

Table 8.1 in the appendix shows an overview of primers and target vectors used for constructs with additional amino acids in the N-terminal linker of KCP-1 and KCP-2.

b) Deletion of amino acids in the N-terminal linker region

Five non-structural C-terminal amino acids of YFP were deleted. A BsrGI site, which usually is adjacent to the C-terminus of EYFP, was deleted at the same time (see Fig. 3.4). The deletions were introduced by PCR on the N-terminal EYFP. The PCR product was cloned into KCP-1 or KCP-2 using AgeI and BspEI.

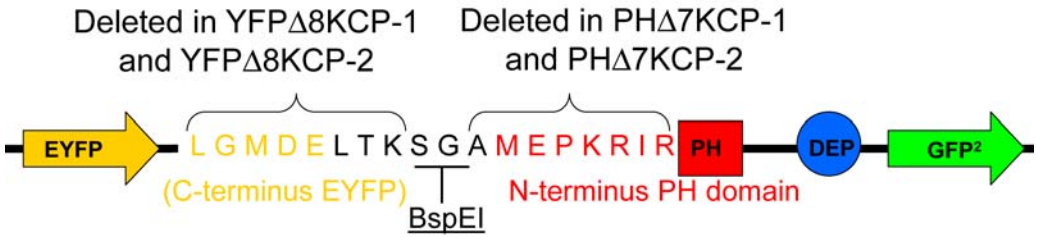

Fig. 3.4 Deletions of amino acids in the N-terminal linker region

Amino acids were deleted at the C-terminus of EYFP and at the N-terminus of the PH domain in the original KCP-1 and KCP-2 constructs.

For a detailed description of cloning, see 3.2.2.2 b.

In a second set of experiments, the first seven amino acids of the PH domain were deleted in order to examine the effect of a reduction in linker length (see Fig. 3.4). These deletions were introduced by PCR on the pleckstrin insert of

KCP-1 or KCP-2. The PCR product was cloned into KCP-1 or KCP-2 using BspEI and BamHI.

Table 8.2 in the appendix shows an overview of primers and target vectors used for constructs with deletions of amino acids in the N-terminal linker region of KCP-1 and KCP-2.

c) Changes in the charge distribution of the PH domain

The PH domain contains three basic residues within the first seven amino acids at the N-terminus: Lys4, Arg5 and Arg7. These amino acids were mutated to glutamic acid, to replace the positive charges with negative charges in the NegPH constructs. In the NeutPH constructs, amino acids 4 and 5 were mutated to leucine and amino acid 7 to serine (see Fig. 3.5). These mutations were introduced by PCR on the pleckstrin insert of KCP-1 or KCP-2. The PCR product was cloned into KCP-1 or KCP-2 using BspEI and BamHI.

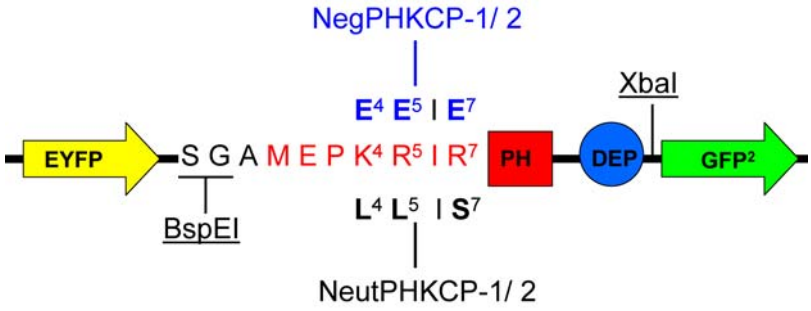

Fig. 3.5 Changes in the charge distribution of the PH domain

Three basic amino acids in the N-terminus of the PH domain were replaced either by acidic or neutral amino acids.

For a detailed description, see 3.2.2.2 c.

So called complementary clones were made, in which we mutated the acidic residues in the acidic loop to basic ones and the basic residues at the beginning of the PH domain to acidic ones. Justin Brumbaugh (EMBL, Heidelberg) made constructs, in which amino acids E^{227} and E^{228} were replaced by arginines and other constructs in which $DDD^{232-234}$ were replaced by arginines. As described in the previous paragraph, the pleckstrin insert for

KCP-1, with either neutral or negative charges in the pH domain, was inserted into these clones, yielding the following constructs: NeutPHKCP-1_RR$^{227/228}$, NeutPHKCP-1_RRR$^{232-234}$, NegPHKCP-1_RR$^{227/228}$ and NegPHKCP-1_RRR$^{232-234}$.

Table 8.3 in the appendix shows an overview of primers and target vectors used for constructs containing changes in the charge distribution of amino acids in the N-terminal part of the PH domain of KCP-1 and KCP-2.

3.2.2.3 Effect of fluorophore dimerization on KCP-1 and KCP-2

The mutation A206K is known to render the normally dimeric fluorescent proteins, derived from *Aequorea Victoria,* as monomeric proteins[270,271] (see structures in the Protein Data Bank under accession numbers 1GFL and 1YFP). The mutation A206K was introduced into the two fluorophores EYFP and GFP^2 of KCP-1 and KCP-2, to study the effect of protein oligomerization on the probe. The mutation was introduced individually into EYFP or GFP^2 with two sets of primers as described in 3.2.1.2 b. GFP^2 was first replaced with mGFP^2 (GFP^2 A206K) in the dummy construct using BamHI and XbaI. The reverse primer for GFP^2 (R1) also introduced a single A→C mutation, deleting the BsrGI site at the end of GFP^2. In this way, BsrGI could be used as a restriction site in the following step. EYFP was replaced with mYFP (EYFP A206K) in the new EYFP-dummy-mGFP^2 construct using NheI and BsrGI. The dummy site was subsequently replaced with either the KCP-1 or KCP-2 sequence.

Constructs containing only one monomeric fluorophore, mGFP^2 or mYFP, were made by introducing the KCP-1 or KCP-2 sequence into a EYFP-dummy-mGFP^2 or a mYFP-dummy-GFP^2 construct.

The mutation L221K in fluorescent proteins derived from *Aequorea victoria* also decreases their ability to dimerize, but to a lesser degree than A206K. While the K_d for A206K variants is about 74 mM (although difficult to determine due to its strong monomeric behavior) the L221K variants still have a K_d of 9.7 mM[270]. This mutation was introduced in the same way as A206K (see 3.2.1.2 b). Different primers were, however, used for S2 and R2.

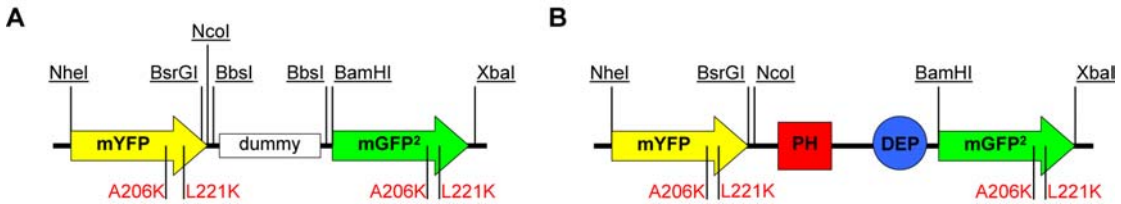

Fig. 3.6 Cloning of monomeric fluorophores in KCP-1 and KCP-2 probes

Mutations (A206K and L221K), destroying the dimeric nature of the fluorescent proteins, were introduced into EYFP and GFP^2.

A Representation of the dummy construct with monomeric fluorescent proteins and the restriction sites used for cloning.

B Representation of the probe with monomeric fluorescent proteins and the restriction sites used for cloning.

For a detailed description of cloning procedures, see 3.2.2.3.

Table 8.4 in the appendix shows an overview of primers and target vectors used for constructs with monomeric fluorophores in KCP-1 and KCP-2.

3.2.2.4 Intra- versus intermolecular FRET in PKC probes

As fluorophores tend to dimerize, they might show FRET not only within the same molecule but also between different molecules. If that is the case, one should be able to observe FRET by co-transfecting two constructs which are only able to FRET between molecules and not within the same molecule.
We designed two sets of experiments to address this question: firstly, either one of the fluorophores was rendered non-fluorescent by introducing a Y66S point mutation into the fluorophore region. The mutation was introduced by site directed mutagenesis (see 3.2.1.2 a) on either KCP-1 or KCP-2, to give Y66SYFP-KCP-1/2-GFP^2 (EYFP non-fluorescent and GFP^2 fluorescent) and EYFP-KCP-1/2-Y66SGFP^2 (EYFP fluorescent and GFP^2 non-fluorescent). For a schematic illustration of constructs, please see Fig. 3.7 A and B.

For the second experiment, constructs were made, which encode only one kind of fluorophore: EYFP-KCP1/2-EYFP and GFP^2-KCP1/2-GFP^2.
For EYFP-KCP1/2-EYFP constructs, PCR was performed on EYFP introducing an N-terminal BamHI site and a C-terminal XbaI site. The PCR product was sub-cloned into the dummy construct to replace GFP^2, resulting

in an EYFP-dummy-EYFP construct. The dummy site was subsequently replaced with either the KCP-1 or KCP-2 sequence.

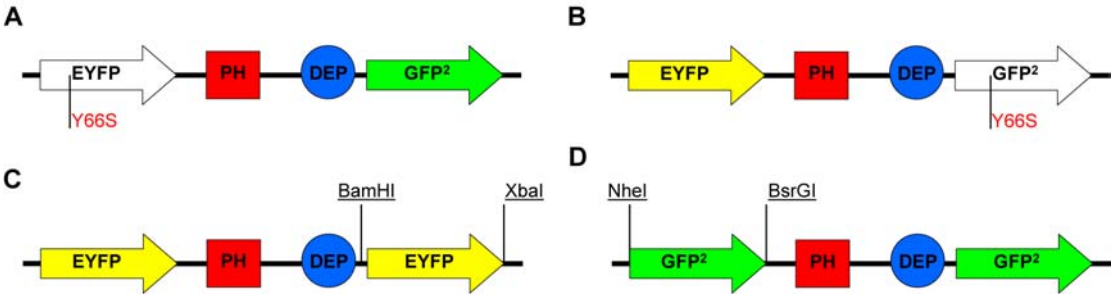

Fig. 3.7 Cloning of probes to discriminate between intra- and intermolecular FRET

To discriminate between intra- and intermolecular FRET, two sets of experiments were designed, with FRET only possible between two molecules, not within one molecule. Probes A and B were used in one experimental set up, probes C and D in another.

A: Probe encoding a non-fluorescent EYFP and a fluorescent GFP^2.

B: Probe encoding a non-fluorescent GFP^2 and a fluorescent EYFP.

C: Probe encoding two yellow fluorescent proteins (EYFP).

D: Probe encoding two green fluorescent proteins (GFP^2).

For GFP^2-KCP1/2-GFP^2 constructs, PCR was performed on GFP^2 to introduce an N-terminal NheI site and a C-terminal BsrGI site. The PCR product was sub-cloned into the dummy construct used in 3.2.2.3 (BsrGI site removed from the C-terminus of GFP^2) to replace with EYFP, resulting in a GFP^2-dummy-GFP^2 construct. The dummy site was subsequently replaced with either the KCP-1 or KCP-2 sequence. For a schematic illustration of constructs please see Fig. 3.7 C and D.

Table 8.5 in the appendix shows an overview of primers and target vectors used for constructs distinguishing between intra- and intermolecular FRET.

3.2.2.5 Changing the FRET pair in PKC probes

a) PKC probes using AGT and chemically synthesized fluorophores

Plasmids of constructs containing ECFP-dummy-EYFP and Citrine-dummy-Citrine were obtained from Andreas Schleifenbaum. PCR was performed on the original AGT clones from Antje Keppler and these were introduced into the ECFP construct using BamHI and XbaI restriction sites. The resulting ECFP-

dummy-AGT was opened with BbsI and the respective KCP-1 or KCP-2 sequence was introduced (see Fig. 3.8 A).

A shorter version of AGT, AGT177 was introduced into EYFP-dummy-GFP^2 by PCR on AGT177. The restriction sites used were NheI and BspEI. As AGT contains an internal BspEI site, a silent G→C mutation was introduced in the cloning process. The resulting AGT177-dummy-GFP^2 was opened with BbsI and the respective KCP-1 or KCP-2 sequence was introduced (see Fig. 3.8 B).

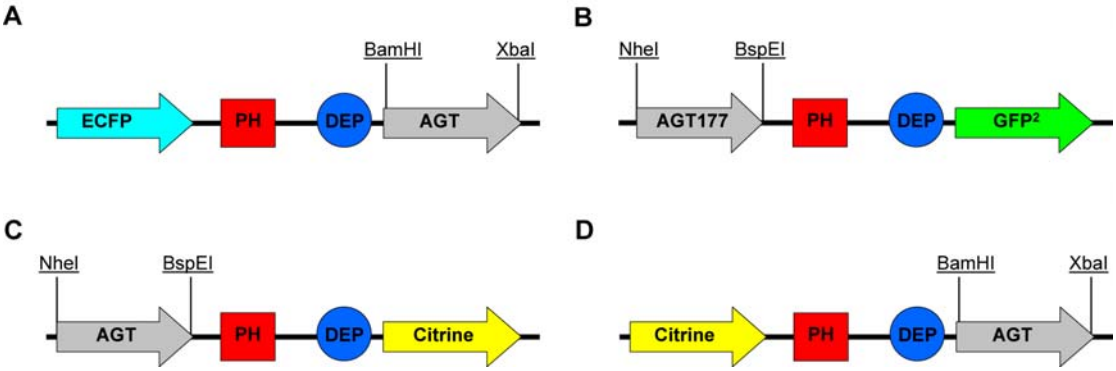

Fig. 3.8 Construction of AGT fusion proteins to be labeled with chemically synthesized fluorophores

Several different constructs were made, combining different genetically encoded fluorescent proteins with AGT.

A AGT was cloned into a construct coding for ECFP as N-terminal fluorophore in KCP-1 and KCP-2 probes.

B A shortened version of AGT, AGT177, was cloned into a construct coding for GFP^2 as C-terminal fluorophore in KCP-1 and KCP-2 probes.

C AGT was cloned into a construct coding for Citrine as C-terminal fluorophore in KCP-1 and KCP-2 probes.

D AGT was cloned into a construct coding for Citrine as N-terminal fluorophore in KCP-1 and KCP-2 probes.

AGT was cloned into the Cit-dummy-Cit construct as replacement for the N-terminal fluorophore using NheI and BspEI. The procedure was similar to the AGT177-dummy-GFP^2 clone, however in this case the template was the full length AGT. The resulting AGT-dummy-Cit was opened with BbsI and the respective KCP-1 or KCP-2 sequence introduced (see Fig. 3.8 C). AGT was also cloned into the double Cit construct as a C-terminal fluorophore using BamHI and XbaI. The resulting Cit-dummy-AGT was opened with BbsI and the respective KCP-1 or KCP-2 sequence was introduced (see Fig. 3.8 D).

Table 8.6 in the appendix shows an overview of primers and target vectors used for constructs with AGT and genetically encoded fluorophore in KCP-1 and KCP-2.

b) PKC probes using FlAsH and ECFP

The tetracysteine motif was introduced into ECFP-KCP-1-AGT and ECFP-KCP-2-AGT (see 2.2.2.3 a) using BamHI and AvaI restriction sites. DNA oligos containing the tetracysteine motif FLNCCPGCCMEP and a stop codon were purchased and ligated into the target vector according to protocol 3.2.1.3 to give ECFP-KCP-1-FlAsH and ECFP-KCP-2-FlAsH (see Fig. 3.9 A).
In addition, constructs with a monomeric ECFP and FlAsH were made. The A206K mutation was introduced into ECFP using standard protocol (see 3.2.1.2) and cloned into ECFP-KCP-1-FlAsH or ECFP-KCP-2-FlAsH using NheI and BsrGI (see Fig. 3.9 B) to give mCFP-KCP-1-FlAsH and mCFP-KCP-2-FlAsH.

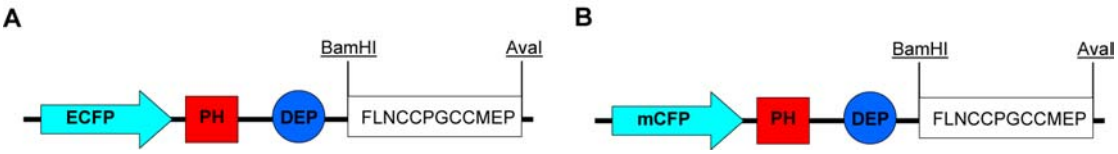

Fig. 3.9 Constructs containing the tetracysteine motif

The C-terminal fluorophore in KCP-1 and KCP-2 was replaced with a 12-amino acid tetracysteine motif for FlAsH labeling.

A Constructs containing ECFP and the tetracysteine motif for FlAsH labeling.

B Constructs containing mCFP and the tetracysteine motif for FlAsH labeling.

Table 8.7 in the appendix shows an overview of primers and template vectors used for constructs encoding the FlAsH labelling sequence in KCP-1 and KCP-2 probes.

4 Results

4.1 Introduction

This thesis has three aims: Firstly, to study different factors that influence protein kinase C probe performance. Secondly, to increase the range of fluorophores used for FRET in order to make the probe more versatile for different applications such as multiparameter imaging. Third, to thoroughly understand the mechanism of action of our probes, we would like to create a probe that is significantly smaller than KCP-2 and can be studied with NMR.

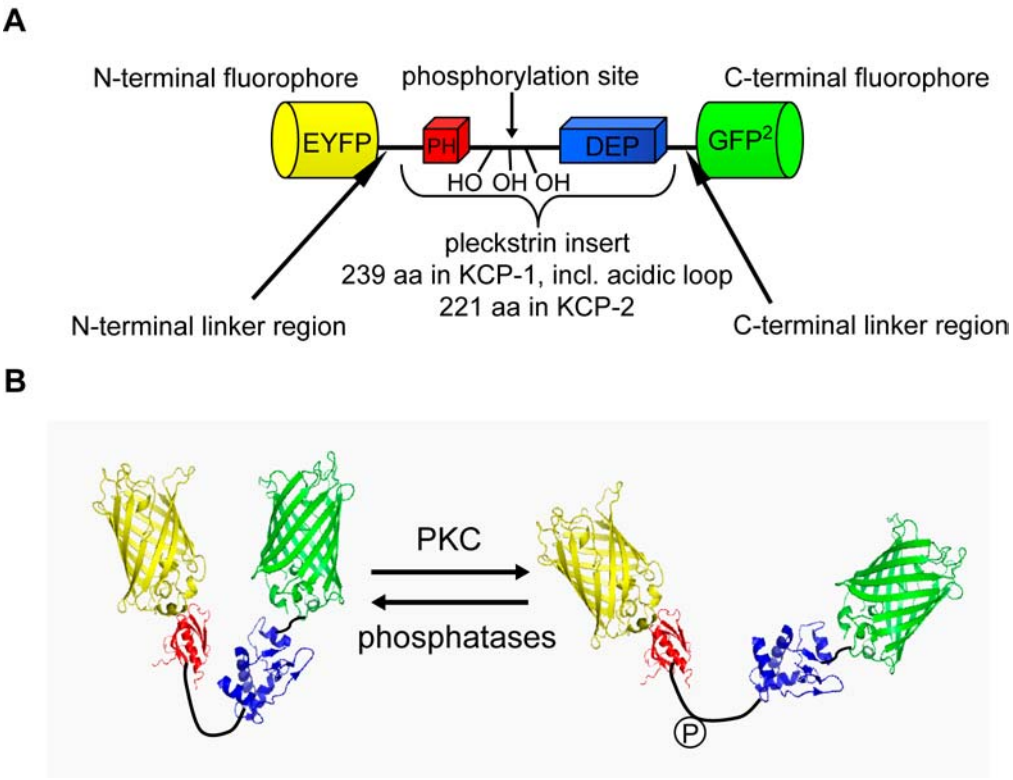

Fig. 4.1 Schematic representation of previously published PKC probes

A Illustration of the set up of our previously published protein kinase C probes. The scheme denotes the different parts of the probe as used in this thesis. The probe consists of a pleckstrin insert sandwiched by two fluorophores (EYFP and GFP^2). KCP-1 and KCP-2 differ only in the length of the pleckstrin insert, which is 239 aa long in KCP-1 and 221 aa long in KCP-2.

B Hypothetic model of conformational change in the KCP-2 probe as suggested by NMR experiments performed with the pleckstrin insert alone: phosphorylation lead to stretching of the probe, which, in the model, would lower the FRET efficiency between both fluorophores. Please note, that the depicted model is *not* actual NMR data, but a model put together from structural data of the individual components.

Two previously published FRET-based probes for PKC activity, KCP-1[1] and KCP-2[2] designed in our lab, are used as references for all newly described probes.

Both are stoichiometric probes containing an N-terminal EYFP and a C-terminal GFP[2]. Between these two fluorophores is a sequence derived from pleckstrin, the major substrate of PKC in platelets[272]. It contains a phosphorylation loop of 14 amino acids recognized by PKC, which is flanked by a PH domain on the N-terminal side and a DEP domain on the C-terminal side. In the original KCP-1, this sequence is 239 amino acids long. KCP-2 is a truncated version of KCP-1, missing the last 18 C-terminal amino acids of pleckstrin (between the DEP domain and the second fluorophore). These 18 amino acids in KCP-1 contain five acidic residues and are therefore named the "acidic loop" (see Fig. 4.1 for a schematic representation of the probes).

Amino acids Ser 113, Thr 114 and Ser 117 of the pleckstrin insert in KCP-1 and KCP-2 are phosphorylated by PKC. This phosphorylation induces a conformational change that leads to increased FRET in KCP-1 and decreased FRET in KCP-2. The emission ratio goes back to starting level if phosphorylation is inhibited, reflecting the activity of phosphatases removing the phosphates from the probe (Fig. 4.2 B).

NMR experiments with the pleckstrin insert of KCP-1 (PH-P-DEP, but lacking both fluorophores) showed a closed conformation which stretched upon phosphorylation (Fig. 4.1 B). This fits well with the result seen in KCP-2: a stretched conformation might lead to an increased distance between the fluorophores and therefore reduces FRET efficiency. KCP-1 seems to undergo a different transformation, possibly due to additional interactions. This question will be addressed in detail in this thesis.

EYFP and GFP[2] are an efficient FRET pair[206] as donor emission and acceptor excitation overlap broadly and the direct excitation of EYFP is below detection levels at the donor excitation maximum (see Fig. 4.2 A).

KCP-1 shows a positive change in EYFP/GFP[2] emission ratio upon PKC stimulation and a drop in emission ratio after inhibition (see Fig. 4.2 B). KCP-2 shows the opposite signal, the EYFP/GFP[2] emission ratio drops upon activation of PKC and increases again after inhibition (see Fig. 4.2 B).

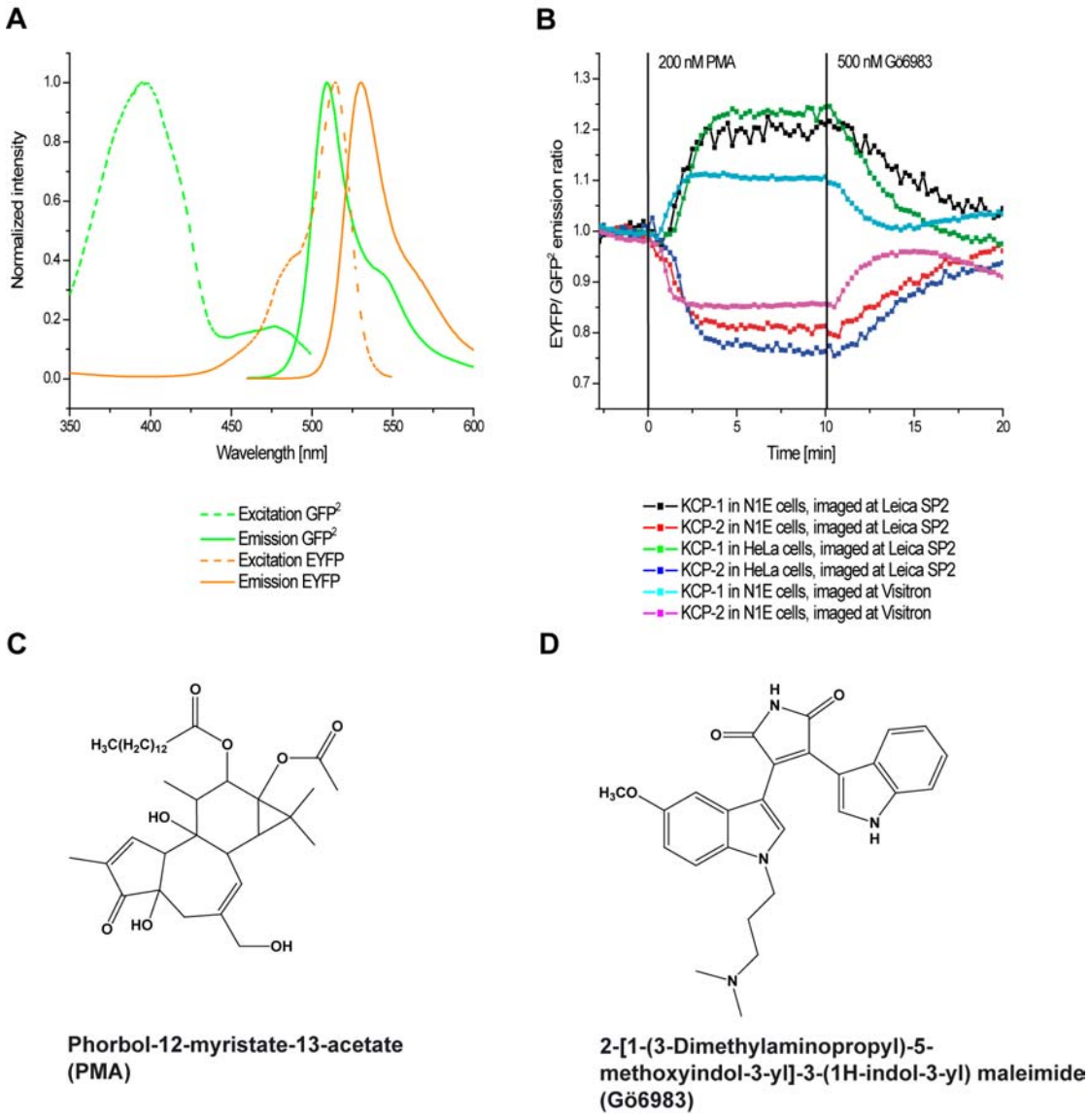

Fig. 4.2 Basic set up of experiments performed to study probe performance

A Normalized spectra of the excitation (dashed line) and the emission (solid line) of GFP^2 (green) and EYFP (orange).

B *In-vivo* experiments with KCP-1 (black, green and cyan) and KCP-2 (red, blue and pink) performed in HeLa (green and blue) or N1E (black, red, cyan and pink) cell lines on two microscopes, Leica SP2 (black, red, green and blue) and Visitron (cyan and pink). The EYFP/GFP^2 emission ratio is plotted over time. PKC activity was first stimulated with PMA then inhibited with Gö6983 after 10 min. Phosphorylation by PKC induced an increase in emission ratio in KCP-1, while it induced a decrease in KCP-2. The inhibition of PKC caused a reversal of the signal back to basal levels in both probes.

C Chemical structure of the PKC activator PMA (phorbol-12-myristate-13-acetate).

D Chemical structure of the PKC inhibitor Gö6983 (2-[1-(3-Dimethylaminopropyl)-5-methoxyindol-3-yl]-3-(1H-indol-3-yl) maleimide).

In order to make probe performance comparable, all experiments have the same basic set up - the PKC probe to be studied is transfected into

mammalian cell lines and imaged on a fluorescence microscope after protein expression. Protein kinase C activity is first stimulated by addition of PMA and, after 10 min, inhibited by Gö6983. The data is analyzed by determination of the ratio of acceptor to donor emission.
PKC stimulation is achieved by addition of PMA (phorbol-12-myistate-13-acetate, see Fig. 4.2 C). This phorbol ester activates PKC specifically and has a long-lasting effect[68,273]. PKC can also be activated with more physiological stimuli, such as histamine[274,275] or bradykinin[276,277]. Addition of these substances leads to phosphorylation of the probe. Their effect is usually short lived and sometimes not as strong as that of phorbol esters. Since the properties of KCP-1 and KCP-2 as a protein kinase C probe have been established and published, there was no need to show their ability to respond to physiological activators. Instead, we wanted to see a reliable, large and sustained response every time, in order to compare probe performance. This is best achieved by stimulating with PMA.
Inhibition of PKC activity is achieved by addition of Gö6983 (see Fig. 4.2 D), which is a potent and cell permeable inhibitor for most PKCs[278].

Two microscopes have mainly been used for this study: a confocal laser scanning microscope (Leica SP2) and a multi-stage wide field system (Visitron). Both show the same kind of signal in both probes, but the amplitude of the signal is different. While the signal in KCP-1 probes increased to 21.5% on the Leica SP2, it only increased to 10.6% on the Visitron system (see Fig. 4.2 B, black, red, green and blue lines). Likewise for KCP-2, the signal on the Leica SP2 decreased by 19-23%, while it only decreased by 15% on the Visitron (see Fig. 4.2 B, cyan and pink lines). This is due to different filter properties in the microscope set up. The SP2 has an AOBS system, which allows the user to define the range of measured emission in nanometer steps thereby allowing a better separation of the two emissions from each other. The Visitron system has preset filters that are more broadly defined and therefore have a much higher bleed through of one detection channel into the other. To compare different constructs to each other, they have to be performed on the same microscope. All results presented here contain the traces of the original probes, KCP-1 and KCP-2, imaged under the same

conditions for comparison. Most experiments have been performed on the Visitron system as it allows fast imaging of several samples in parallel. The Leica SP2 was used to image pairs of fluorophores other than EYFP/GFP[2], or when expression levels had to be determined, as this microscope allows for accurate setting of emissions. An additional advantage of imaging on the Visitron system is that the signal to noise ratio is better than on the Leica SP2. This is especially important when measuring probes that display only small changes in emission ratio.
Traces of changes in emission ratio for each probe are shown as an average of at least ten cells measured in at least three independent experiments.

The original KCP-1 and KCP-2 probes perform well in different cell lines. Fig. 4.2 B shows that the cell line chosen did not influence the signal amplitude or shape. KCP-1 showed an increase in emission ratio of approximately 20% upon PKC activation on the Leica SP2 microscope, independent of the cell type (N1E= black line; HeLa= green line). The same is true for KCP-2, which showed a decrease in emission ratio of 20% upon PKC activation on the Leica SP2 microscope for both cell lines (N1E= red line; HeLa= blue line). N1E cells were preferred to HeLa cells as they have a round morphology and therefore small focus drifts during a longer time course only had a small effect.

4.2 Variations in the N-terminal linker region

4.2.1 Additional amino acids in the N-terminal linker region

As FRET efficiency strongly depends on the distance between the fluorophores, we first studied the effect of an increased linker length in the N-terminal linker region (Fig. 4.1 A). In the original KCP-1 and KCP-2 probes this linker has a length of six amino acids (Leu-Tyr-Lys-Ser-Gly-Ala). It contains three restrictions sites for cloning. One of these sites, BspEI, was used to introduce additional amino acids and elongate the linker region (see 3.2.2.2 A). If more than six amino acids were added, the sequence was designed to code for short α-helical stretches.

Clone	Inserted DNA sequence	Additional aa inserted between Ser and Gly
3SKCP	TCC GGT GCG GCC GGA	Ser-Gly-Ala-Ala-Gly
3RKCP	TCC GGC CGC ACC GGA	Ser-Gly-Arg-Thr-Gly
6SKCP	TCC GGC GCC AAC ATC GTG TCC GGA	Ser-Gly-Ala-Asn-Ile-Val-Ser-Gly
6RKCP	TCC GGA CAC GAT GTT GGC GCC GGA	Ser-Gly-His-Asp-Val-Gly-Ala-Gly
10SKCP	TCC GGC ATG TTC TCT ATC AAC CGC GTG TAC GCC GGA	Ser-Gly-Met-Phe-Ser-Ile-Asn-Arg-Val-Tyr-Ala-Gly
10RKCP	TCC GGC GTA CAC GCG GTT GAT AGA GAA CAT GCC GGA	Ser-Gly-Val-His-Ala-Val-Asp-Arg-Glu-His-Ala-Gly
6R6SKCP	TCC GGA CAC GAT GTT GGC GCC GGC GCC AAC ATC GTG TCC GGA	Ser-Gly-His-Asp-Val-Gly-Ala-Gly-Ala-Asn-Ile-Val-Ala-Gly

Table 4.1 DNA and amino acid sequences introduced into KCP-1 or KCP-2

Nucleotides inserted into the BspEI restriction site of KCP-1 or KCP-2 site are shown in red, the BspEI restriction site (TCCGGA) is shown in black. Additional amino acids in the protein are shown in blue, flanked by the original ones in black.

As only one restriction site was used, the oligonucleotides were able to anneal in two different orientations: the sense orientation, which yielded amino acids with the desired secondary structure (called "S" constructs, see Table 4.1); and the reverse orientation, introducing a different sequence of the same length with random structure (named "R" constructs, see Table 4.1). The constructs were named with numbers, according to the number of additional amino acids, and an "S" or "R" according to the orientation in which the oligonucleotide was introduced into the restriction site. KCP-1 or KCP-2

indicated into which probe the amino acids were inserted. For example, the construct 6SKCP-1 has six additional amino acids, introduced in sense orientation into the original KCP-1 construct.

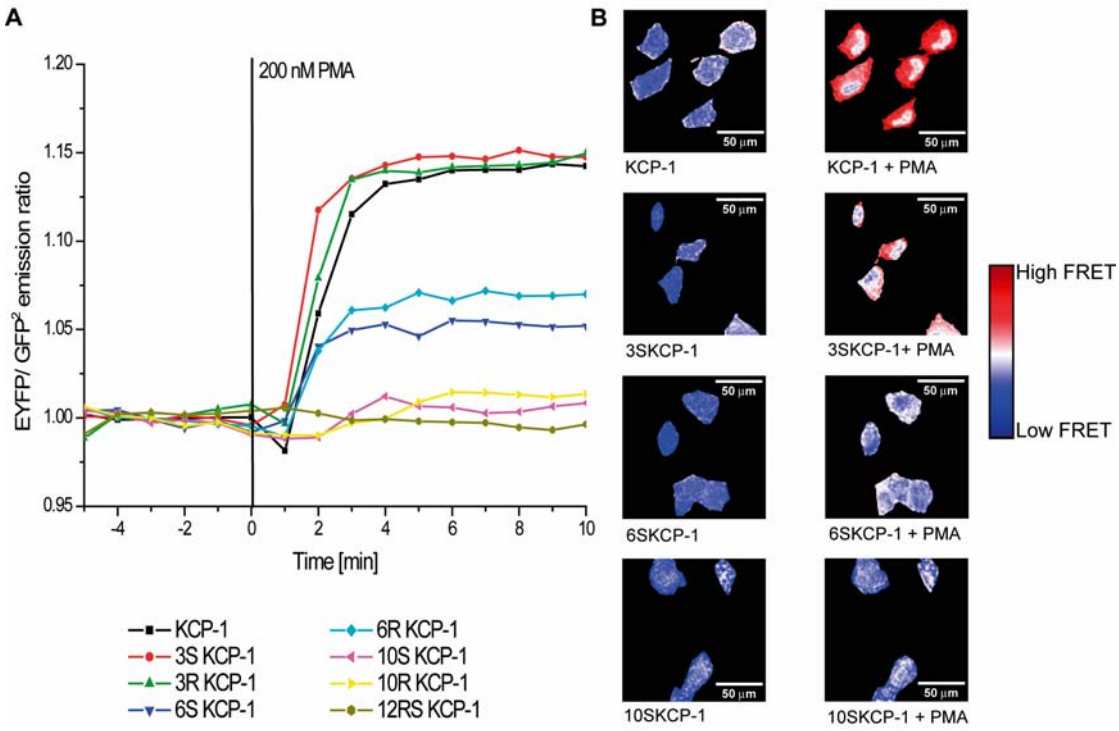

Fig. 4.3 Introduction of additional amino acids in the N-terminal linker region of KCP-1

Additional amino acids were introduced in the N-terminal linker region of KCP-1. Experiments were performed on the Visitron system on slides spotted with DNA and covered with HeLa cells.

A PKC activity was stimulated by addition of 200 nM PMA after 6 min and the EYFP/GFP^2 emission ratio measured over time. PKC activity was inhibited 10 min after activation by addition of 500 nM Gö6983, but data is not shown for clarity. The emission ratio of the original probe KCP-1 (black line) increased substantially upon PKC activation. With increasing length of the N-terminal linker, the amplitude of the signal became gradually smaller.

B Single cell examples from the experiments are color-coded according to FRET level. A change in emission ratio, i.e. FRET level, is seen as a change in color. Introduction of more than three amino acids led to reduced or abolished signal in KCP-1 probes.

The constructs were spotted on welled cover slips and imaged simultaneously on the Visitron system (3.2.1.6). One image per spot per minute was taken and a maximum of 27 spots (nine constructs in triplicate), imaged in parallel. The original KCP-1 or KCP-2 probes were spotted on every cover slip as a reference and a control.

A strong effect of linker length on probe performance could be observed in KCP-1 derived probes: the longer the linker, the weaker the change in

emission ratio upon PKC stimulation (see Fig. 4.3). The original KCP-1 probe showed an increase in EYFP/GFP^2 emission ratio of 14% (Fig. 4.3 A, black line) upon activation of PKC with PMA. If three amino acids were added in the N-terminal linker region, the same increase of 14% was detected (Fig. 4.3 A, red and green lines). If six amino acids were added, the increase in emission ratio was only 5.5-7% (Fig. 4.3 A, dark and light blue lines), half the increase shown by the original probe. If ten or twelve amino acids were added the signal was abolished (Fig. 4.3 A, yellow, pink and khaki lines). This effect is independent of the orientation in which the oligonucleotides were inserted.

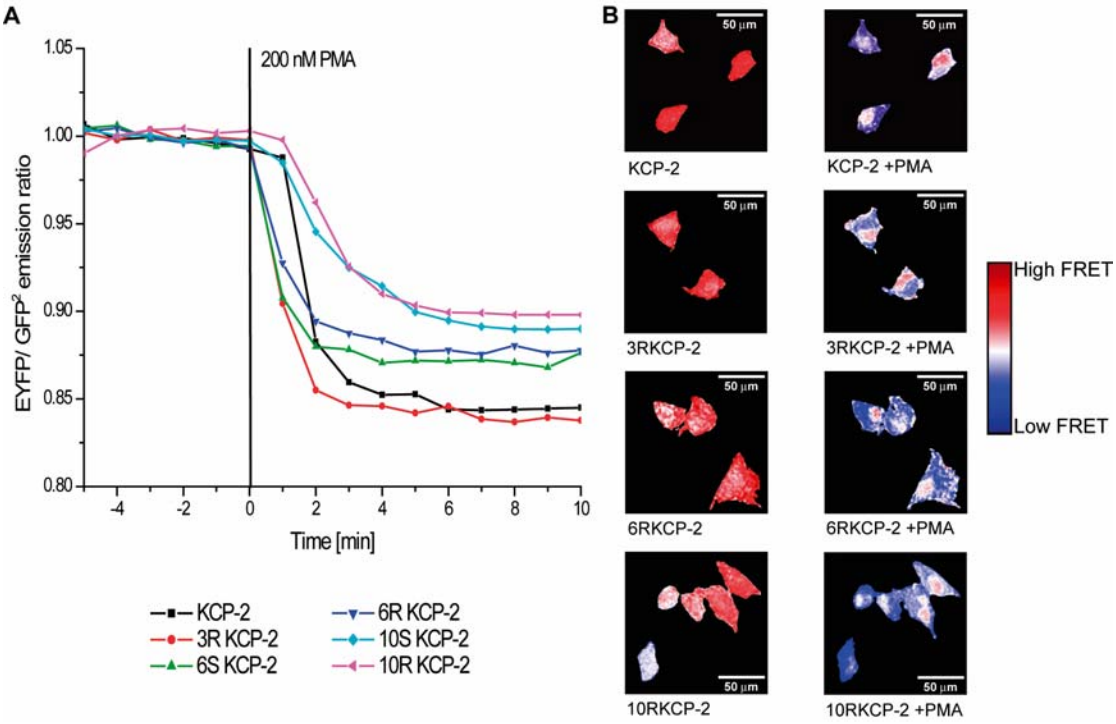

Fig. 4.4 **Introduction of additional amino acids in the N-terminal linker region of KCP-2**

Additional amino acids were introduced in the N-terminal linker region of KCP-2. Experiments were performed on the Visitron system on slides spotted with DNA and covered with HeLa cells.

A PKC activity was stimulated by addition of 200 nM PMA after 6 min and the EYFP/GFP^2 emission ratio measured over time. PKC activity was inhibited 10 min after activation by addition of 500 nM Gö6983, but data is not shown for clarity. The emission ratio of the original probe KCP-2 (black line) decreased substantially upon PKC activation. Increasing the length of the N-terminal linker slightly diminished the amplitude of the signal.

B Single cell examples from the experiments are color-coded according to height of FRET level. A change in emission ratio, i.e. FRET level, is seen as change in color. Introduction of amino acids led to a slightly reduced signal in KCP-2 probes.

The effects of increased linker length on probe performance in KCP-2 samples were similar to KCP-1 (Fig. 4.5). The original KCP-2 probe showed a

decrease in EYFP/GFP^2 emission ratio of 16% upon PKC activation (Fig. 4.4 A, black line). The change in emission ratio was also 16% if three amino acids were added to the N-terminal linker region. With six additional amino acids, the emission ratio decreased by 12-13%, and with ten additional amino acids, the signal decreased by 10-11%. The longer the introduced linker, the smaller the change in emission ratio for the KCP-2 probes. These results for KCP-2 showed the same trend as in KCP-1, although significantly less pronounced (Fig. 4.5).

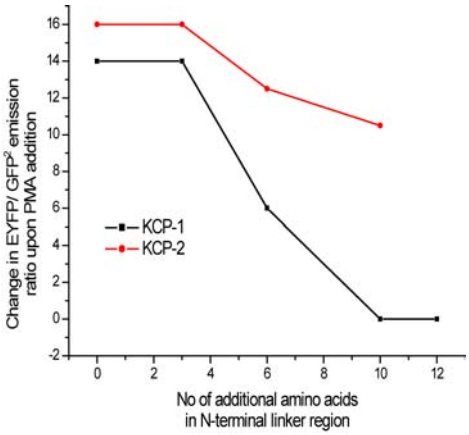

Fig. 4.5 Change in emission ratio after phosphorylation in KCP-1 and KCP-2 probes

The change in EYFP/GFP^2 emission ratio (in %) is shown depending on the amount of amino acids introduced in the N-terminal linker region of PKC probes. Addition of amino acids leads to reduced probe performance in both probes, although the effect is much stronger in KCP-1 (black line) than KCP-2 (red line).

The cell pictures in Fig. 4.3 B and Fig. 4.4 B were color-coded according to FRET level. Blue stands for low FRET levels, red for high FRET levels. Original cell pictures were taken from both channels and the ratio calculated using ImageJ. A strong color change indicates a strong change in emission ratio. This color coding is used throughout this thesis to demonstrate changes in FRET levels directly on the cells. As can be seen in both figures, Fig. 4.3 B and Fig. 4.4 B, the change in emission ratio of the probes only took place in the cytosol, not in the nucleus. The nucleus remained white or blue in the color-coded KCP-1 pictures (first and second panel, Fig. 4.3 B), while the cytosol turned red after PKC activation, indicating a decrease in EYFP/GFP^2 emission ratio. The same was found for all KCP-2 samples: the nuclei remained red or white, while the cytosol turned blue, indicating a decrease in EYFP/GFP^2 emission ratio. This was expected as PKC is not active in the

nucleus. Observation of the signal in the nucleus was a good control showing that the probes indeed measured activation or inhibition of PKC and not an artifact. If the measurements had resulted from an artifact, we would expect the signal to be in the whole cell, not only in certain compartments.

4.2.2 Deletion of amino acids in the N-terminal linker region

As we could show that an increase in linker length had a significant effect on the performance of KCP-1 derived probes, we were interested in studying the effect of a decreased linker length in these probes.

According to the crystal structure of GFP and its variants (PDB ID: 1GFL, 1YFP), the C-terminal end (aa 231-236) of the fluorescent protein is flexible and not involved in the overall fluorophore structure[196,279].

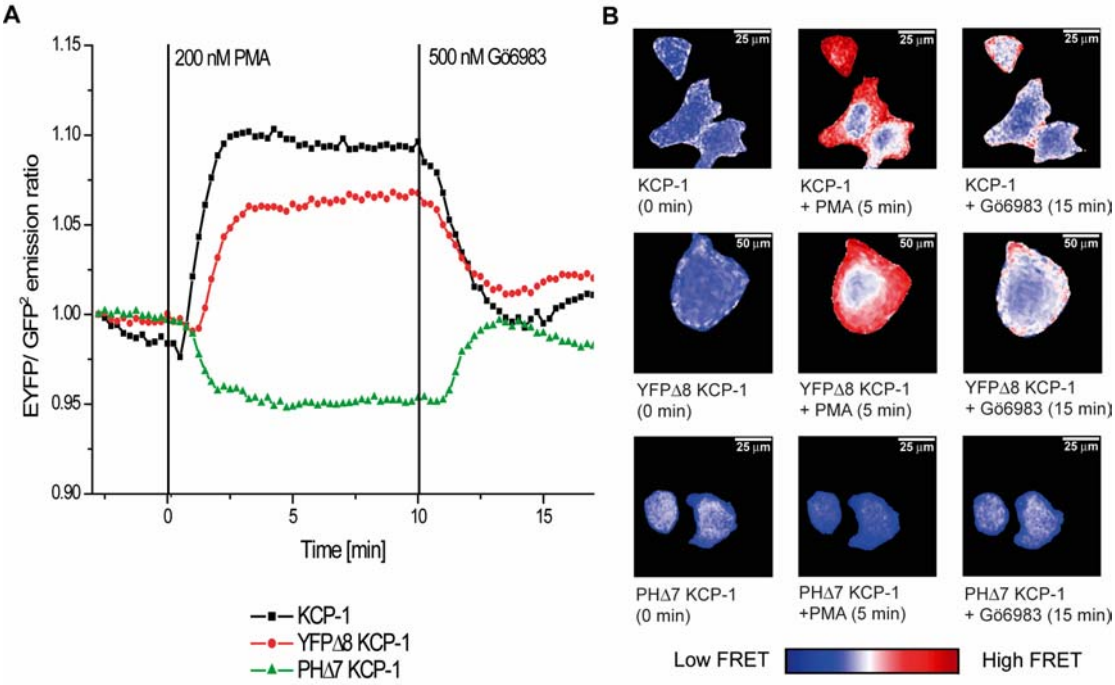

Fig. 4.6 Deletion of amino acids in the N-terminal linker region of KCP-1

Amino acids were deleted in the N-terminal linker region of KCP-1. Experiments were performed with HeLa cells on the Visitron system.

A PKC activity was stimulated by addition of 200 nM PMA after 2.75 min and inhibited with Gö6983 after 10 min. The EYFP/GFP^2 emission ratio of different probes was plotted against time. The original KCP-1 probe (black line) showed an increase in emission ratio upon PKC activation. YFPΔ8KCP-1 (red line) showed a similar response, though the signal was smaller than the original one. In PHΔ7KCP-1 (green line) the signal was reversed: phosphorylation resulted in a decrease in emission ratio.

B Single cell examples from the experiments are color-coded according to FRET level. A color change, indicating a change in emission ratio of the probes, could be seen in all panels, although the direction of the signal was reversed in PHΔ7KCP-1.

We deleted these five C-terminal amino acids, as well as a BsrGI restriction site, which is usually adjacent to the C-terminus of EYFP. In total, eight amino acids were deleted from the linker region between the N-terminal EYFP and

the PH domain of pleckstrin in the KCP-1 and KCP-2 probes (3.2.2.2). These constructs were named YFPΔ8KCP-1 and YFPΔ8KCP-2.

In addition, we deleted the first seven amino acids of the PH domain, at the beginning of the pleckstrin insert and an alanine ahead of the start-methionine. These constructs were called PHΔ7KCP-1 and PHΔ7KCP-2.

Deletion of eight amino acids in YFPΔ8KCP-1 resulted in a decrease in signal amplitude of about 35%. While the emission ratio upon phosphorylation increased to about 9.6% in the original KCP-1 probe, it only increased to 6.3% in the shortened probe (Fig. 4.6 A). The emission ratio was lowered after addition of Gö6983, reflecting the activity of phosphatases dephosphorylating the probe.

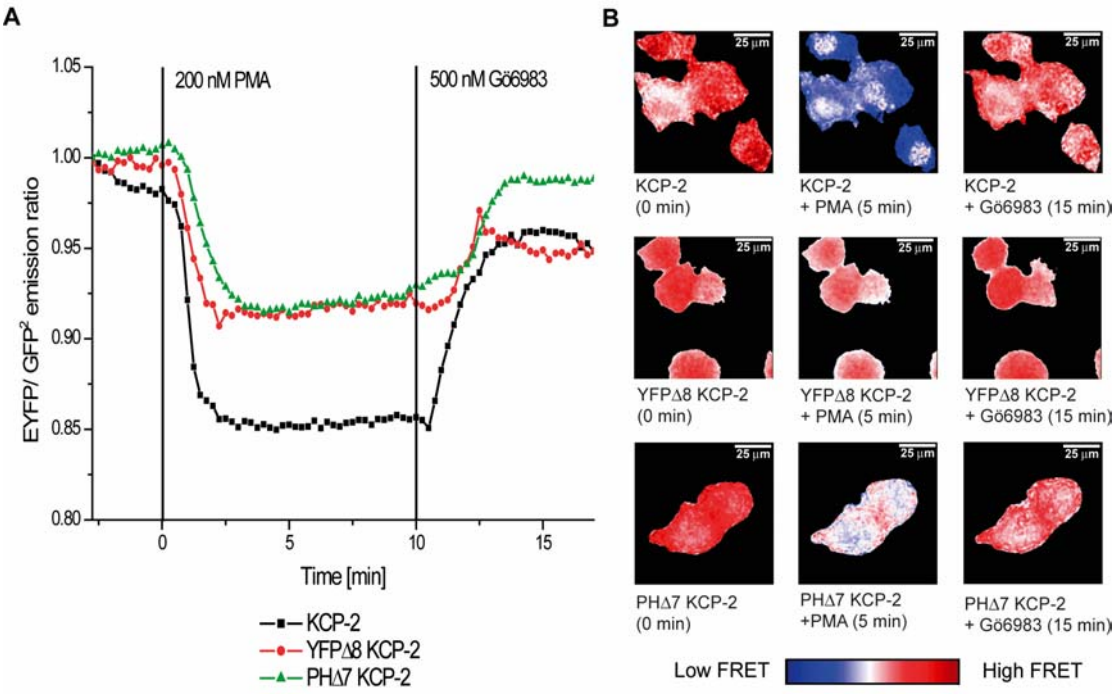

Fig. 4.7 Deletion of amino acids in the N-terminal linker region of KCP-2

Amino acids were deleted in the N-terminal linker region of KCP-2. Experiments were performed with HeLa cells on the Visitron system.

A PKC activity was stimulated by addition of 200 nM PMA after 2.75 min and inhibited with Gö6983 after 10 min. The EYFP/GFP^2 emission ratio of different probes was plotted against time. The original KCP-2 probe (black line) showed a decrease in emission ratio upon PKC activation. In both shorter samples (YFPΔ8KCP-2, red line and PHΔ7KCP-2, green line) the amplitude of the signal was smaller than in the original KCP-2 probe.

B Single cell examples from the experiments are color-coded according to FRET level. A color change, indicating a change in emission ratio of the probes, could be seen in all panels, although it was much smaller in the shorter probes.

Deletions of amino acids in the PH domain (PHΔ7KCP-1), however, led to a reversal of the signal: upon PKC activation the EYFP/GFP^2 emission ratio decreased to -5%. Addition of Gö6983 reversed the signal and brought it back to basal level.

A significant effect could also be observed when deleting the same amino acids in the KCP-2 probes. While the original KCP-2 showed a decrease in emission ratio of 15% after PKC activation, the signal was weaker in the shortened probes, only 8% in YFPΔ8KCP-2 and PHΔ7KCP-2. Although there was a clear signal, it was only 55% of the original amplitude of KCP-2.

Deletion of amino acids in the N-terminal linker had strong effects on both probes. If the C-terminus of EYFP was shortened, both probes showed significantly reduced probe performance. If the N-terminus of the PH domain was deleted, the effect in PHΔ7KCP-1 was even stronger than in YFPΔ8KCP-1 as the signal was reversed in direction. As we will see in the next paragraphs, this is not due to linker shortage, but mainly due to changes in the PH domain.

4.2.3 Changes in the charge distribution of the PH domain

As mentioned before, the only difference between KCP-1 and KCP-2 is a stretch of 18 amino acids at the C-terminus of the pleckstrin insert. This so-called acidic loop contains two glutamates (residues 227 and 228 of the pleckstrin insert) and three aspartates (residues 232-234 of the pleckstrin insert). The different responses of the two KCP probes might be due to interactions of these amino acids with other residues in the molecule (Fig. 4.8).

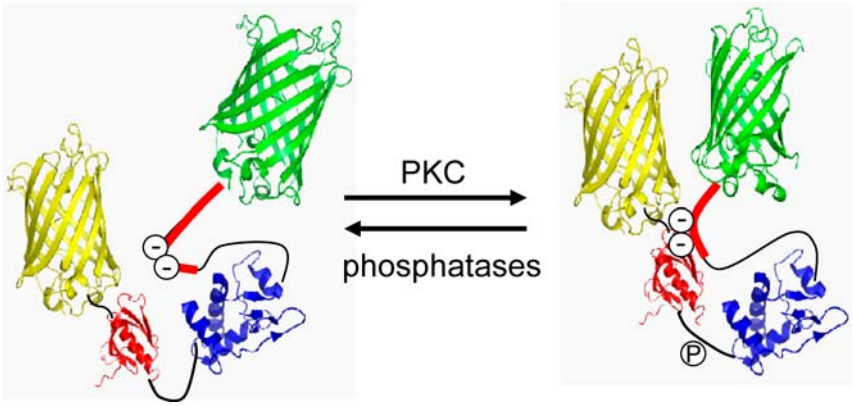

Fig. 4.8 Working model for KCP-1

A model for the conformational change in the KCP-1: in an unphosphorylated state the negatively charged residues in the acidic loop do not interact. The longer linker separates both fluorophores further in KCP-1 than in KCP-2. Phosphorylation leads to a conformational change that induces closer interaction of the negatively charged residues in the acidic loop with positively charged amino acids in the PH domain. Please note the depicted model is not actual structural data, but a model put together from structural data of the individual components.

The PH domain at the beginning of the pleckstrin insert contains three basic residues within the first seven amino acids: Lys4, Arg5 and Arg7. These amino acids might be interaction partners for polar interactions with the acidic loop. To test this hypothesis, we mutated these three amino acids in the PH domain to either neutral (NeutKCP-1 or NeutKCP-2) or negative (NegKCP-1 or NegKCP-2) residues.

Replacing these basic amino acids with neutral ones (K4L, R5L and R7S) in KCP-1 led to a reduced signal. Instead of an increase of 9.6% as in the

original KCP-1 probe, we saw an increase of only 6% in the emission ratio after PKC stimulation.

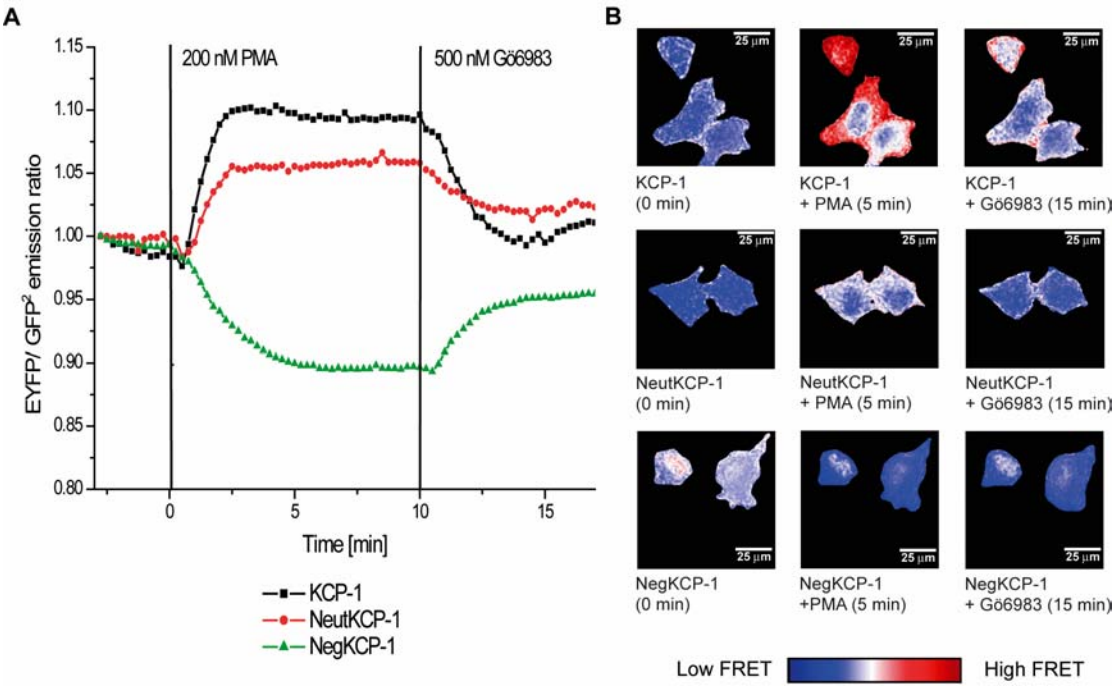

Fig. 4.9 Changes in the charge distribution of the pH domain of KCP-1

The basic charges at the start of the PH domain in KCP-1 were exchanged with neutral (NeutKCP-1) or acidic (NegKCP-1) ones. Experiments were performed in N1E cells on the Visitron system.

A PKC activity was stimulated by addition of 200 nM PMA after 2.75 min and inhibited with Gö6983 after 10 min. The EYFP/GFP^2 emission ratio of different probes was plotted against time. The original KCP-1 probe (black line) showed an increase in emission ratio upon PKC activation. NeutKCP-1 (red line) still had a positive response to PKC stimulation, but with smaller amplitude. The signal was reversed in NegKCP-1 (green line).

B Single cell examples from the experiments are color-coded according to FRET level. A distinctive color change, indicating a significant change in emission ratio of the probe, was seen in the first panel (showing the original KCP-1 probe). NeutKCP-1 showed an increase of FRET after phosphorylation, but with smaller amplitude. NegKCP-1 displayed the opposite behavior, the emission ratio dropped after PKC stimulation.

Replacing the amino acids with negatively charged ones (K4E, R5E and R7E) had a stronger effect on the probe: the signal was reversed. After phosphorylation by PKC the EYFP/GFP^2 emission ratio of NegKCP-1 dropped by 10% instead of increasing as in KCP-1. While addition of Gö6983 usually brought the emission ratio of probes back to starting level, it only went back to about -5% in the NegKCP-1 probe. The kinetics of the probe also seemed to be altered. The change in emission ratio after phosphorylation was usually quite fast. This fast response was also observed in most modified probes, not

only in KCP-1 and KCP-2. In the NegKCP-1 probe, however, the drop in emission ratio was much slower than in other probes.

Similar replacements in KCP-2 led to reduced probe performance. The direction of the signal, though, remained the same.

While the EYFP/GFP^2 emission ratio of the original KCP-2 probe decreased by 15% upon phosphorylation, it only decreased by 9% in the NeutKCP-2 probe and by 12% in the NegKCP-2 probe (Fig. 4.10 B, red and green line). This corresponds to 80% of the original signal in NegKCP-2 and 60% in NeutKCP-2.

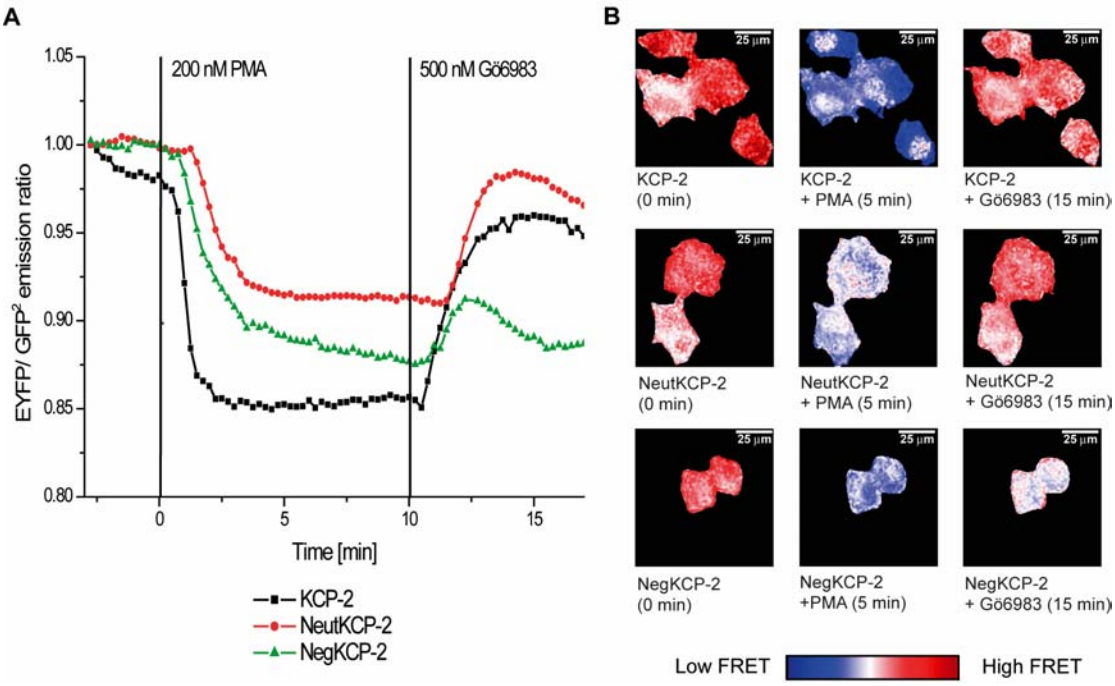

Fig. 4.10 Changes in the charge distribution of the pH domain of KCP-2

The basic charges at the beginning of the PH domain in KCP-2 were exchanged for neutral (NeutKCP-2) or acidic (NegKCP-2) ones. Experiments were performed in N1E cells on the Visitron system.

A PKC activity was stimulated by addition of 200 nM PMA after 2.75 min and inhibited with Gö6983 after 10 min. The EYFP/GFP^2 emission ratio of different probes was plotted against time. The original KCP-2 probe (black line) showed a decrease in emission ratio upon PKC activation. NeutKCP-2 (red line) and NegKCP-1 (green line) also displayed a negative response to PKC stimulation, but with smaller amplitude.

B Single cell examples from the experiments are color-coded according to FRET level. A distinctive color change, indicating a significant change in emission ratio of the probe, is seen in the first panel showing the original KCP-2 probe. NeutKCP-2 and NegKCP-2 showed some change in FRET levels, but not as pronounced as for the original KCP-2 probe.

The results observed, when the basic amino acids were replaced with neutral or negatively charged residues, are similar to the experiments discussed in

the previous chapter, where amino acids of the PH domain were deleted from the sequence.

Based on the model in Fig. 4.8, there is another explanation for the conformational change in KCP-1, which takes the reversal of the signal in the NegKCP-1 probe into account. If the acidic loop is interacting with the amino acids in the PH domain, destroying this interaction might lead to a reversal of signal: the additional interaction is missing, therefore the probe is stretching. This leads to a greater distance between the two fluorophores resulting in a decrease in FRET (according to the model for KCP-2 in Fig. 4.1 B).
If there is an interaction between the acidic loop and the residues 4, 5 and 7 of the PH domain that was determined by the charge of those amino acids, the interaction might be restored by creating complementary probes, in which we introduce basic amino acids into the acidic loop and acidic amino acids into beginning of the PH domain.
Justin Brumbaugh (Schultz group, EMBL) made constructs in which he replaced the amino acids Glu227 and Glu228 in the acidic loop with arginines. He also replaced three glutamates, amino acids 232-234, with arginines in a second construct. The previously shown constructs, encoding for either neutral or negative charges in aa 4, 5 and 7 of the PH domain, were introduced into these vectors, creating four different clones having either a PH domain with neutral amino acids and positive charges in the acidic loop, or a PH domain with negative charges and positive charges in the acidic loop: NeutKCP-1RR$^{227/228}$, NeutKCP-1RRR$^{232-234}$, NegKCP-1RR$^{227/228}$ and NegKCP-1RRR$^{232-234}$.
Both constructs with neutral amino acids in the PH domain, showed a small positive response upon phosphorylation (Fig. 4.11 A). If DDD$^{232-234}$ were replaced by arginines, the increase was 5.6%, whereas if EE$^{227/228}$ were replaced by arginines the increase was only 2.6%. This relates to 58% of the signal of the original probe in the NeutKCP-1RRR$^{232-234}$ construct and to 27% in the NeutKCP-1RR$^{227/228}$ construct. This was similar to the results for the constructs with neutral amino acids in the PH domain, but unchanged acidic loop (Fig. 4.9 A).

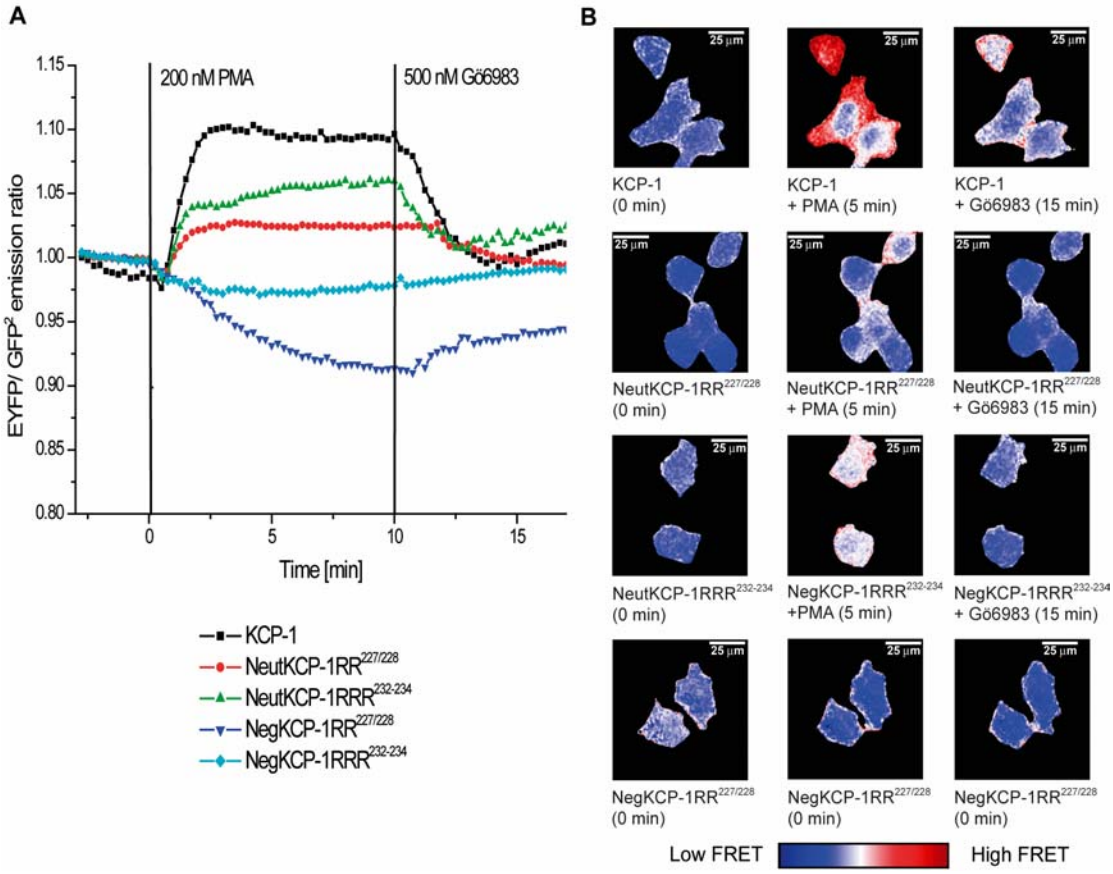

Fig. 4.11 Complementing charge changes in KCP-1

The basic charges at the start of the PH domain in KCP-1 were exchanged for neutral or acidic ones. At the same time negative charges in the acidic loop were replaced by positive ones. Experiments were performed in N1E cells on the Visitron system.

A PKC activity was stimulated by addition of 200 nM PMA after 2.75 min and inhibited with Gö6983 after 10 min. The EYFP/GFP^2 emission ratio of different probes was plotted against time. The original KCP-1 probe (black line) showed an increase in emission ratio upon PKC activation. The neutral constructs showed a positive change in emission ratio, but with smaller amplitude. The negative constructs displayed a decrease in emission ratio.

B Single cell examples from the experiments were color-coded according to FRET level. A distinctive color change, indicating a significant change in emission ratio of the probe, was seen in the first panel showing the original KCP-1 probe.

If the construct had a PH domain with negatively charged amino acids and positive charges in the acidic loop, the direction of the signal was reversed (Fig. 4.11 A), similar to the result seen for the NegKCP-1 construct (Fig. 4.9 A). While the signal in NegKCP-1RRR$^{232-234}$ decreased by 2.7%, the signal in the NegKCP-1RR$^{227/228}$ probe decreased by 7.5%. Comparable to the result in the NegKCP-1 clone (Fig. 4.9 A), the shape of the response was also different. The signal took longer to develop and did not go back to basal levels after inhibition of PKC activity in NegKCP-1RR$^{227/\ 228}$ and in NegKCP-1.

Taken together, these experiments do not confirm any model, in which these particular amino acids in the PH domain and the acidic look are interacting with each other.

4.3 Effect of fluorophore dimerization on KCP-1 and KCP-2

Most fluorescent proteins (FPs) are known to have the tendency to oligomerize[271]. The degree and stoichiometry, with which they oligomerize, vary from organism to organism. Fluorescent proteins from *Aequorea victoria* are the only ones that do not form obligate oligomers. These FPs form weak dimers[196] (see Fig. 4.12). When measuring the interaction of tagged proteins with FRET, it is crucial that the reporter proteins do not in any way interfere with, or even create, an interaction. Effects due to dimerization of the FPs in the three-dimensional cytosol have not yet been shown, but it has been shown to create artifacts in membrane-protein systems[270].

There is a hydrophobic patch at the dimer interface that is thought to be responsible for the dimerization (Fig. 4.12 A, cyan box). Independent mutations of any of the three hydrophobic amino acids in this patch (Ala206, Leu221 and Phe223) to a lysine or an arginine greatly reduce the dimerization tendency.

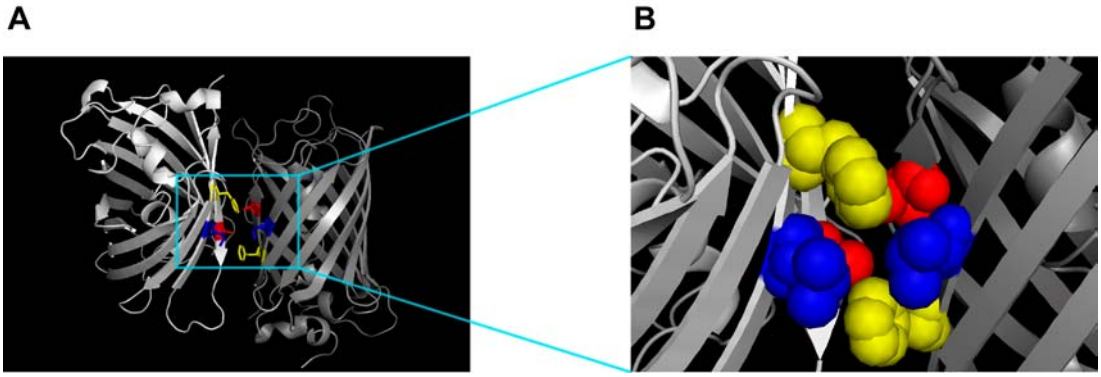

Fig. 4.12 Crystal structure of GFP

A Crystal structure of GFP from *Aequorea victoria*[196]. Monomers of GFP form a head to tail dimer, but substitution of any of the three indicated residues with a positively charged amino acid reduces the molecule's tendency to dimerize. Ala^{206} is shown in red, Leu^{221} in blue and Phe^{223} in yellow. (PDB no 1GFL)

B Enlarged picture of the three residues in the hydrophobic patch responsible for FP dimerization in *A. victoria*.

While the dissociation constant (K_d) for the wild type protein is about 0.11 mM, it is 9.7 mM if Leu^{221} is mutated to lysine. The mutation A206K has the strongest effect, increasing the K_d to 74 mM. A reliable determination of this

value was however not possible due to the extreme monomeric nature of the protein[270].

We first introduced the A206K mutation into both, EYFP and GFP^2, in KCP-1 and KCP-2 probes, and then individually into one fluorophore at a time. Additionally, the L221K mutation was introduced into EYFP and GFP^2, to study the effect of a lower dimerization tendency that is not entirely monomeric. Monomeric fluorophores were named "m" for monomeric, the L221K constructs were named m221 for distinction from the truly monomeric FPs.

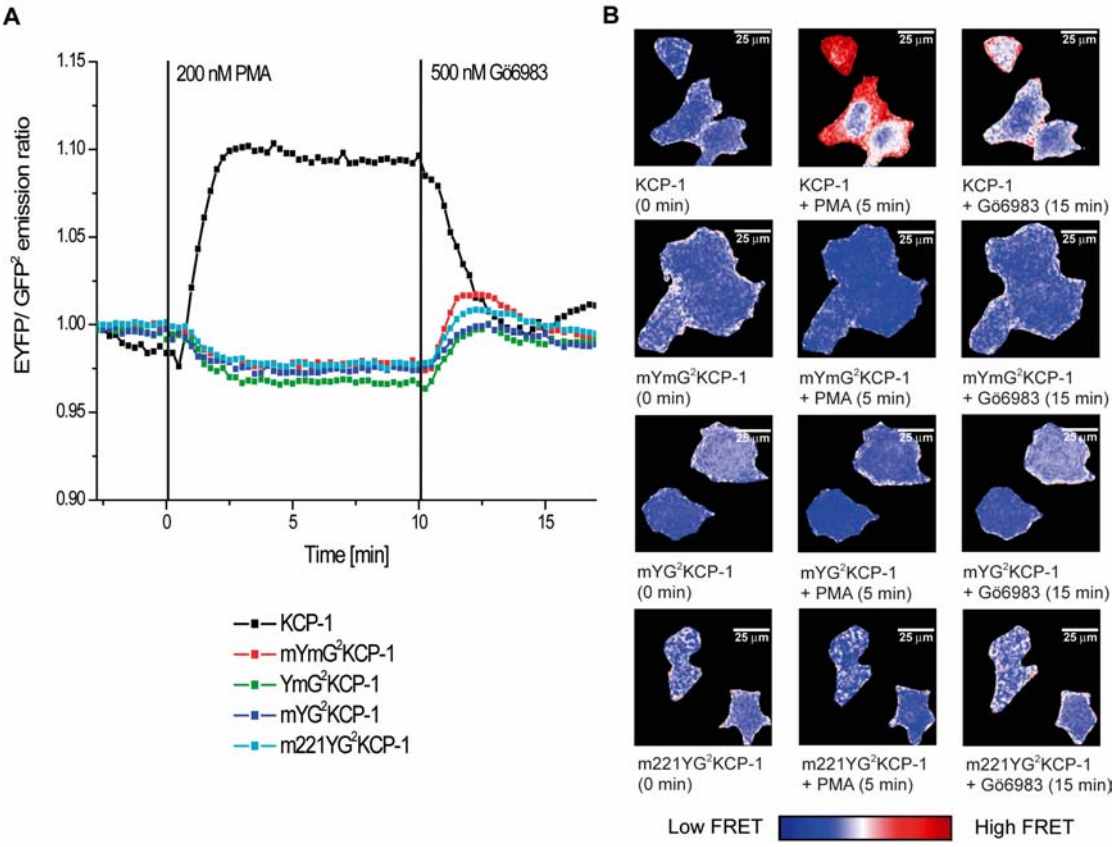

Fig. 4.13 Introduction of monomeric fluorescent proteins into KCP-1

Mutations that decreased the proteins ability to dimerize were introduced into EYFP and GFP^2 of KCP-1. Experiments were performed in N1E cells on the Visitron system.

A PKC activity was stimulated by addition of 200 nM PMA after 2.75 min and inhibited with Gö6983 after 10 min. The EYFP/GFP^2 emission ratio of different probes was plotted against time. While the original probe KCP-1 showed a clear increase in emission ratio upon stimulation with PMA, all probes containing one or more monomeric proteins displayed a small decrease in emission ratio.

B Single cell examples from the experiments are color-coded according to FRET level. A distinctive color change, indicating a significant change in emission ratio of the probe, is seen only in the first panel showing the original KCP-1 probe.

The effect of these mutations was very pronounced and consistent for all KCP-1 probes tested (Fig. 4.13 A). Irrespective of whether one or both fluorophores were monomeric, whether it was the strong monomeric mutation, A206K, or the weaker one, L221K, the EYFP/GFP^2 emission ratio always decreased to 2.4-3.1%. The result was reproducible in signal amplitude and direction.

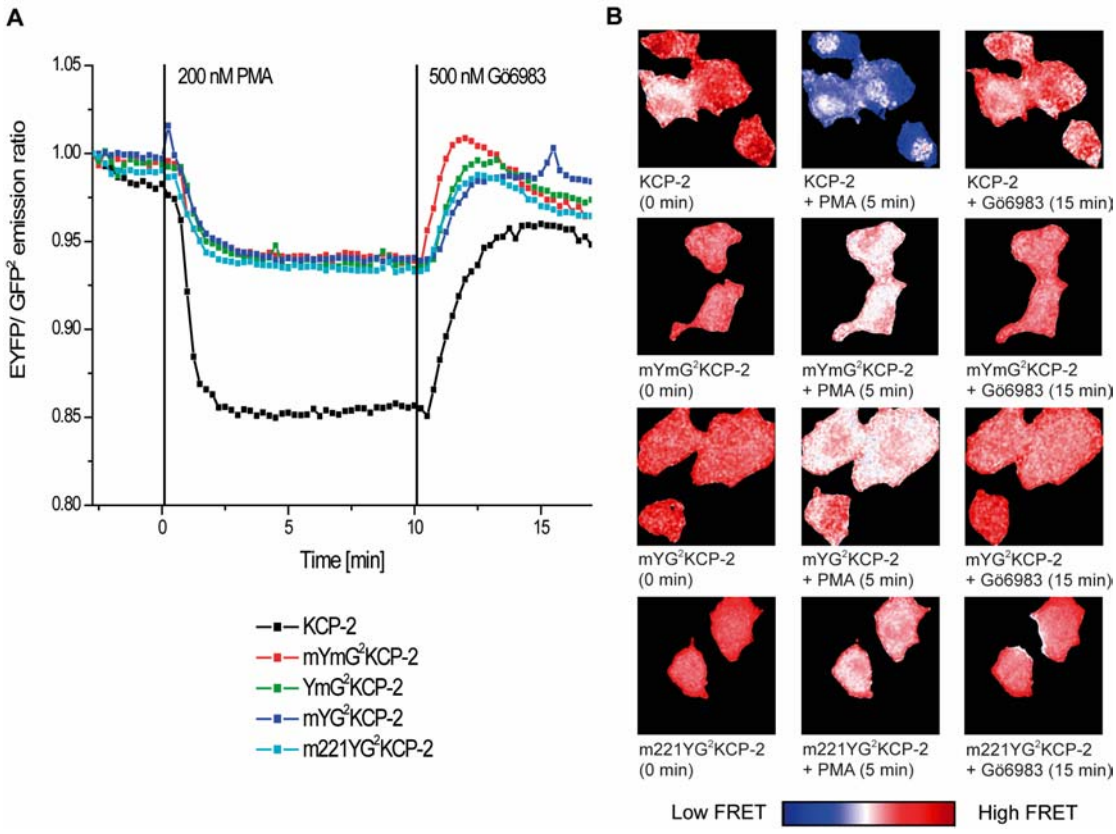

Fig. 4.14 Introduction of monomeric fluorescent proteins into KCP-2

Mutations that decrease the proteins ability to dimerize were introduced into EYFP and GFP^2 of KCP-2. Experiments were performed in N1E cells on the Visitron system.

A PKC activity was stimulated by addition of 200 nM PMA after 2.75 min and inhibited with Gö6983 after 10 min. The EYFP/GFP^2 emission ratio of different probes was plotted against time. While the original probe, KCP-2, showed a significant decrease in emission ratio upon stimulation with PMA, all probes containing one or more monomeric proteins displayed only a minor decrease in emission ratio.

B Single cell examples from the experiments are color-coded according to FRET level. A distinctive color change, indicating a significant change in emission ratio of the probe, is seen only in the first panel showing the original KCP-2 probe.

A strong effect can also be observed in the KCP-2 probes carrying monomeric fluorescent proteins. In these experiments, the direction of the signal did not change compared to the original KCP-2 probe, but the amplitude was significantly smaller (Fig. 4.14 A). While the emission ratio in the original

probe decreased about 15% upon phosphorylation, the ratio in the monomeric probes only decreased to 6-6.4% of basal level. This corresponds to about 42% of the response of the original probe. Again, this effect was independent of whether one or both of the fluorescent proteins were monomeric.

To study whether our probes generally depended on the dimeric state of the fluorophores, or if this was only the case if using *A. victoria* FPs, we exchanged GFP^2 and EYFP with monomeric FPs from *Discosoma*. These monomeric proteins were published at the end of 2004 and provided real monomers with good spectral properties from yellow to red[210]. We used mOrange as donor (replacing GFP^2) and mCherry as acceptor (replacing EYFP) in KCP-1 and KCP-2. Previous experiments in the lab had shown that these FPs could be used as a FRET pair, although their FRET efficiency was lower in amplitude than that for EYFP/ECFP or EYFP/GFP^2 (Alen Piljić, unpublished data).

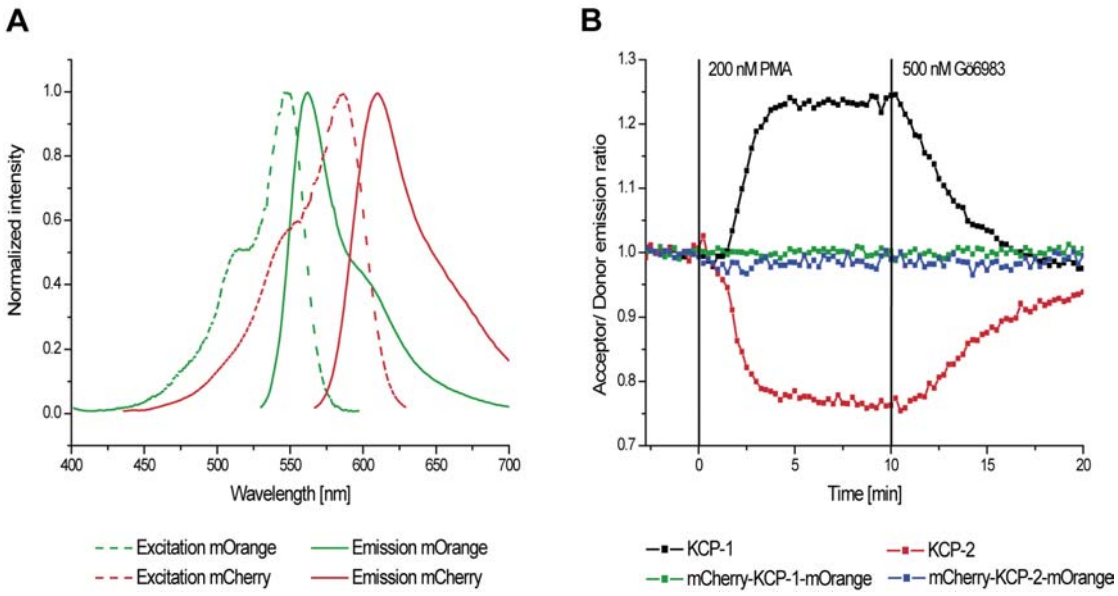

Fig. 4.15 KCP-1 and KCP-2 with monomeric FPs mCherry and mOrange

A Normalized spectra of the excitation (dashed line) and the emission (solid line) of mOrange (green) and mCherry (red).

B PKC activity was stimulated by addition of 200 nM PMA after 2.75 min and inhibited with Gö6983 after 10 min. The EYFP/GFP^2 emission ratio of different probes was plotted against time. The monomeric probes with mOrange and mCherry displayed no change in emission ratio upon phosphorylation.

Neither of the two probes with mCherry and mOrange showed any change in mCherry/mOrange emission ratio after PKC stimulation with PMA.

Taken together these experiments showed that dimerization of the fluorophores in pleckstrin-based PKC probes is crucial for good probe performance. Even though all monomeric or partly monomeric probes with fluorophores derived from *A. victoria* showed changes in emission ratio upon PKC phosphorylation, these changes were much smaller than in the original dimerizing probes.

4.4 Summary of mutational data on KCP-1 and KCP-2

The following table summarizes all results shown so far. The percentage of probe performance normalized to the respective KCP-1 or KCP-2 probe under same conditions is shown for each altered probe.

KCP-1 derived probe	% of the original signal	KCP-2 derived probe	% of the original signal
3S KCP-1	**103.52**	3R KCP-2	**104.49**
3R KCP-1	**100.00**	6S KCP-2	**82.05**
6S KCP-1	**38.73**	6R KCP-2	**78.85**
6R KCP-1	**50.00**	10S KCP-2	**71.15**
10S KCP-1	**2.11**	10R KCP-2	**65.38**
10R KCP-1	**10.56**		
12RS KCP-1	**-2.11**		
YFPΔ8 KCP-1	**65.63**	YFPΔ8 KCP-2	**54.73**
PHΔ7 KCP-1	**-52.08**	PHΔ7 KCP-2	**54.73**
NeutKCP-1	**59.38**	NeutKCP-2	**58.11**
NegKCP-1	**-104.17***	NegKCP-2	**78.38***
NeutKCP-1RR$^{227/228}$	**27.08**		
NeutKCP-1RRR$^{232-234}$	**58.33**		
NegKCP-1RR$^{227/228}$	**-78.13***		
NegKCP-1RRR$^{232-234}$*	**-28.13**		
mYmG^{2}KCP-1	**-25.00**	mYmG^{2}KCP-2	**40.54**
YmG^{2}KCP-1	**-32.29**	YmG^{2}KCP-2	**43.24**
mYG^{2}KCP-1	**-27.08**	mYG^{2}KCP-2	**40.54**
m221YG^{2}KCP-1	**-25.00**	m221YG^{2}KCP-2	**43.24**

Table 4.2 Table summarizing the results for all mutations in KCP-1 and KCP-2 described so far

A * denotes probes in which the probes' performance is severely disturbed and reversibility of the signal is not given. The percentage of response from the original probe is therefore not described accurately.

4.5 FRET efficiency of selected constructs

We have so far studied the change in emission ratio in different PKC probes using *in vivo* measurements. We observed an increase or decrease from a certain starting level of FRET, without really looking at absolute FRET efficiencies. In order to examine the effect that certain mutations have on the probe, we need to know whether FRET levels in different probes are similar or not. Introducing mutations might have led to changes in the architecture of the probe, which influenced the FRET efficiency. If there was no longer any FRET between the two fluorophores, it would explain the lack of changes in emission ratio.

We determined FRET efficiencies with two different methods, acceptor photo bleaching (AccPB, 3.2.1.12) and trypsination experiments using a fluorimeter (3.2.1.13).
In AccPB experiments, the donor is imaged at its excitation maximum before and after bleaching of the fluorophore. The FRET efficiency is calculated as the percentage of the total excitation energy transferred from donor to acceptor, as measured by the emitted fluorescence.
The AccPB showed a clear change in FRET efficiency of KCP-1 and KCP-2 after phosphorylation (Fig. 4.16 A). The unphosphorylated KCP-1 probe had a starting FRET level of 17%, which increased to 26% after phosphorylation. The unphosphorylated KCP-2 probe on the other hand, had a starting FRET level of 28.5% that decreased to 17% after phosphorylation. This is consistent with the live cell imaging data: the emission ratio of KCP-1 increased after phosphorylation, while it decreased in KCP-2 (Fig. 4.2 B). In all of the probes, that contained any of the monomeric mutations (A206K or L221K), in EYFP and/or GFP^2, the FRET efficiency was between 13-21%. The changes seen, when going from the unphosphorylated to phosphorylated probe, where usually very small, with the FRET efficiency being slightly lower after PKC activation than before. This again, corresponded well with the live cell imaging data.

The AccPB data suggested that FRET still occurred in the monomeric probes, but the change upon phosphorylation was abolished by introducing the mutations.

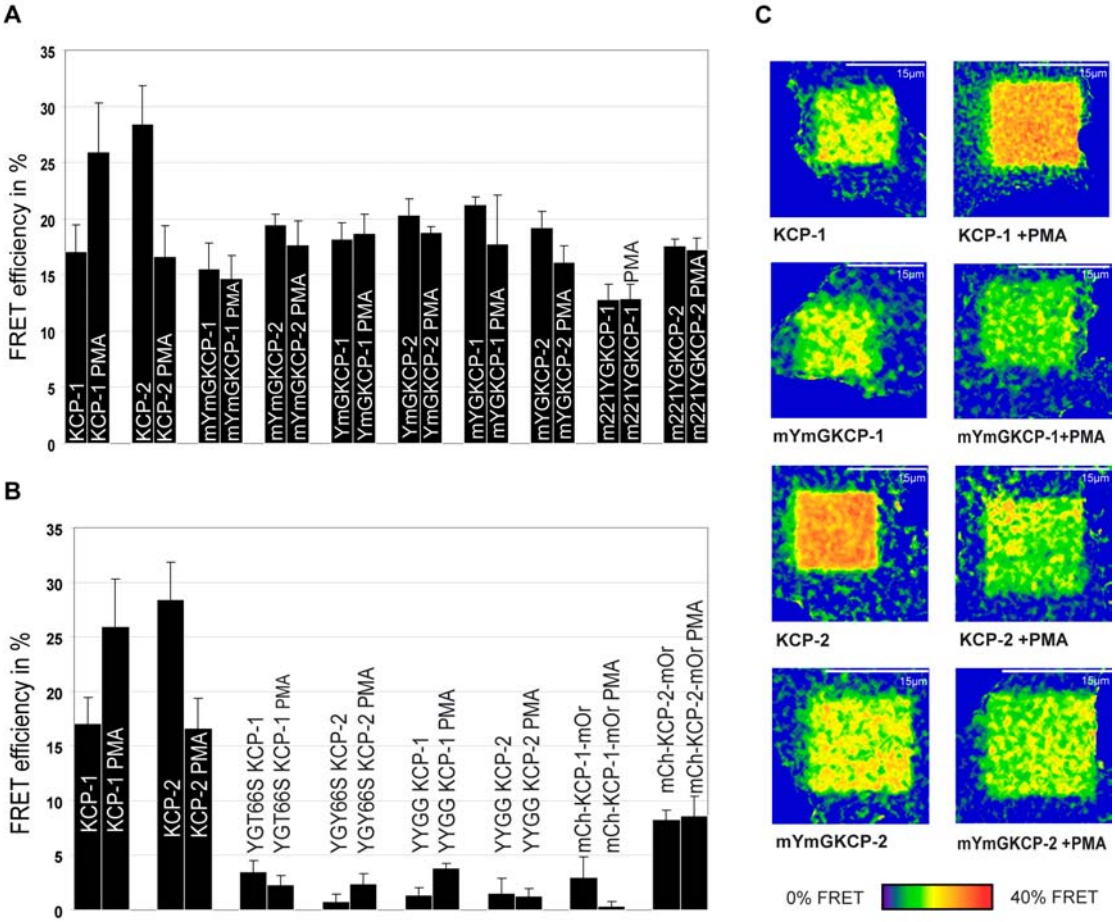

Fig. 4.16 Comparison of FRET efficiency as measured with acceptor photo bleaching

A Comparison of FRET efficiencies of the original KCP-1 and KCP-2 probes and their monomeric or partly monomeric constructs, as measured with acceptor photo bleaching.

B Comparison of FRET efficiencies of the original KCP-1 and KCP-2 probes and selected other constructs used in this thesis, as measured with acceptor photo bleaching.

C Single cell examples of the original data from the acceptor photo bleaching experiments. FRET efficiency is shown before and after PKC stimulation in the two original probes KCP-1 and KCP-2 and, as an example for all other samples, in the probes carrying the A206K mutation in both fluorophores, EYFP and GFP[2]. The level of FRET efficiency is color-coded, from blue (no FRET) to red (high FRET).

We also determined the FRET efficiency of our other monomeric probes, mCherry-KCP-1-mOrange and mCherry-KCP-2-mOrange (Fig. 4.16 B). The FRET efficiency of mCherry-KCP-1-mOrange was very low, around 3% unphosphorylated and 0.5% after phosphorylation. The FRET efficiency of mCherry-KCP-2-mOrange was slightly higher, around 8% unphosphorylated

and 8.5% after phosphorylation. In both probes, FRET efficiency was rather low in the first place and it did not change much depending on the phosphorylation state. This explained the lack in any change of emission ratio in the probes (Fig. 4.15 B).
The constructs that we used for discrimination of inter- versus intramolecular FRET all had very low levels of FRET efficiency, between 0.5 to 3.8% (Fig. 4.16 B). This is not surprising as we did not expect those probes to exhibit FRET at all, since they should not be interacting closely.

FRET efficiency was also measured with trypsination experiments (3.2.1.13). In these experiments, the acceptor was not bleached away as in AccPB, but removed by trypsin. Trypsin cleaved the probe, but left both fluorophores intact. The donor emission was measured in the fluorimeter before and after trypsin cleavage of the probe. The FRET efficiency was calculated as the percentage of the total excitation energy transferred from donor to acceptor, as measured by the emitted fluorescence.
The trypsination experiments also showed a clear difference in the FRET efficiencies of KCP-1 and KCP-2, before and after phosphorylation (Fig. 4.17). The unphosphorylated KCP-1 probe had a starting FRET level of 16%, which increased to 20% after phosphorylation. The unphosphorylated KCP-2 probe, on the other hand, had a starting FRET level of 25.3% that decreased to 16% after phosphorylation. Again, this was in agreement with the live cell imaging data: the emission ratio of KCP-1 increased after phosphorylation while it decreased in KCP-2 (Fig. 4.2 B).
While FRET efficiencies for KCP-1 and KCP-2 measured in trypsination or AccPB experiments compared well with each other, the results are less homogenous for the monomeric or partly monomeric EYFP/GFP^2 samples. The measured FRET efficiency was between 2.3-5.6% for most KCP-1 derived samples. For the m221YGKCP-1 probe, however, the result was over 13%. In KCP-2 derived samples, the FRET efficiency varied from 4 to 10.5%. The FRET efficiency was usually lower after phosphorylation, as observed in the live cell experiments. Only in the mYGKCP-1 and mYGKCP-2 samples, did the apparent FRET efficiency increase after phosphorylation.

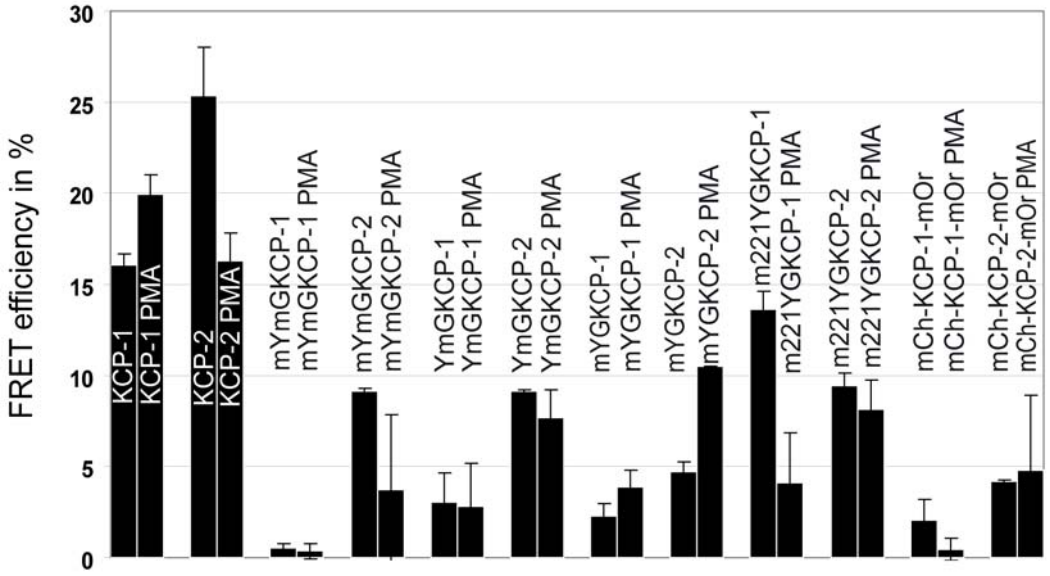

Fig. 4.17 Comparison of FRET efficiencies as measured with trypsination experiments

Comparison of FRET efficiencies of the original KCP-1 and KCP-2 probes and monomeric or partly monomeric constructs, as measured with trypsination experiments.

The FRET efficiencies determined by trypsination experiments for the monomeric probes using mCherry and mOrange were similar to those determined by AccPB: 2% for Ch-KCP-1-Or before and 0.5% after phosphorylation. It was slightly higher for Ch-KCP-2-Or with 4.1% before and 4.8% after phosphorylation.

Levels of calculated FRET efficiencies from trypsination experiments varied greatly and the error in FRET efficiencies was higher than if the values were determined by AccPB. Cell lysates are not the best environment for determination of FRET efficiencies as the cellular environment is too difficult to control. Other kinases and phosphatases might act on the probe as well as proteases. Determination of FRET efficiencies by trypsination is a very good method for purified samples, as there is no risk in bleaching the donor as well. Values might therefore be slightly more accurate than with AccPB. For a fast determination of many samples, however, AccPB is the faster and more reliable method.

4.6 Intra- versus intermolecular FRET in KCP-1 and KCP-2

Since we showed that the dimerization state of the fluorophores used for PKC probes is very important, we had to consider the possibility of **inter**molecular FRET, as well as **intra**molecular FRET. Thus far, we have assumed that the FRET, measured in all KCP-1 and KCP-2 probes, stemmed from an energy transfer between GFP^2 and EYFP within one protein. According to our hypothesis, a conformational change within the probe led to a change in FRET efficiency after PKC activation or inactivation.
Knowing the importance of fluorophore dimerization for probe performance, another model is possible: in the unphosphorylated state, the fluorophores of different probe molecules might be in close enough proximity for FRET, due to their oligomerization tendency. Misleading effects in FRET probes, due to fluorescent protein dimerization, have been reported before[270]. Phosphorylation might then lead to a conformational change, which enhances the dimerization in neighboring molecules in KCP-1 probes, while it destroys it in KCP-2 probes.

Discrimination between inter- and intramolecular FRET is possible using two different experimental set ups. Both follow the same reasoning: FRET between the two fluorescent proteins of one molecule has to be inhibited, while still allowing for FRET between fluorophores of different molecules.
In the first experiment, we introduced an Y66S mutation into either EYFP or GFP^2. Y66S is one of the core amino acids forming the fluorophore in FPs from *A. victoria*[196]. If it is replaced by non-aromatic amino acids, the FP is rendered non-fluorescent.
Two altered constructs were co-transfected for each probe: one with a functional GFP^2 but a non-fluorescent EYFP (EYFPY66S KCP-1 or EYFPY66S KCP-2), and the second one with a functional EYFP but a non-fluorescent GFP^2 (GFP^2Y66S KCP-1 or GFP^2Y66S KCP-2). This set up still allowed FRET between the functional GFP^2 of one probe molecule and the fluorescent EYFP of another probe molecule, but not within the same probe (see schematic illustration Fig. 4.18 A).

Before each experiment with these constructs, expression levels of both proteins had to be checked. Both constructs have to be expressed at the same level to allow any statement about the change in FRET. As the original probes are stoichiometric probes, they were used as reference for equal expression levels. The individual fluorescence levels had to be determined individually for KCP-1 and KCP-2 individually as they have different basal FRET levels.

The experiments were performed in HeLa and N1E cells, but a change in EYFP/ GFP^2 emission ratio could not be observed in any experiment (Fig. 4.18 B, blue and green line, imaged in HeLa cells), neither with KCP-1 nor with KCP-2. This indicated that intermolecular FRET was not occurring in this experiment.

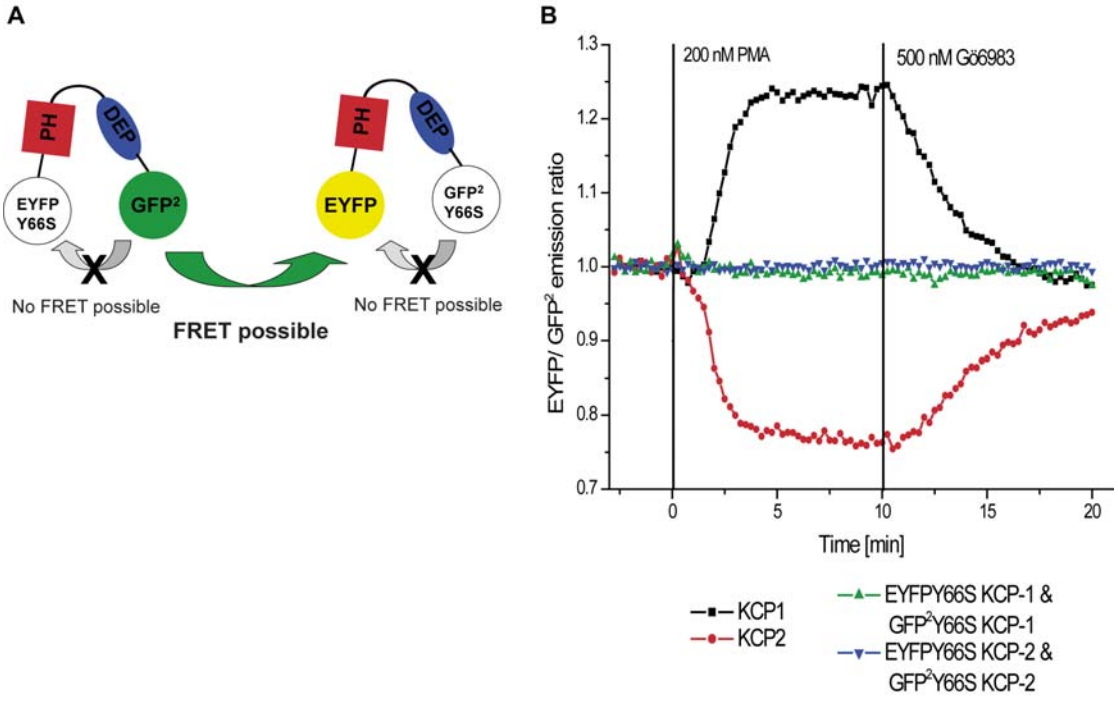

Fig. 4.18 Discrimination between inter- and intramolecular FRET in PKC probes

A Schematic representation of the experiment: each molecule contained only one fluorescent protein, the second one was rendered non-fluorescent. This arrangement excludes any intramolecular FRET, while intermolecular FRET is still possible.

B PKC activity was stimulated by addition of 200 nM PMA and inhibited with Gö6983 after 10 min. The EYFP/GFP^2 emission ratio of different probes was plotted against time. Both KCP-1 (EYFPY66S KCP-1 and GFP^2Y66S KCP-1) or both KCP-2 (EYFPY66S KCP-2 and GFP^2Y66S KCP-2) constructs were co-transfected into HeLa cells and their signal compared to the original probes. While the original probes showed a clear signal, the co-transfected probes showed none.

In the second set of experiments, addressing the same question, we made probes that encode only on species of fluorescent protein. In one construct, the N-terminal EYFP was replaced by a second GFP^2; in another construct, the C-terminal GFP^2 was replaced by a second EYFP (see 3.2.2.4). Both constructs were co-transfected (EYFP-KCP-1-EYFP with GFP^2-KCP-1-GFP^2 or EYFP-KCP-2-EYFP with GFP^2-KCP-2-GFP^2, respectively) into cells and the FRET ratio measured after stimulation of PKC activity. Again, this set up made FRET within one molecule impossible, while it was still possible between two different molecules (for a schematic illustration, see Fig. 4.19 A). As in the first experiments, care had to be taken to choose cells with equal expression levels of both constructs.

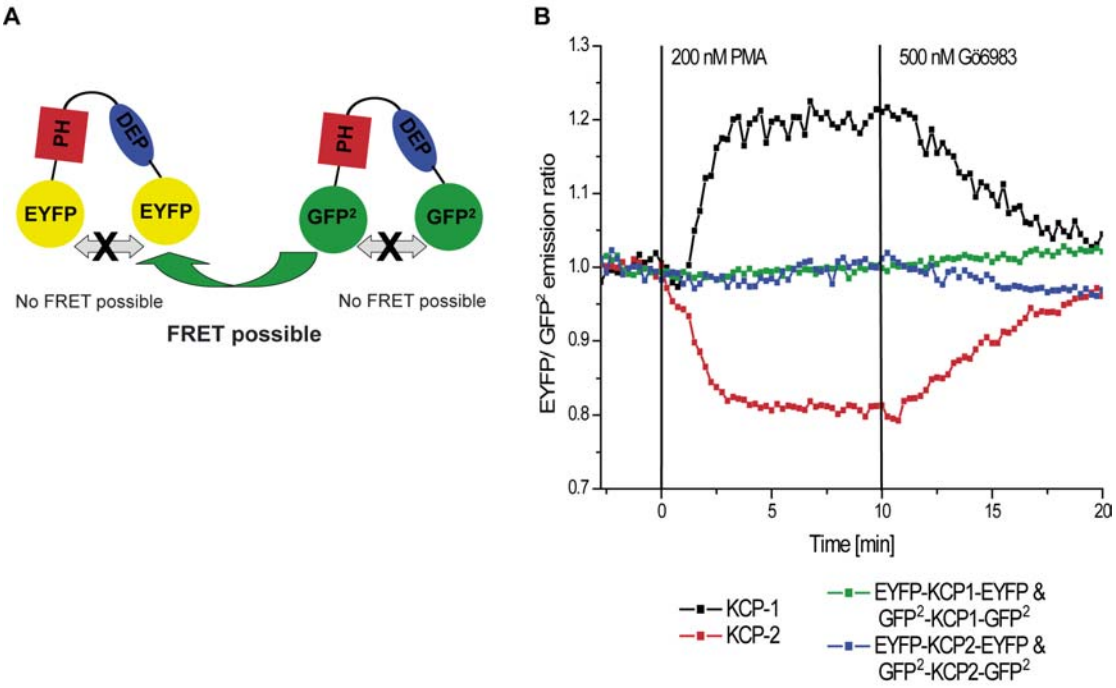

Fig. 4.19 Discrimination between inter- and intramolecular FRET in PKC probes –part 2

A Schematic representation of the experiment: each molecule contained two fluorescent proteins of the same kind. This arrangement excludes any intramolecular FRET, while intermolecular FRET is still possible.

B PKC activity was stimulated by addition of 200 nM PMA and inhibited with Gö6983 after 10 min. The EYFP/GFP^2 emission ratio of different probes was plotted against time. Both KCP-1 (EYFP-KCP-1-EYFP and GFP^2-KCP-1-GFP^2) or both KCP-2 (EYFP-KCP-2-EYFP and GFP^2-KCP-2-GFP^2) constructs were transfected into HeLa cells and their signal compared to the original probes. While the original probes showed a clear signal, the co-transfected probes showed none.

Experiments were performed in N1E and HeLa cells, but changes in emission ratio could be observed in neither (Fig. 4.19 B, green and blue line, imaged in

N1E cells). Again, this showed clearly that intramolecular FRET was not taking place.

Together, these experiments demonstrated, that the effect observed in KCP-1 and KCP-2 probes, is due to intramolecular FRET rather than intermolecular. Dimerization has effects within the probe, but that effect does not extend to other molecules.

4.7 Changing the FRET pair in PKC probes

4.7.1 PKC probes using the AGT-labeling approach and chemically synthesized fluorophores

Changing the FRET pair in our PKC probes has two main advantages:
Firstly, it would aid multiparameter imaging. If we want to measure other parameters in a single experiment using other probes, they usually need to be in different wavelength areas of the visible spectrum. Many existing probes use ECFP/EYFP as a FRET pair, e.g. calcium sensors[165,166], a cAMP sensor[280] or in translocation and self-association assays of annexin 4 on membrane surfaces[281].
Secondly, shifting probes to higher excitation and emission wavelength not only aids multiparameter imaging, but also decreases the risk of photodamage. Imaging with red light would even allow imaging of tissue or whole animals, as it penetrates deeper than blue or green light and is less harmful.

As it had been shown in a previous thesis from our lab[282], combinations of other possible FRET pairs, using differently-colored genetically encoded fluorophores, yielded only weak probes (Cit-KCP-2-ECFP, Cit-KCP-2-mRFP). Mostly these probes failed to show any change in emission ratio at all (Cit-KCP-1-ECFP, Cit-KCP-1-RFP).
We therefore decided to use AGT labeling[227,228]. This technique is based on a genetically encoded tag that can be covalently labeled with small organic molecules inside living cells (Fig. 2.6). It enabled us to test a wide range of chemically synthesized fluorophores with different genetically encoded fluorescent proteins.
ECFP and fluorescein (Fig. 4.20 A) have appropriate spectral properties to make FRET likely (Fig. 4.20 B): donor emission and acceptor excitation overlap well and both emissions are well separated. The O^6-benzylguanine (BG) derivative of fluorescein-diacetate, BGAF, is readily hydrolyzed to BG-

fluorescein (BGFL) by esterases within the cell and is known to label AGT efficiently *in vivo*[228].

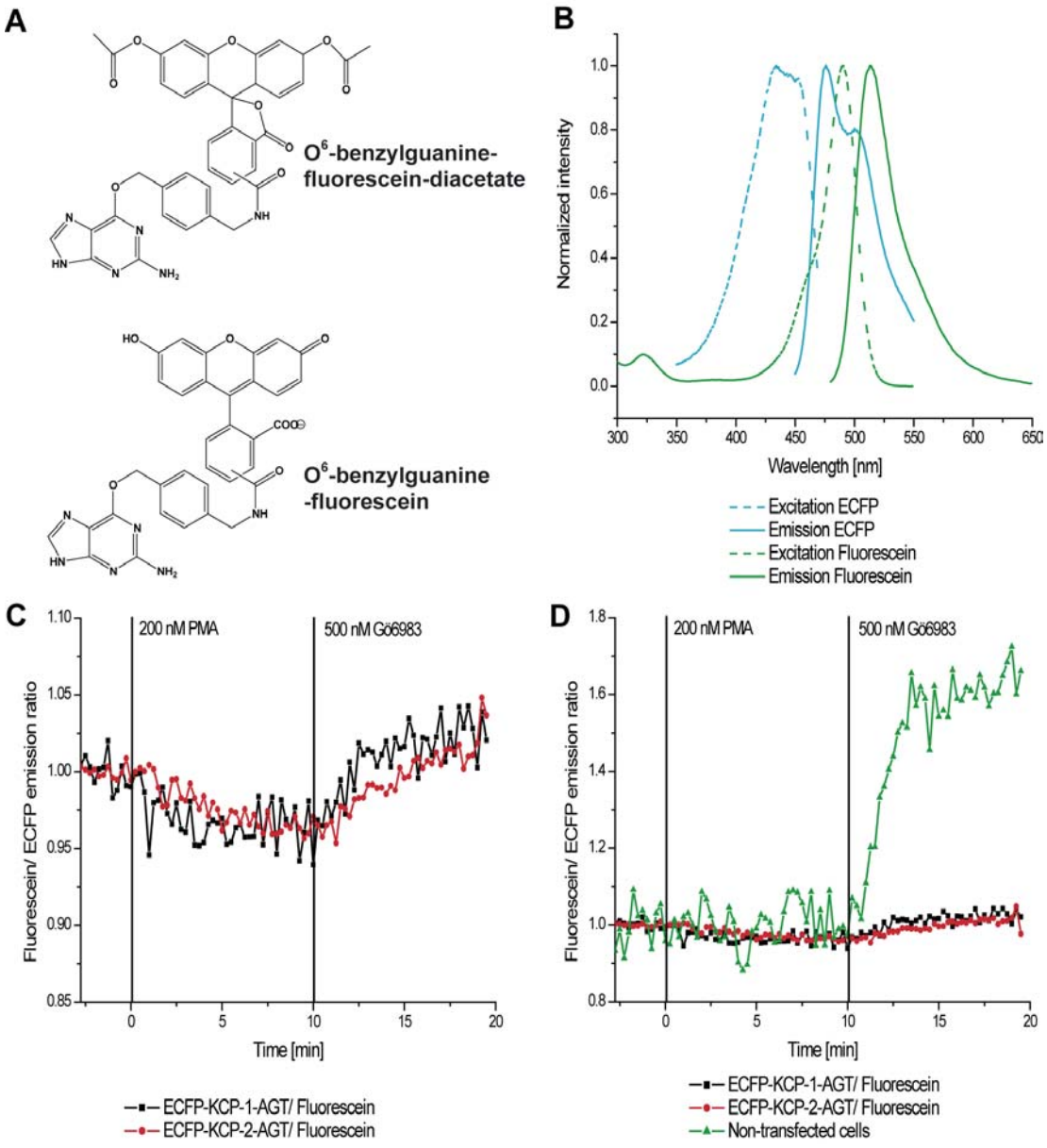

Fig. 4.20 PKC probe using AGT labeled with fluorescein and ECFP

A Chemical structure of O^6-benzylguanine-fluorescein-diacetate and O^6-benzylguanine-fluorescein

B Normalized spectra of the excitation (dashed line) and the emission (solid line) of ECFP (cyan) and fluorescein (green).

C Cells were transfected with ECFP-KCP-1(or KCP-2)-AGT and labeled with fluorescein before the experiment. PKC activity was stimulated and subsequently inhibited with Gö6983. The emission ratio was measured over time. A small decrease in emission ratio upon phosphorylation and an apparent increase after Gö addition could be seen in both probes.

D Same experiment as in C, however, the trace of non-transfected cells is included. It shows a huge increase in emission ratio in non-transfected cells due to addition of Gö6983.

Cell labeling with fluorescein in experiments using ECFP-KCP-1-AGT or ECFP-KCP-2-AGT worked well and the background to signal ratio was good. Stimulation of PKC activity with PMA led to a small decrease in emission ratio in both probes. Inhibition of PKC activity led to an increase in emission ratio that exceeded basal level (Fig. 4.20 C).

As Gö6983 has a strong orange color, we had to examine whether it was influencing the signal. We analyzed a non-transfected cell that was adjacent to the transfected ones (Fig. 4.20 D). The trace in this experiment increased very strongly after PMA addition. The signal was clearly an artifact due to the color of the inhibitor itself, as no probe was present that could have detected any PKC activity. As fluorescein is not as bright as most genetically encoded FPs, the color of Gö6983 affected the signal more strongly than it did in the original probes. This effect had to be taken into account with all fluorophores, especially if they were further red-shifted than fluorescein, as most chemical fluorophores are not as bright as FPs.

In addition, it was difficult to tell, whether the decrease in emission ratio after phosphorylation in the transfected cells was in fact due to any changes in the probe, or whether it was due to bleaching of the fluorescein. Fluorescein has a relatively high extinction coefficient (68.000 $cm^{-1}M^{-1}$, pH 8), a very good quantum yield (0.9) and is water soluble[283], but it is not very photo-stable[284]. If the acceptor molecule pool decreased due to bleaching, it would also result in a decrease in the fluorescein/ECFP emission ratio. The signal to noise ratio in both traces (Fig. 4.20 C) was very bad compared to the original probes (compare Fig. 4.2 B). This also indicated that, if there was an actual signal, it was very weak and unreliable.

In another set of experiments, we used Citrine[202] (Cit) as a donor and a variety of red dyes as acceptor. These experiments were performed only in KCP-2 probes, as we had previously shown that KCP-1 is more sensitive to changes than KCP-2.

Cy3 is a water soluble cyanine dye (Fig. 4.21 A), which is brighter and more photo-stable than fluorescein. This dye had to be microinjected as it is not cell-permeable. The emissions of Cit and Cy3 are nicely separated, although the excitation of Cy3 and the emission of Cit are not ideally suited for FRET

(Fig. 4.21 C). Cy 3 has a shoulder in its excitation spectra that falls within the excitation of Cit. We still thought it useful to test this pair as the cellular environment always influences the fluorophores and might enable FRET.

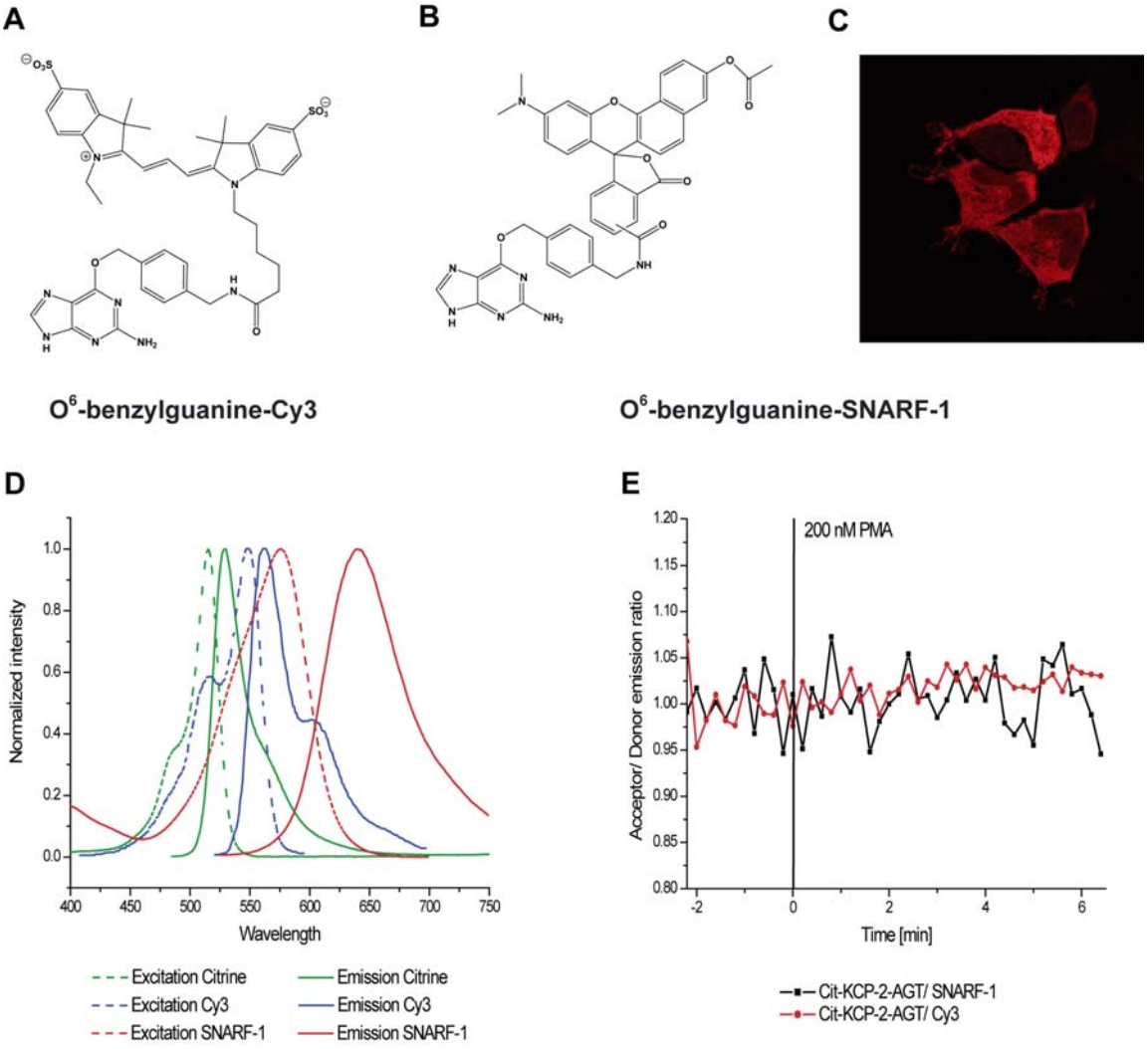

Fig. 4.21 PKC probe using AGT with different labels and Citrine

A Chemical structure of O^6-benzylguanine-Cy3.

B Chemical structure of O^6-benzylguanine-SNARF-1.

C Image of HEK-293 cells transfected with Cit-KCP-2-AGT and labeled with BG-SNARF. Excitation at 594 nm, emission measured from 600 to 660 nm.

D Normalized spectra of the excitation (dashed line) and the emission (solid line) of Citrine (green), Cy3 (blue) and SNARF (red).

E Cells were transfected with Cit-KCP-1(or KCP-2)-AGT and labeled with BG-Cy3 or BG-SNARF before the experiment. PKC activity was stimulated with PMA and the emission ratio was measured over time. No change in acceptor/donor emission ratio could be seen for any probe.

Cells expressing Cit-KCP-2-AGT were microinjected with Cy3 and imaged after 90 min. Cy3 was excited at 561 nm to control labeling of AGT with the

dye. While the labeling worked well, no change in Cy3/Cit emission ratio could be observed after stimulation of PKC with PMA (Fig. 4.21 D, black line).
In a second set of experiments the Cit-KCP-2-AGT construct expressed in HeLa cells was labeled with O^6-benzylguanine-SNARF-1 (BG-SNARF, Fig. 4.21 B). SNARF-1 is a long wavelength PH indicator developed by *Molecular Probes*[283]. Its excitation and emission maxima are quite broad, but Cit could be excited with 488 nm or 514 nm, where SNARF is only excited to a small extent (Fig. 4.21 C).
No change in SNARF/Cit emission ratio could be observed after stimulation of PKC with PMA (Fig. 4.21 D, red line).

One drawback in using AGT is the fact that it – being a full sized protein - is relatively large. We do not know in which orientation relative to the FP the fluorophore is bound to the AGT. It may be that the orientation was making FRET impossible, as the distance between the two fluorophores could be too large for FRET, or the transition dipole moments might not have been arranged in a suitable way.
We tried to circumvent this problem, by using a shorter version of AGT[228]. AGT177 lacks the 28 C-terminal amino acids of the full length human AGT (207 amino acids[285]). These amino acids had previously shown not to be crucial for AGT activity[286]. We wanted to test whether the fluorophore in a shorter version of AGT, would be bound in a more favorable orientation for FRET with respect to the genetically encoded FP.
As donor, we chose GFP^2, as the clear separation between excitation and emission wavelength made exclusive donor excitation possible and reduced acceptor excitation significantly.
The first FRET pair studied with the short AGT construct was GFP^2 and O^6-benzylguanine-tetramethylrhodamine (BG-TMR, Fig. 4.22 A). TMR has an emission maximum at 553 nm and is more photo-stable than fluorescein. The overlap between donor emission and acceptor excitation is not very large, but FRET might still feasible as the donor could be excited without any acceptor excitation. In addition, the two emissions are nicely separated from each other, minimizing bleed-through of one emission into the other.

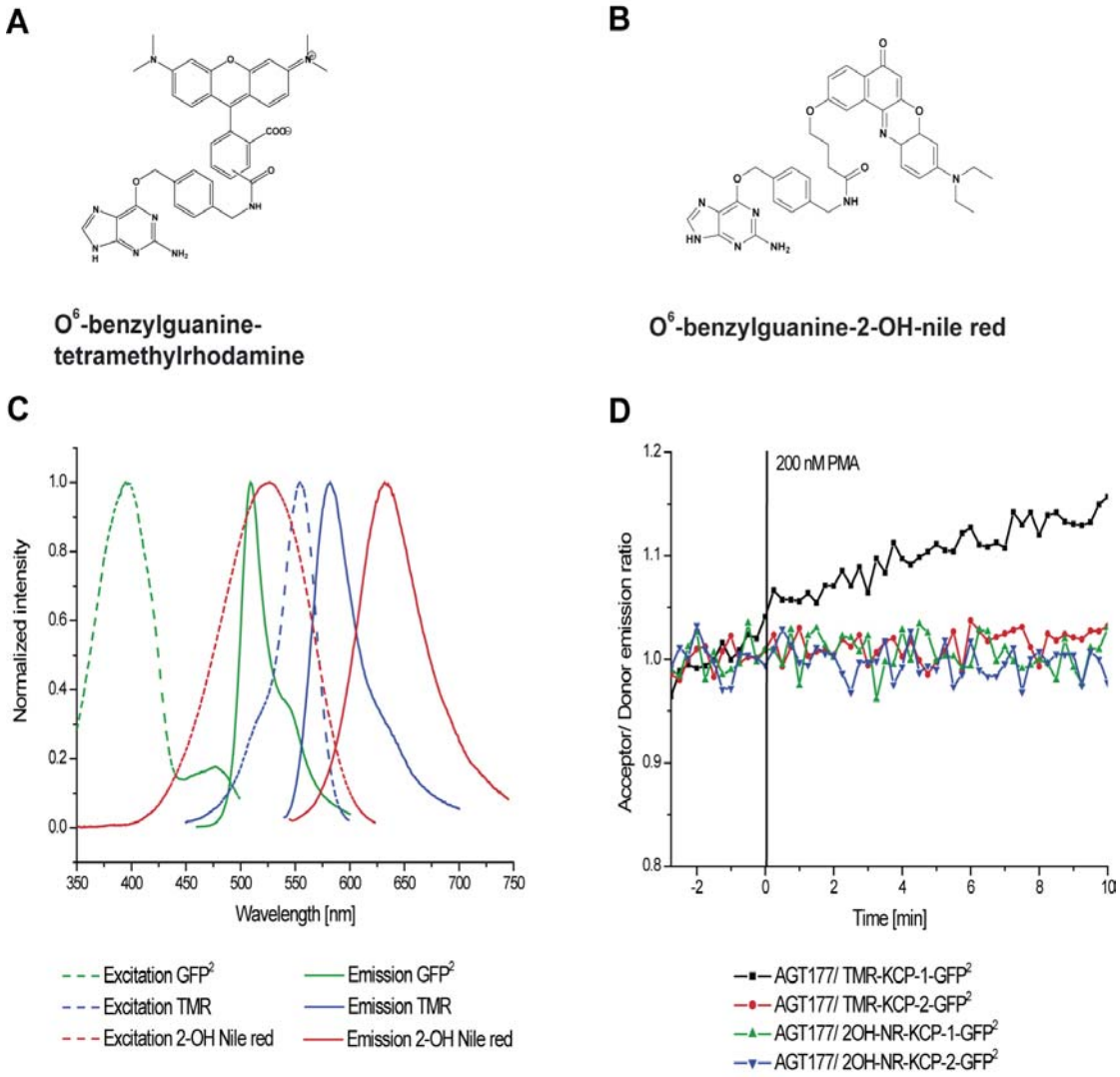

Fig. 4.22 PKC probe using AGT with different labels and GFP^2

A Chemical structure of O^6-benzylguanine-tetramethylrhodamine (BG-TMR)

B Chemical structure of O^6-benzylguanine-2-OH-nile red (BG-NR)

C Normalized spectra of the excitation (dashed line) and the emission (solid line) of GFP^2 (green), TMR (blue) and 2-OH-nile red (red).

D Cells were transfected with GFP^2-KCP^2-1(or KCP-2)-AGT177 and labeled with BG-TMR or BG-NR before the experiment. PKC activity was stimulated with PMA and the emission ratio was measured over time. No change in acceptor/ donor emission ratio could be seen for any probe.

After stimulation of PKC with PMA, no change in TMR/GFP^2 emission ratio could be observed, neither in the KCP-1 derived sample nor in the KCP-2 derived one (Fig. 4.22 D).

The second dye used was O^6-benzylguanine-2-OH-nile red (BG-NR, Fig. 4.22 B), which was synthesized in our lab by Shannon Black. This dye has a broad

excitation band, which covers the emission range of GFP^2 completely. Its emission is red shifted with a maximum at 633 nm (Fig. 4.22 C).

Labeling with BG-NR worked inefficiently compared to the other dyes. The dye was cell permeable, but background labeling was high. In *in vivo* experiments, no change in NR/GFP^2 emission ratio could be seen after stimulation of PKC with PMA, no matter whether the probe was KCP-1 or KCP-2 derived.

Taking all experiments together, it did not seem likely that new PKC probes could be developed using the AGT-labeling technique. The dyes used in these experiments, with the exception of 2-OH Nilered, were all well established for AGT labeling. Cells without donor fluorescence never showed any acceptor fluorescence ruling out unspecific labeling. Unsuccessful labeling of the probe was therefore not expected and probe-intrinsic reasons were responsible for lack of probe performance. Measurements of absolute FRET efficiencies were not performed as no ratio change could be observed.

4.7.2 PKC probes using FlAsH and ECFP

Another method of labeling proteins with chemically synthesized fluorophores is FlAsH labelling[233,287]. A short tetracysteine motif flanked by additional amino acids is introduced at the C- or N-terminus of the protein to be tagged and labeled with FlAsH-EDT_2 (Fig. 4.23 A) before the experiment.
We used an amino acid motif of 12 amino acids with the sequence FLNCCPGCCMEP, which has been shown to have higher fluorescence quantum yields and improved dithiol resistance compared to other tetracysteine motifs[234]. As a FRET partner for FlAsH, we chose ECFP. FRET between these two fluorophores has been previously used in a probe system[178]. Donor emission and acceptor excitation overlap nicely and both emission peaks are sufficiently well separated for ratiometric emission measurement (Fig. 4.23 A).
We expected FRET between ECFP and FlAsH to be possible in our probes as FlAsH bound to the tetracysteine motif is much smaller than a second FP or AGT. This might facilitate a suitable orientation of both fluorophores, thereby allowing for FRET. We also used the monomeric version of ECFP, mCFP, as a donor for FlAsH. We did not expect to see differences in the probes using ECFP or mCFP, as dimerization is not expected to be of major importance in these probes.

The FlAsH labeled KCP-1 probe only gave a small positive response after PKC stimulation. The original KCP-1 probe only showed an increase in EYFP/GFP^2 emission ratio of about 3% in this particular microscope set up (Zeiss Axiovert 135), the mCFP-KCP-1-FlAsH FlAsH/ ECFP ratio increased by 6% (Fig. 4.23 B). The ECFP-KCP-1-FlAsH probe did not show a clear signal, but the ratio increased after addition of PMA and decreased after Gö6983 addition. Bleaching effects seemed much stronger for these probes.
If cloned into the KCP-2 probe, the change in emission ratio was very strong after PKC activation (Fig. 4.23 D). Both samples, using ECFP or mCFP, showed a decrease of 18-20%, which is the same signal as for the original KCP-2 probe. The ECFP-KCP-2-FlAsH probe seemed slightly altered in its

kinetics and more affected by bleaching as the FRET level did not reach basal levels again. This effect was much smaller than in the corresponding KCP-1 sample, though.

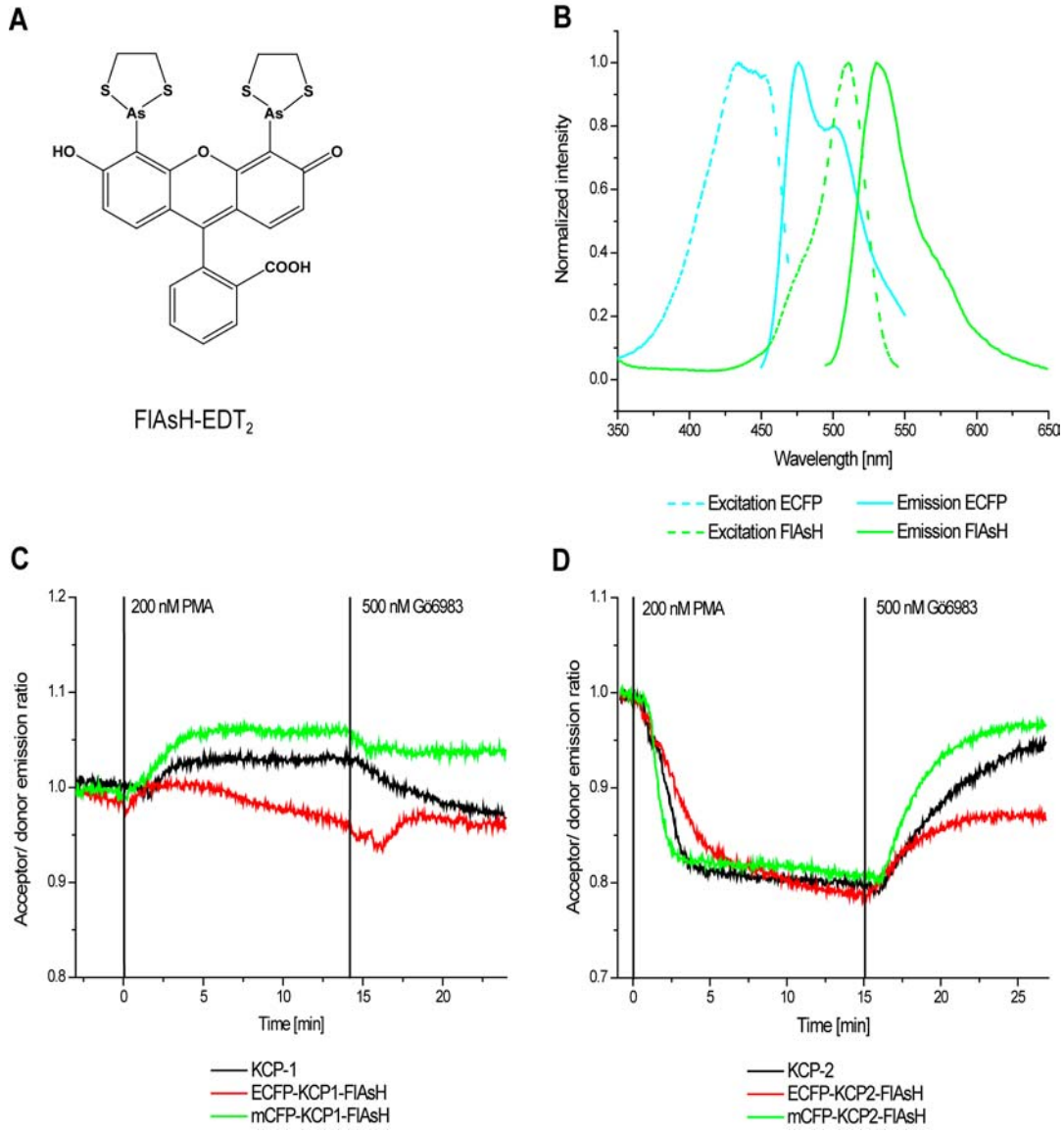

Fig. 4.23 PKC probe using FlAsH and ECFP

A Chemical structure of FlAsH-EDT$_2$.

B Normalized spectra of the excitation (dashed line) and the emission (solid line) of ECFP (cyan) and FlAsH (green).

C Cells were transfected with ECFP(or mCFP)-KCP-1-FlAsH and labeled with FlAsH-EDT$_2$ before the experiment. PKC activity was stimulated with PMA and the FlAsH/ECFP (or mCFP) emission ratio was measured over time. Only a small change could be seen in the original probe and mCFP-KCP-1-FlAsH.

D Cells were transfected with ECFP(mCFP)-KCP-2-FlAsH and labeled with FlAsH-EDT$_2$ before the experiment. PKC activity was stimulated with PMA and the FlAsH/ECFP (mCFP) emission ratio was measured over time. All probes show a clear response to phosphorylation.

We studied the FRET efficiency of the different FlAsH based probes by adding 5 mM BAL (British-Anti-Lewisite, 2,3-dimercapto-1-propanol) to the experiment. BAL is a vicinal dithiol with a higher affinity for arsenicals than EDT or FlAsH. It strips FlAsH off the tetracysteine motif very effectively and leads to recovery of ECFP fluorescence[236].

This can clearly be seen by a very fast and steep decrease in FlAsH fluorescence emission accompanied by a simultaneous increase in ECFP fluorescence at the same time (Fig. 4.24 A). FRET efficiency is calculated as the quotient of the difference in ECFP fluorescence at the beginning of the experiment and after BAL treatment divided by the maximal fluorescence. The start value was taken just before addition of PMA, the maximal value after BAL addition when the curve had reached its maximum.

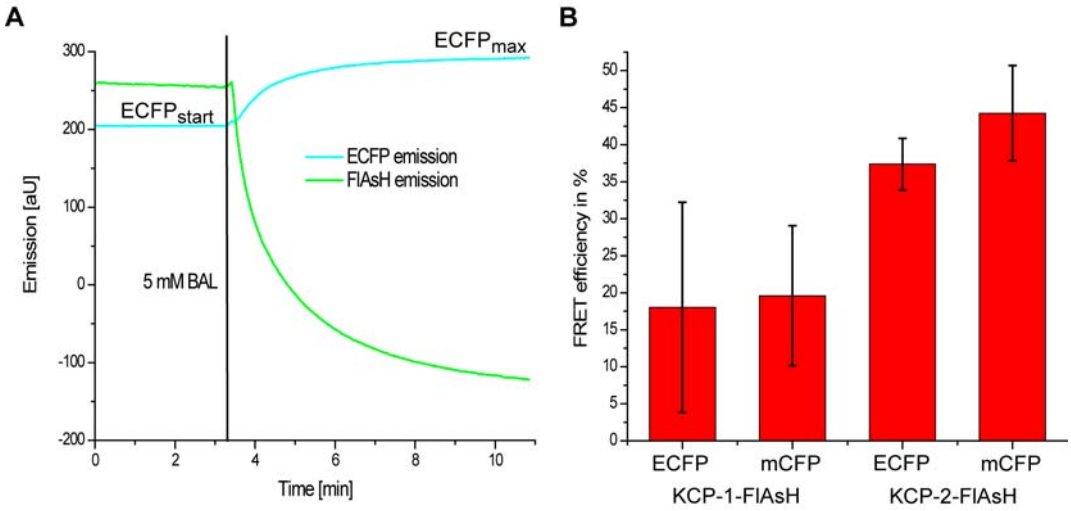

Fig. 4.24 Measurement of FRET efficiency for FlAsH based PKC probes

A Emission channels of EYFP and FlAsH during BAL treatment.

B Comparison of FRET efficiencies determined after BAL addition to the experiment.

Both KCP-1 derived probes had significantly lower FRET efficiency than the KCP-2 derived probes. The ECFP-KCP-1 probe had an efficiency of 18%, while the mCFP-KCP-1 probe had 19.5% (Fig. 4.24 B). For both samples, the error is very high, which corresponds to the results found during live cell experiments, where imaging proved more difficult than with KCP-2 samples. The difference in FRET efficiency between the monomeric and the dimerizing KCP-1-FlAsH probes was not significant.

The FRET efficiency in KCP-2-FlAsH probes showed at least double that of the efficiency in KCP-1-FlAsH probes. The ECFP-KCP-2-FlAsH probe had a FRET efficiency of 37.5%, while the monomeric version had 44.5% (Fig. 4.24 B). The monomeric KCP-2-FlAsH probe had a 15% higher FRET efficiency than ECFP-KCP-2-FlAsH while the difference was only 8% in the monomeric KCP-1 FlAsH probe.

The KCP-2 FlAsH probe is the first example of a FRET based probe combining FlAsH labeling with a genetically encoded fluorophore in the cytosol. We therefore named it KCP-F. KCP-F proves that background labeling of FlAsH in living cells can be small enough for background sensitive applications like FRET. This, however, requires careful optimization of labeling conditions.

5 Discussion

5.1 Models showing the mechanism of action in KCP-1 and KCP-2 probes

Based on the data collected in this work, we are able to present modified models for the mechanism of action of two previously published PKC probes, KCP-1 and KCP-2.

Both models will be introduced at the beginning of this chapter and the implication of all results, in terms of these models, will be discussed subsequently. I will start with the model describing KCP-2.

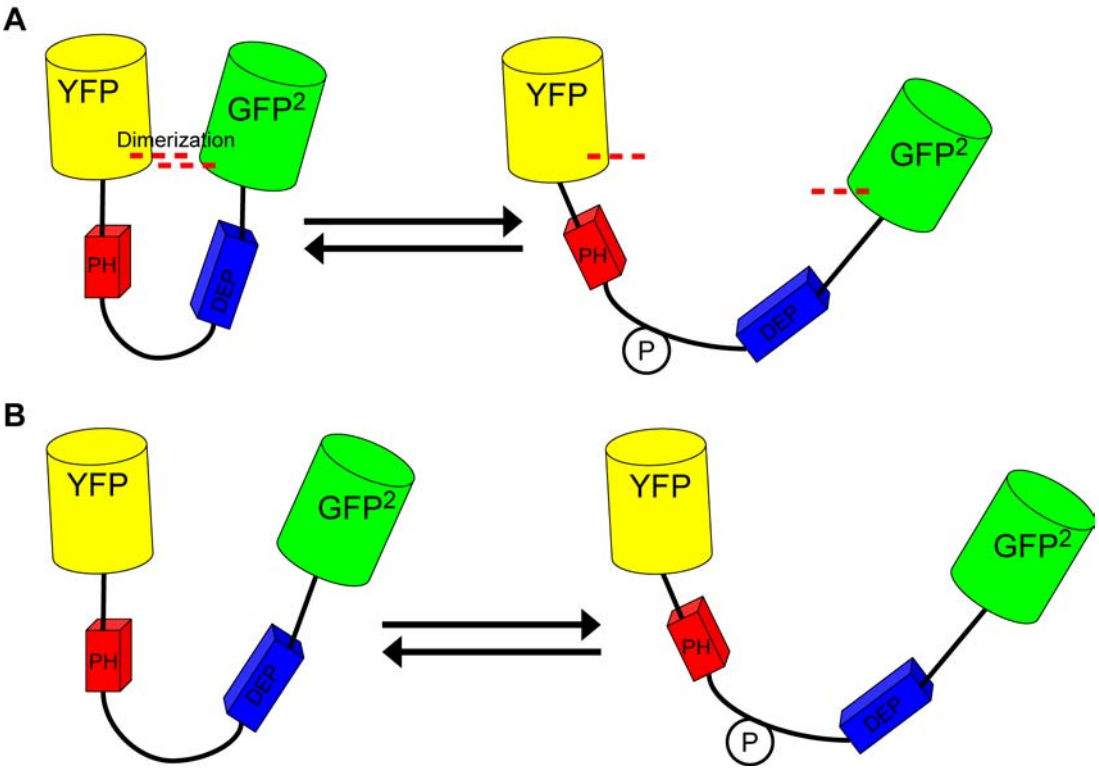

Fig. 5.1 Model for the mechanism of action of KCP-2

A The unphosphorylated KCP-2 probe exhibits high FRET efficiency due to the dimerization of fluorophores, which pulls the probe to a more closed confirmation. Phosphorylation of the probe leads to stretching of the phosphorylation loop, resulting in lower FRET efficiency.

B If dimerization is hindered, the fluorophores are further apart, even in the unphosphorylated probe, and KCP-2 exhibits lower FRET efficiency than before. Phosphorylation of the probe leads to stretching of the phosphorylation loop into the open conformation. As the initial distance was larger, the change in distance from phosphorylated to unphosphorylated is smaller. Hence, the change in emission ratio is smaller as well.

Unphosphorylated KCP-2 displays relatively high FRET efficiency. Phosphorylation of the probe through PKC leads to a decrease in FRET. NMR studies (unpublished data by Bernd Simon, Sattler group, EMBL Heidelberg) of the non-fluorophore-labeled pleckstrin insert of KCP-1, have shown that the unphosphorylated insert adopts a closed conformation (Fig. 5.2).

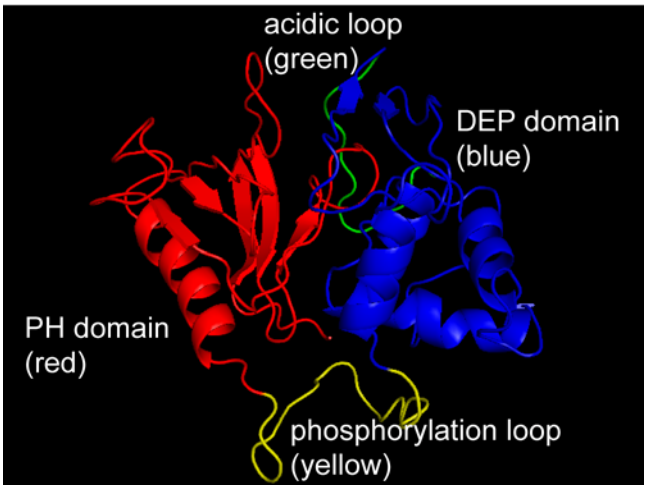

Fig. 5.2 Closed structure of the pleckstrin insert

NMR structure (Sattler group, EMBL Heidelberg) of the non-fluorophore labeled pleckstrin insert in the closed, unphosphorylated conformation. The PH domain is shown in red, the phosphorylation loop in yellow, the DEP domain in blue and the acidic loop in green.

This conformation opens upon phosphorylation and the pleckstrin insert assumes a more stretched conformation. This leads to an increase in the distance between the PH and DEP domain, which in turn also increases the distance between the fluorophores. FRET data obtained with KCP-2 support these NMR data, as the FRET efficiency is reduced after phosphorylation.

In this thesis, we have shown that there is an additional important element for good probe performance. Dimerization of fluorophores leads to a closer conformation of the domains than seen in the NMR data. According to the model proposed in this thesis, phosphorylation, and the subsequent conformational change in the phosphorylation loop, breaks the dimerization force, the probe opens up and adopts an open confirmation (Fig. 5.1 A). If we abolish the ability of the fluorophores to dimerize, they are already on average further apart in the initial conformation than in the original KCP-2 probe. The change in distance upon phosphorylation is therefore smaller, which results in a smaller change in the EYFP/GFP^2 emission ratio.

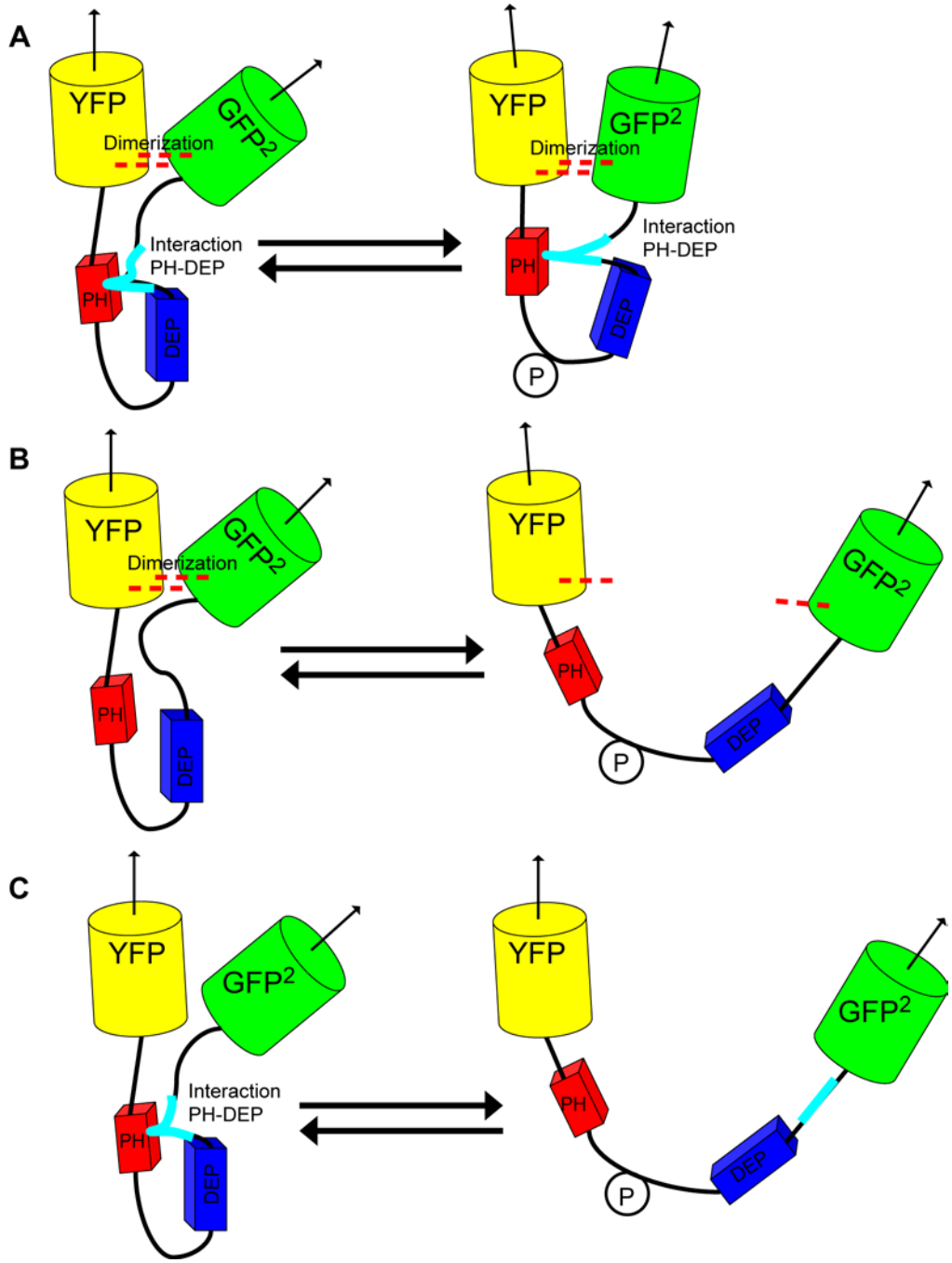

Fig. 5.3 Model for the mechanism of action of KCP-1

A Two forces determine the architecture of KCP-1, dimerization of the fluorophores and an interaction between the PH and the DEP domain. The second interaction leads to a different orientation of the fluorophores compared to KCP-2, resulting in lower FRET efficiency. Phosphorylation leads to a conformational change that rearranges the transition dipole moment of the fluorophores and leads to an increase in FRET efficiency.

B If the PH-DEP interaction is disturbed (by changes in the PH domain), phosphorylation breaks the remaining dimerization force and the molecule opens up. This leads to reduced FRET efficiency after phosphorylation.

C If the fluorophores are no longer able to dimerize, phosphorylation breaks the remaining PH-DEP interaction and the molecule opens up. This leads to reduced FRET efficiency after phosphorylation. *The orientation of the transition dipole is indicated by an arrow in all models.*

In our present model, fluorophore dimerization is only one of two forces determining the conformation of KCP-1 (Fig. 5.3 A). When imaging KCP-1 in living cells, we see an increase in FRET upon PKC activation. This indicates that the fluorophores are better positioned for FRET after phosphorylation than before, either due to distance or to relative orientation of the transition dipole moments. The only difference between KCP-1 and KCP-2 is the acidic loop of the DEP domain. We assume that this loop is responsible for the additional interaction, presumably by interacting with the PH domain (Fig. 5.3 A). This PH-acidic loop interaction leads to a less favorable orientation of the transition dipole moments of the fluorophores, which results in lower initial FRET efficiency. Phosphorylation of the probe rearranges the structure of the phosphorylation loop, but it does not lead to a separation of fluorophores. Instead, the transition dipole moments of the fluorophores are changed to a more favorable orientation than in the unphosphorylated state. The force exerted by the phosphorylation is not enough to break the combined forces of dimerization and PH-DEP interaction. Instead, the force is deviated into rearranging the orientation of the fluorophores (Fig. 5.3 A).
If one of the two interactions is missing in KCP-1, the phosphorylation-induced rearrangement is strong enough to break the remaining bond and the probe opens up resulting in a loss of FRET efficiency (Fig. 5.3 B and C). KCP-1 with only one intramolecular interaction (e.g. KCP-1 probes with monomeric fluorophores) behaves like KCP-2: the EYFP/GFP^2 emission ratio decreases upon phosphorylation.

5.2 Variations in the N-terminal linker region

5.2.1 Additional amino acids in the N-terminal linker region

Addition of amino acids in the N-terminal linker region has an impact on both probes, KCP-1 and KCP-2 (Fig. 4.3 and Fig. 4.4). In KCP-2, this is straightforward to explain. Increased linker length leads to an increase in the distance between the two fluorophores and thereby decreases initial FRET between them. The change in emission ratio after phosphorylation of the longer KCP-2 probes is still between 65-105% of the change in the original probe. The effect is relatively small as the dimerization of fluorophores still

functions as a clamp, holding the FPs in a closed confirmation. If dimerization is hindered, on the other hand, the change in emission ratio of the monomeric probes is only 40-43% of the original probe (Fig. 4.14), showing the greater importance of dimerization as compared to linker length.

The KCP-1 probe is more sensitive to additional linker length. Addition of ten amino acids leads to near abolishment of probe function, while KCP-2 still keeps 65% of its performance. KCP-1 is more sensitive to changes than KCP-2, as two forces – dimerization and PH-DEP interaction - act on the probe. If additional amino acids are introduced in the linker region between EYFP and the pleckstrin insert, an additional strain is introduced. The additional amino acids have to be accomodated in the linker, leading to less ideal spacing of both interaction sites. This strain is stronger the more residues are added. There is an equilibrium between the functional and non-functional probes, where part of the molecules display the normal KCP-1 signal, while others do not. Introduction of three amino acids has no effect, while six additional residues already lead to a reduced probe performance of 40-50%. Introduction of more than six amino acids shifts the equilibrium towards the non-functional probes and the overall signal upon phosphorylation is even lower. If 12 residues are added, the strain on the both interactions upon phosphorylation is so strong that they brake apart in most probes. The signal of the probe reverses its amplitude and is now similar to KCP-2.

Justin Brumbaugh performed similar experiments in the C-terminal linker region of KCP-1[2]. He introduced a linker of 10 amino acids between the acidic loop and the C-terminal GFP[2]. These probes, however, displayed normal KCP-1 signals upon phosphorylation by PKC. Apparently, the C-terminal linker is flexible enough to allow for both interactions to still take place.

5.2.2 Deletion of amino acids in the N-terminal linker region

If additional amino acids influence the signal of KCP-1 and KCP-2 probes, shortening of the linker might also have an impact on probe performance.

Deletion of residues at the C-terminus of EYFP leads to decreased probe performance in both probes (Fig. 4.6 and Fig. 4.7). YFPΔ8KCP-1 still retains 65% of the original performance, while YFPΔ8KCP-2 retains 55%. We

suggest that reducing the linker at the end of EYFP has effects on the orientation of the fluorophores in both probes. The amino acids responsible for dimerization are located quite close to the C-terminus of the FP (A^{206}, L^{221} and F^{223} in a protein of 239 residues). In order to still allow dimerization in the shorter probes, the angle of the FPs in relation to each other must change. Shortening the linker reduces the flexibility needed for dimerization and thereby changes the transition dipole moment in KCP-2 to a less favorable position and weakens the dimerization. Weaker dimerization shifts the equilibrium more towards the open conformation, which results in a smaller signal than in the original probe.

In KCP-1, the additional strain introduced by shortening the probe leads to breakdown of both interactions in some molecules, reducing the ratio of functional to non-functional probes. The equilibrium, however, is still on the side of the functional molecules, leading to a probe performance that is still relatively high. This is similar to the results in probes with very long linkers.

Deletion of the first seven amino acids of the PH domain has an effect on the function and structure of this domain. In KCP-1, it destroys one of the two crucial interactions: the PH-DEP interaction (Fig. 5.3 C). The probe now is similar to KCP-2 and the FRET ratio decreases upon phosphorylation. The initial FRET efficiency is higher in this probe compared with KCP-1 (Fig. 5.4), indicating that it is more similar to KCP-2.

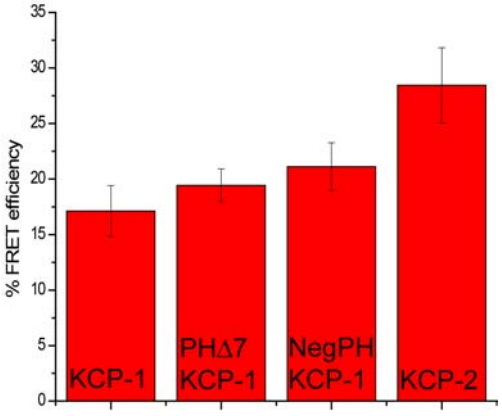

Fig. 5.4 Initial FRET efficiencies of KCP-1 and KCP-2 in comparison with KCP-1 probes that have a changed PH domain

Besides disturbing the PH-DEP domain interaction, deletion of amino acids will also generally affect the PH domain and therefore lead to reduced probe

performance (Fig. 4.7 and Fig. 4.10). In particular, Arg^7 might be crucial for the overall architecture of the PH domain as it is part of a β-sheet that interacts with an α-helix in the domain. Changes in the PH domain are likely to have effects, besides influencing the PH-DEP interaction. Firstly, the domain architecture is disturbed. The N-terminal PH domain of pleckstrin is known to be involved in both, protein-protein and protein-lipid interactions[143,288-290]. Changes in its architecture could therefore alter those interactions and lead to decreased phosphorylation of the probe. Secondly, the changed PH domain architecture will influence the orientation of the fluorophores to each other. These two effects, induced by changes in the PH domain, are also relevant KCP-2. In KCP-2, deleting the first seven amino acids of the PH domain leads to a signal similar to YFPΔ8KCP-2. The N-terminal linker region of KCP-2, while less sensitive to elongations (Fig. 4.4 A), is relatively sensitive to shortening (Fig. 4.7 A). As discussed above, a possible explanation is that a longer linker is still flexible enough to allow proper dimerization in KCP-2, while a shortened linker reduces this flexibility. If the two molecules are not set correctly, the interaction is too loose and the resulting change in emission ratio is small (compare Fig. 5.1 B). It is important to note, however, that the major impact in PHΔ7KCP-2, is the disturbance of the PH domain, not shortening of the linker. As will be discussed in the following paragraphs, the integrity of the PH domain is important also for proper performance in KCP-2 probes.

5.2.3 Changes in the charge distribution of the PH domain

In our initial model, we assume that the interaction between the PH domain and acidic loop is based on charges. We suspected that aspartates and glutamates in the acidic loop were interacting with the basic residues at the start of the PH domain. In KCP-2, exchanging the basic residues with neutral ones (NeutKCP-2, Fig. 4.9 A), reduces the probe performance to 58% of the signal of the original probe. This is similar to the effect observed in the shorter probes, YFPΔ8KCP-2 and PHΔ7KCP-2, where the probes only exhibited 54% of the original signal. From our model for the mechanism of action of KCP-2, we would not expect large changes in the probe's performance when

introducing mutations in the PH domain, since we expect the mechanism to be independent of a PH-DEP interaction. We have to consider, however, that the overall architecture of the PH domain is disturbed, resulting in an altered orientation of the fluorophores. Introducing negative charges will disturb the domain architecture even more severely than introducing neutral residues. The EYFP/GFP^2 emission ratio for NegKCP-2 decreases upon phosphorylation of the probe. The signal exhibits an apparent 78% of the original probe's performance, however, it does not go back to basal level after inhibition of PKC but stays at a significantly lower level. The fact, that the probe's performance is no longer reversible indicates severe changes have occurred in the overall architecture of the probe.

In NeutPHKCP-1, the neutral amino acids have a similar effect as seen in the shorter probe, YFPΔ8 KCP-1. The signal is decreased showing only 60% of the original KCP-1 signal. If the same amino acids are replaced with negative residues, the effect is much stronger. The signal reverses and shows a decrease in FRET ratio upon phosphorylation. This could be expected since we are destroying one of the two crucial interactions in KCP-1 (Fig. 5.3) and thereby making it more similar to KCP-2. We would also expect the initial FRET to be higher than in KCP-1, as the orientation of the fluorophores should be more KCP-2-like due to the disturbed PH-DEP interaction. Indeed, the initial FRET efficiency is higher in the NegKCP-1 probe, than in the original probe, reflecting an overall structure that is more similar to KCP-2. NegKCP-1 has a FRET efficiency that is 4 percentage points higher than the original probe. In YFPΔ8KCP-1, the FRET efficiency is 2.5 percentage points higher (Fig. 5.4). Introducing neutral residues at the beginning of the PH domain has an effect on the architecture of the PH domain and will probably disturb the PH-DEP interaction. Introducing negative charges has a stronger effect, since they disturb this interaction even more severely. As in NegPHKCP-2, we see that the NegKCP-1 probe no longer reaches basal level anymore after inhibition of PKC activity. Again, the probes architecture seems to have been thoroughly disturbed.

As we observed a big impact of negative charges on the probes performance, we tested whether it could be rescued by introducing positive charges in the acidic loop. If the probe depended on charge-charge interactions, this should

yield a functional KCP-1 probe. We created constructs that had positive charges in the acidic loop but negative charges in the PH domain. Fig. 4.11 A shows that the interaction between PH and DEP domain does not rely on this particular charge distribution. Using complementary charges (positive in acidic loop and negative in PH domain) did not re-establish the KCP-1 probe function. Instead, the neutral probes (NeutKCP-1RR$^{227/228}$ and NeutKCP-1RR$^{232-234}$) gave a signal similar to NeutKCP-1, while the negative probes (NegKCP-1RR$^{227/228}$ and NegKCP-1RR$^{232-234}$) displayed a decrease in emission ratio comparable to NegKCP-1 (Fig. 4.11). Again, reversibility was not given anymore in the negative probes, showing the severe impact of the changes on the probe. The fact that the complementation probes were not able to rescue a KCP-1 like behavior rules out a simple charge-charge interaction.

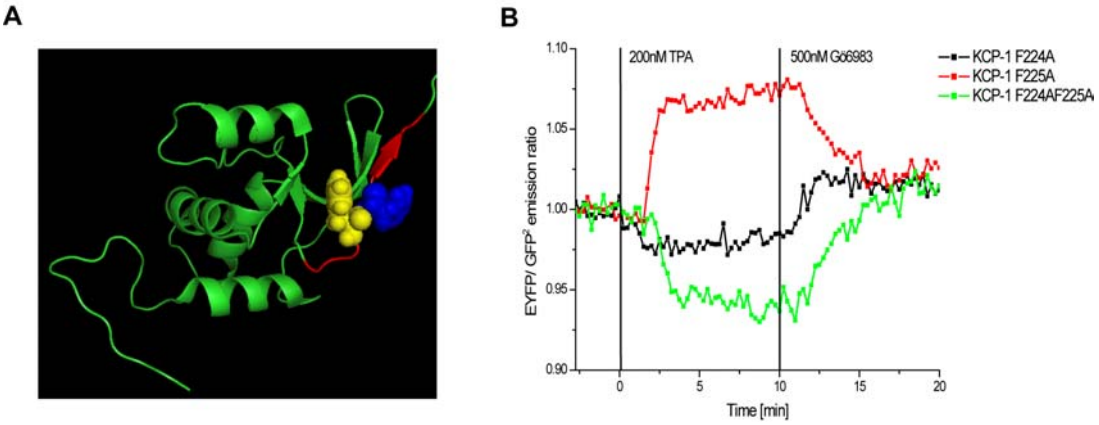

Fig. 5.5 Recent NMR structure of the DEP domain of human pleckstrin

A Solution structure of human the DEP domain from human pleckstrin, solved by NMR (PDB no 1CSO by Yokoyama *et al*). Residues 221 to 229 are shown in red, residues F^{224} and F^{225} are shown in blue and yellow (numbering according to numbering in this thesis).

B Residues F^{224} and F^{225} were replaced by alanines. The response is a KCP-1 like response, if only F225A is present (red line), but it is KCP-2 like if F224A is introduced (black line). The response is also KCP-2 like, if both mutations are present in the molecule (green line). Experiments were performed by Justin Brumbaugh.

A recent structure of the DEP domain has given important clues as to the nature of the PH-DEP interaction. The NMR structure of the DEP domain (PDB no 1CSO, to be published) was deposited in the protein data bank by S. Yokoyama *et al* (RIKEN Structural Genomics/Proteomics Initiative, Japan) in November 2005. The structure defines the DEP domain as slightly longer on both, the C- and N-termini, than the structure previously used by the Sattler

group (Fig. 5.2). Residues 221 to 229 are an integral part of the DEP domain, according to the more recent structure (see Fig. 5.5 A and B).

Using the new NMR data, the structure of the closed pleckstrin insert could be re-calculated. The new calculations show that F^{225} interacts with a β-finger inside the DEP domain, while F^{224} packs into the PH domain. F^{224} is therefore likely to form part of the PH-DEP interaction in KCP-1 probes. This was confirmed by recent experiments in our lab (performed by Justin Brumbaugh). If F^{224} is mutated to alanine, the PH-DEP interaction is severely disturbed and the KCP-1 probe acts as a KCP-2 probe, exhibiting a negative change in emission ratio upon PKC activation (Fig. 5.5, black line). Mutation of F^{225} to alanine does not change the direction of the signal (Fig. 5.5, red line). Introduction of F224A inevitably leads to reversal of the signal, independent of whether F225 is mutated or not (Fig. 5.5, green line). These experiments identify residue F^{224} as crucial for determining the PH-DEP interaction in KCP-1 and clearly show that it is not charge-charge but hydrophobic interactions, which are responsible for the PH-DEP interaction. While confirming the NMR data, they also explain why replacing the charges could not restore a KCP-1 like signal.

The NMR structure by Yokoyama *et al* also shows that residues after 229 are not important for the overall structure. Any changes after residue 229 are less likely to have a strong effect on KCP-1 probes, while changes before that residue will severely impair the interaction of the PH and DEP domain. This was confirmed by experiments performed in our lab, which showed that mutations or deletions of amino acids after 229 still yield a functional KCP-1 probe (experiments performed by Justin Brumbaugh). It was also confirmed by the experiments using complementary charges in the acidic loop and the PH domain (Fig. 4.11 A). The direction of the signal is determined by whether the residues at the beginning of the PH domain are neutral or negative. Neutral residues will lead to a positive but reduced response upon phosphorylation as the architecture of the PH domain is slightly disturbed. Negative residues will lead to a negative response, as the PH domain, and therefore the PH-DEP domain interaction, is severely perturbed. The amplitude of the respective signals, however, is modulated by which amino acids in the acidic loop have been replaced by arginines. Replacement of

residues 232-234 has a less pronounced effect than replacement of residues 227 and 228. This corresponds to the findings that amino acids after 229 are not crucial for DEP domain architecture, while those before 229 are essential.
It is important to point out that the acidic loop is an intrinsic part of the DEP domain, not an additional feature of KCP-1. KCP-2 always has a disturbed PH-DEP domain interaction due to it having an incomplete DEP domain.

5.3 Effect of fluorophore dimerization on KCP-1 and KCP-2

The monomeric versions of both constructs show significantly reduced probe performance. Their signals are so weak that they are unsuitable for routine experiments. Monomeric KCP-1 samples show not only a decrease in signal amplitude but also a reversal of the signal direction upon phosphorylation. As illustrated in Fig. 5.1, the dimerization of the two fluorophores in KCP-2 functions as a clamp, pulling them into a better orientation for FRET. If that interaction is missing, the fluorophores are on average further apart in the unphosphorylated state than they would be in the KCP-2 probe with dimerizing fluorophores. The change in distance upon going from the closed to the open conformation upon phosphorylation is not as pronounced anymore.
In our model, dimerization is one of two forces determining the conformation of the probe molecule in KCP-1 (Fig. 5.3). The additional force in KCP-1, as compared to KCP-2, results in a different orientation of the fluorophores in the unphosphorylated probe. Subsequent phosphorylation does not lead to a greater distance between the fluorophores but to a rearrangement of the fluorophores resulting in a better orientation of the transition dipole and hence a higher FRET efficiency. If one of the two forces, e.g. dimerization or the PH-DEP interaction, is broken, the probe behaves like KCP-2 and opens upon phosphorylation.
It does not matter which of the fluorophores are monomeric, since the hydrophobic patch has to be present in both molecules for dimerization.
Using other monomeric proteins, such as mCherry or mOrange (Fig. 4.15 B), is inefficient for the same reasons. Without the potential for dimerization, the probes could, at most, exhibit a very low FRET efficiency. Alen Piljić, in the

group, showed that the efficiency of mCherry and mOrange as a FRET pair is much smaller than ECFP/EYFP. While the FRET pair ECFP/EYFP in his assay displayed an emission change of a 150%[281], the change was only 25-30% when using mOrange/mCherry. These results indicate that the mCherry/mOrange FRET pair probably has a much smaller R_0 than EYFP/ECFP. If we transpose this to the KCP probes, we would expect to see a signal, where the amplitude is about 1/5 of the signal for the monomeric probes. In KCP-1, this would mean a signal of about 0.5%, in KCP-2 a signal of about 1.2%. These signals are too small to be measured efficiently. It is therefore not surprising that we could not use the mOrange/mCherry FRET pair for this probe.

5.4 FRET efficiency of selected constructs

Comparing the results obtained in live cell imaging with the results from AccPB (Fig. 4.16 A) we have to conclude that there are limitations to the AccPB method when analyzing small changes in FRET efficiency. Although most of the monomeric probes show a slightly higher FRET efficiency before phosphorylation, the results are not as consistent as the live cell data. Phosphate groups are prone to detaching from the probe even if probes were measured on the same day. This leads to a higher observed FRET efficiency than we would expect in phosphorylated, monomeric probes. Experiments with KCP-1 and KCP-2 show the susceptibility of phosphates for detaching. If FRET efficiencies were measured on the same day, both original probes show clear differences in FRET efficiency, corresponding to the live cell experiments. If, however, the same sample was measured on the next day, we see a different result for both probes. The FRET efficiency of KCP-1 is smaller after phosphorylation than it used to be the day before. The FRET efficiency of phosphorylated KCP-2 is higher than it was the day before. Both of these results indicate that some of the phosphates have detached. As the changes, when going from the unphosphorylated to the phosphorylated probes, are much smaller in the monomeric constructs, they are more sensitive to this effect.

5.5 Intra- versus intermolecular FRET in KCP-1 and KCP-2

Knowing the importance of fluorophore dimerization for probe performance, it was necessary to verify that FRET was taking place within the molecule and not with adjacent molecules. We could clearly show for the KCP probes, the FRET observed was a result of intramolecular and not intermolecular energy transfer. We set up two different experiments where FRET between fluorophores of one molecule was impossible but could still occur between FPs from different probe molecules. No change in FRET ratios could be detected upon phosphorylation, or subsequent dephosphorylation of the probes. The initial FRET efficiency in these probes was close to zero.

Even though the possibility of intermolecular FRET had to be assessed, it is not very likely to take place. The fluorescent proteins from *A. victoria* form dimers, although relatively weak ones with a K_D of 0.11 mM[270]. It is plausible, that dimerization takes place within one molecule but it seems less likely to extend to other molecules as well. The fact that the dimerization force is overcome by phosphorylation is another indication of its relative weakness.

5.6 Changing the FRET pair in PKC probes

Changing the FRET pair in PKC probes is desirable for multiparameter imaging and wider application of the probe. As we have extensively discussed in the paragraphs above, dimerization is crucial for probe performance.

Previous experiments in the lab[282] had shown that a KCP-2 probe with ECFP and Citrine showed a reduced signal amplitude, while KCP-1 with ECFP and Citrine did not work at all. This was very surprising as these fluorophores are otherwise known to be a very good FRET pair. When designing FRET probes, it is desirable to have a large Förster radius for the FRET pair used. R_0 for the EYFP and ECFP pair has been reported to be 4.92 nm, R_0 for EYFP and GFP[2] 5.64 nm (R_0 of EYFP/GFP[2] was assumed to be the same as for EYFP/GFP as the donor emission/acceptor excitation overlap is the same)[223]. The difference in FRET efficiency at different distances for two Förster radiuses (4.9 corresponding to EYFP/ECFP and 5.6 corresponding

toEYFP/GFP[2]) has been plotted in Fig. 5.6. The reduced R_0 explains the smaller signal in KCP-2, but not the lack in signal in KCP-1. It is likely that the transition dipole in ECFP is different from GFP[2]. This might result in a different rearrangement of the relative orientations after phosphorylation of the probe that is not favorable for FRET anymore.

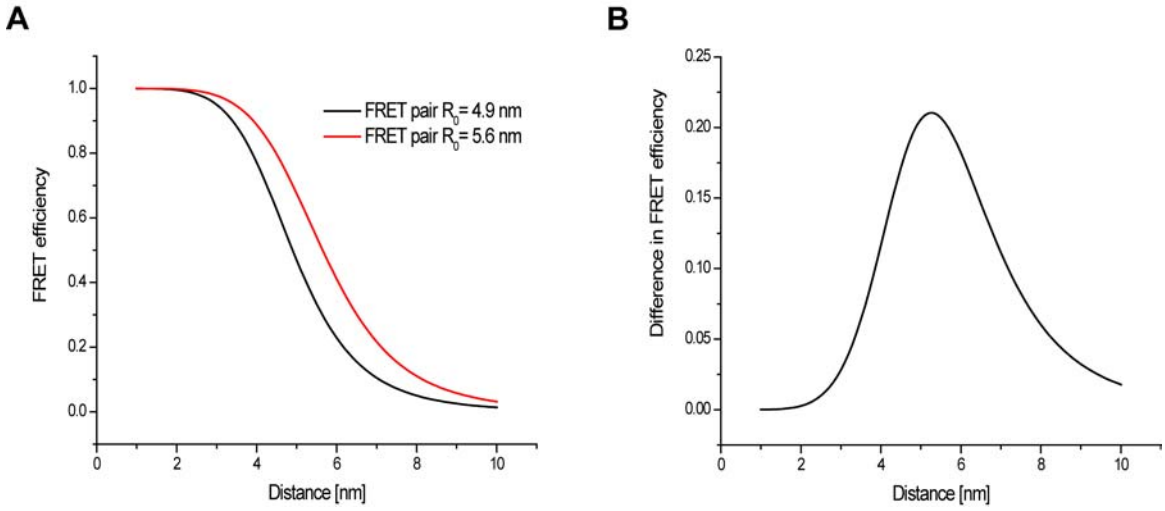

Fig. 5.6 Dependence of FRET efficiency for different R_0 at distances from 1-10 nm

While the difference in R_0 for the two FRET pairs might not be crucial in other assays, it has a big impact in our PKC probes. We have previously seen that the probes are very sensitive to changes in their architecture and in the orientation of the fluorophores with respect to each other. It is therefore not surprising that they need a FRET pair with relatively high Förster radius.

It is also not surprising that none of the probes combining AGT and a genetically encoded fluorophore yielded usable results. AGT with a bound fluorophore is only slightly smaller than GFP. The orientation of the chemical dye bound to AGT relative to the FP can vary greatly. It is not pulled in a closer orientation, as AGT cannot dimerize with FPs. The maximum response we could have expected, when using AGT labeled with a dye is about the same response as for the monomeric KCP-1 or KCP-2 probes. Even this result could only be observed if the dye were bound to AGT in a way that optimizes the relative orientation for the FP and the dye. This was obviously not the case, as we could not see any changes in emission ratio in the probes,

even when using ECFP and fluorescein, which are otherwise known to work as a FRET pair.

The situation is different when looking at the FRET based probe based on ECFP and FlAsH. FlAsH, bound to the tetracysteine motif, is so small that dimerization no longer plays a role as it can get very close to the other fluorophore (Fig. 5.7).

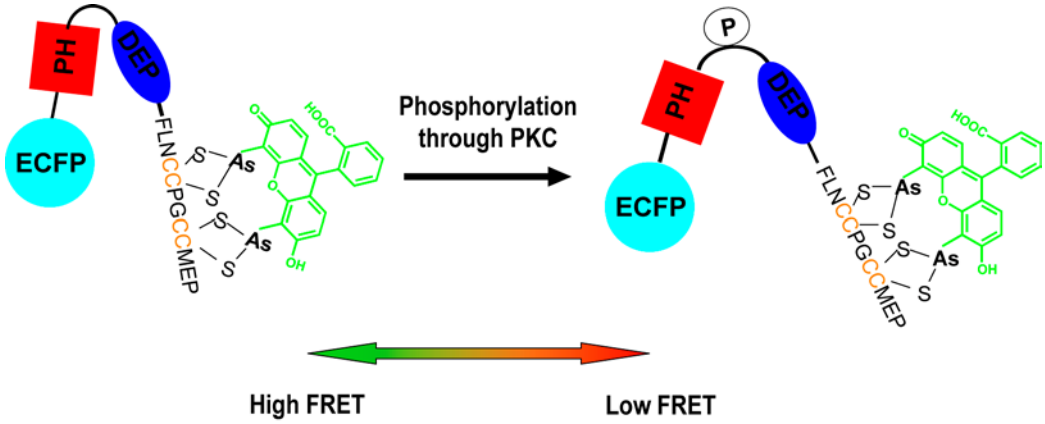

Fig. 5.7 Model for the mechanism of action on KCP-F

Unphosphorylated KCP-F is in a closed conformation with high initial FRET efficiency. Phosphorylation of the probe by PKC leads to stretching of the pleckstrin insert and greater distance between the two fluorophores. The FRET efficiency therefore decreases.

The PKC probe based on the FlAsH/ECFP FRET pair (KCP-F) is the first cytosolic FlAsH based FRET probe known so far. Only one other FRET probe using FlAsH has so far been published (Hoffmann *et al*[178]). This probe measures activation of G protein coupled receptors (GPCR) in living cells via FRET. FlAsH labeling has usually been used for the for the labeling of cellular substructures that have a very high concentration of tagged protein, e.g. connexins[237], as this labeling is not generally very efficient. We have been able to show that using FlAsH is a valuable alternative to FP based FRET, even in a cytosolic environment. This is important for probe design, as the small size of FlAsH makes it a better label for most applications[291]. The study by C. Hoffmann *et al*[178], also imaged GPCR activation using ECFP/EYFP as a FRET pair. This however, caused the downstream signaling to adenylyl cyclase to be perturbed. This problem was overcome by using the small tetracysteine tag and FlAsH. An additional advantage of FlAsH compared to FPs, is that it does not require any folding or maturation time. FP folding is not

instantaneous, which might influence the protein of interest even more than the size. This problem has, however, been greatly reduced in the new generation of fluorescent proteins.

The reduced molecular size of KCP-F makes NMR analysis of the molecule possible. This will allow thorough understanding of the probe and will elucidate the probes' mechanism of action on a molecular level. This will be done in collaboration with M. Sattler at EMBL in Heidelberg.

6 Conclusions

In the work presented in this thesis, we have investigated different aspects of protein kinase C probe performance.

We were able to present improved models for the conformational switch of two previously published PKC probes, KCP-1 and KCP-2. In these models, we were able to demonstrate that dimerization of fluorophores can be used as a tool for increased probe performance. This is in contrast to the previously widely accepted view that fluorophore dimerization was a major caveat when using fluorescent proteins[271]. Dimerization can produce artifacts, but it can also be helpful for developing new probes. In our probes, no artifacts from dimerization were observed. Whether dimerization is foe or friend has to be individually decided for each application.

Care has to be taken when influencing interactions within the probe molecule. In our probes, changes in the PH domain significantly affected probe performance, suggesting a previously undefined molecular interaction in the pleckstrin insert. Intramolecular structures, stemming e.g. from the substrate, and their impact on probe performance have to be considered, but can also be used to obtain information about the substrate proteins' function.

In addition, we demonstrated that linker length between the substrate loop for PKC phosphorylation and the N-terminal fluorophore determines good probe performance. While long linkers are too flexible for efficient energy transfer between two fluorophores, short linkers might be too stiff. This again, depends on the individual application and needs to be examined on a case by case basis.

The newly developed FlAsH based FRET probe, KCP-F, proves that FlAsH labeling is a useful addition to the arsenal of FRET probes. Its small size, compared to FPs, make it less likely to interfere with protein function. The small size of the probe will permit structural analysis of the probe by NMR in the future.

The resulting data will allow thorough understanding of the mechanism of action of pleckstrin-based PKC probes. Based on this information, existing probes might be improved and new probes developed.

7 Outlook

We were able to show that dimerization of the fluorophores is not *per se* a problem for probe development. In fact, it can be utilized to increase the signal amplitude by clamping the fluorophores in a favorable position for FRET. In our KCP-2 probe, for example, the initial FRET efficiency could be increased by 10% when using dimerizing fluorophores. This could be exploited in probes with weakly defined conformational changes locking either the initial or the final structure into a state where the fluorophores are in close proximity. In our case, we demonstrated that the concentration of the probes was not high enough to result in intramolecular FRET as a result of fluorophore dimerization. One should consider developing other molecular clamps to serve the same purpose. This would not be easy, however, as a balance has to be maintained with the interaction acting as a clamp but not dominating the protein structure. The weak dimerization of *A. victoria* FPs seems to be ideally suited for this purpose.

Thus far, we have gathered a wealth of information about KCP-1 and KCP-2 probes based on mutational analysis ([1,2], this thesis and unpublished work by Justin Brumbaugh). An in depth understanding of the structure-activity relationship inevitably requires a high resolution structure. The KCP probes, containing two full sized FPs (27 kD each), are too big for NMR analysis. The newly developed KCP-F probe has a size more suited to NMR studies. The structure will be solved in collaboration with M. Sattler's group at EMBL, Heidelberg. This will allow comparison of the structural and mutational data. Combining structural and mutational data might facilitate the design of probe variants with greatly improved signal, which could then be suitable for high throughput screening for PKC inhibitors.

Having established the feasibility of a FlAsH based probe opens the possibility of using EYFP and ReAsH has a FRET pair. This would be a first step towards shifting the probes emission to longer wavelengths. As mentioned previously, this is important for multiparameter and deep tissue imaging. Another approach would be to use other weakly dimeric FPs with different photophysical properties.

The spatial resolution of PKC signal detection could be increased even further by combing an EYFP/ReAsH probe with electron microscopy (EM). In a method developed by M. Ellisman's group[237], proteins labeled with ReAsH could be used for photoconversion of diaminobenzidine (DAB). The dye-catalyzed formation of singlet oxygen causes highly localized polymerization of DAB to an insoluble osmiophilic precipitate, visible by EM.

There is indirect evidence[282] that KCP-1 and CKAR, a PKC probe developed in R. Tsien's laboratory[119], have differing isoenzymes specificity. This will be verified by using isoenzyme-specific inhibitors. Isoenzyme specific probes would be a valuable tool for elucidating the involvement of certain isoforms in specific pathways or different subcellular locations. It is likely that existing probes are phosphorylated by several PKCs but they might be able to be tailored towards greater specificity.

The emission ratio in probes that had severely altered PH domains (NegKCP-1 and NegKCP-2) did not return to basal levels after phosphorylation and subsequent dephosphorylation. The fact that reversibility is no longer given for some of the mutated probes could be exploited for the design of "memory probes". Rare transient phosphorylation/dephosphorylation events, for instance during the cell cycle, are hard to detect. A memory probe would retain the changed FRET efficiency after phosphorylation, even after the termination of the signal and subsequent dephosphorylation. This would be of particular interest in the study of transient signals, for example from Aurora kinases.

8 Appendix

8.1 Primers used for cloning of constructs

8.1.1 Variations in the N-terminal linker region

a) Additional amino acids in the N-terminal linker region

Name	Target vector	Sense primer	Reverse primer
3sKCP-1	KCP-1	KCP-1+3aa_s	gKCP-1+3aa_rev
6sKCP-1	KCP-1	KCP-1+6aa_s	gKCP-1+6aa_rev
10sKCP-1	KCP-1	KCP-1+10aa_s	gKCP-1+10aa_rev
3rKCP-1	KCP-1	gKCP-1+3aa_rev	KCP-1+3aa_s
6rKCP-1	KCP-1	gKCP-1+6aa_rev	KCP-1+6aa_s
10rKCP-1	KCP-1	gKCP-1+10aa_rev	KCP-1+10aa_s
6r6sKCP-1	KCP1	gKCP-1+10aa_rev KCP-1+10aa_s	KCP-1+10aa_s gKCP-1+10aa_rev
6sKCP-2	KCP-2	KCP-1+6aa_s	gKCP-1+6aa_rev
10sKCP-2	KCP-2	KCP-1+10aa_s	gKCP-1+10aa_rev
3rKCP-2	KCP-2	gKCP-1+3aa_rev	KCP-1+3aa_s
6rKCP-2	KCP-2	gKCP-1+6aa_rev	KCP-1+6aa_s
10rKCP-2	KCP-2	gKCP-1+10aa_rev	KCP-1+10aa_s

Table 8.1 Introduction of additional amino acids into KCP-1 and KCP-2 via oligonucleotide ligation

b) Deletion of amino acids in the N-terminal linker region

Name	Template DNA	Sense primer	Reverse primer
YFPΔ8KCP-1	EYFP	AgeI_YFP232_s	BspEI_YFP232_rev
YFPΔ8KCP-2	EYFP	AgeI_YFP232_s	BspEI_YFP232_rev
PH Δ7KCP-1	Pleckstrin insert	BspEI-7aaPH_s	BamHI-XaaPH_rev
PH Δ7KCP-2	Pleckstrin insert	BspEI-7aaPH_s	2BamHI-XaaPH2_rev

Table 8.2 Overview of primers and template DNA for constructs with deletion of amino acids in the N-terminal linker of KCP-1 and KCP-2

c) Changes in the charge distribution of the PH domain

Name	Template DNA	Sense primer	Reverse primer
NegPHKCP-1	Pleckstrin insert KCP-1	BspEI_neg_s	BamHI-XaaPH_rev
NegPHKCP-2	Pleckstrin insert KCP-2	BspEI_neg_s	2BamHI-XaaPH2_rev
NeutPHKCP-1	Pleckstrin insert KCP-1	BspEI_Neutr_s	BamHI-XaaPH_rev
NeutPHKCP-2	Pleckstrin insert KCP-2	BspEI_Neutr_s	2BamHI-XaaPH2_rev
NegPHKCP1_DD	KCP-1_DD$^{227/228}$	BspEI_neg_s	BamHI-XaaPH_rev
NegPHKCP1_DDD	KCP-1_DDD$^{232-234}$	BspEI_neg_s	2BamHI-XaaPH2_rev
NeutPHKCP1_DD	KCP-1_DD$^{227/228}$	BspEI_Neutr_s	BamHI-XaaPH_rev
NeutPHKCP1_DDD	KCP-1_DDD$^{232-234}$	BspEI_Neutr_s	2BamHI-XaaPH2_rev

Table 8.3 Overview of primers and template DNA for constructs with changes in the charge distribution of amino acids in the N-terminal part of the PH domain of KCP-1 and KCP-2

8.1.2 Effect of fluorophore dimerization on KCP-1 and KCP-2

Name	Template DNA	Sense primer	Reverse primer
mGFP^2 PCR1	GFP^2	S1_GFP2_BamHI	R2_A206K_rev
mGFP^2 PCR2	GFP^2	S2_A206K_sense	mGFP_XbaI_rev
EYFP-dummy-mGFP^2 PCR3	PCR 1/ PCR2 GFP^2	S1_GFP2_BamHI	mGFP_XbaI_rev
mYFP PCR1	EYFP	mYFP_NheI_sense	R2_A206K_rev
mYFP PCR2	EYFP	S2_A206K_sense	mYFP_BsrGI_rev
mYFP-dummy-mGFP^2 PCR3	PCR 1/ PCR2 YFP	mYFP_NheI_sense	mYFP_BsrGI_rev
m221GFP^2 PCR1	GFP^2	S1_GFP2_BamHI	R2_L221K_rev
m221GFP^2 PCR2	GFP^2	S2_L221K_sense	mGFP_XbaI_rev
YFP-dummy-m221GFP^2 PCR3	PCR 1/ PCR2 GFP^2	S1_GFP2_BamHI	mGFP_XbaI_rev
m221YFP PCR1	EYFP	mYFP_NheI_sense	R2_L221K_rev
m221YFP PCR2	EYFP	S2_L221K_sense	mYFP_BsrGI_rev

m221YFP-dummy-m221GFP^2 PCR3	PCR 1/ PCR2 YFP	mYFP_NheI_sense	mYFP_BsrGI_rev

Table 8.4 Overview of primers and template DNA for constructs with monomeric fluorophores in KCP-1 and KCP-2

8.1.3 Intra- versus intermolecular FRET in PKC probes

Name	Template DNA	Sense primer	Reverse primer
Y66SYFP-KCP1-GFP^2	KCP-1	T66S_YFP_sense	T66S_YFP_rev
Y66SYFP-KCP2-GFP^2	KCP-2	T66S_YFP_sense	T66S_YFP_rev
EYFP-KCP1-Y66SGFP^2	KCP-1	T66S_GFP2_sense	T66S_ GFP2_rev
EYFP-KCP2-Y66SGFP^2	KCP-2	T66S_ GFP2_sense	T66S_ GFP2_rev
EYFP-dummy-EYFP	EYFP-dummy-GFP^2 + KCP-1	S1_GFP2_BamHI	mGFP_XbaI_rev
GFP^2-dummy-GFP^2	EYFP-dummy-GFP^2	mYFP_NheI_sense	mYFP_BsrGI_rev

Table 8.5 Overview of primers and template DNA for constructs discriminating between intra- and intermolecular FRET

8.1.4 Changing the FRET pair in PKC probes

a) Clones using AGT and chemically synthesized fluorophores

Name	Template DNA	Sense primer	Reverse primer
ECFP-dummy-AGT	pNuc-GEhAGT-B	BamHI-AGT-GUT_sens	AGT-TAA-XbaI reverse primer
AGT177 PCR1	AGT177	S1_NheI-AGT	R2_primer_AGT-BspEI
AGT177 PCR2	AGT177	S2_primer-AGT-BspEI	R1_AGT-BspEI
AGT177-dummy-GFP^2 PCR3	AGT177	S1_NheI-AGT	R1_AGT-BspEI
AGT PCR1	AGT	S1_NheI-AGT	R2_primer_AGT-BspEI
AGT PCR2	AGT	S2_primer_AGT-BspEI	R1_AGT-BspEI

AGT-dummy-Cit[2] PCR3	AGT	S1_NheI-AGT	R1_AGT-BspEI
Cit-dummy-AGT	AGT	BamHI-AGT-GUT_sens	AGT-TAA-XbaI_rev

Table 8.6 Overview of primers and template DNA for constructs using AGT and chemically synthesized fluorophore in KCP-1 and KCP-2

b) PKC probes using FlAsH and cyan fluorescent protein

Name	Target vector/ DNA	Sense primer	Reverse primer
ECFP-KCP-1-FlAsH	ECFP-KCP-1-AGT	optFlAsH_sense	optFlAsH_rev
ECFP-KCP-2-FlAsH	ECFP-KCP-2-AGT	optFlAsH_sense	optFlAsH_rev
mCFP / PCR1	ECFP	YFP_NheI_sense	R2_A206K_rev
mCFP / PCR2	ECFP	S2_A206K_sense	YFP_BsrGI_rev
mCFP-KCP-1-FlAsH	ECFP-KCP-1-AGT	YFP_NheI_sense	YFP_BsrGI_rev
mCFP-KCP-2-FlAsH	ECFP-KCP-2-AGT	YFP_NheI_sense	YFP_BsrGI_rev

Table 8.7 Overview of primers and template DNA forKCP-1 and KCP-2 constructs designed for FlAsH labelling

8.2 List of primers

Name	Sequence
KCP-1+3aa_s	5'-CCGGTGCGG-3'
KCP-1+6aa_s	5'-CCGGCGCCAACATCGTGT-3'
KCP-1+10aa_s	5'-CCGGCATGTTCTCTATCAACC GCGTGTACG-3'
gKCP-1+3aa_rev	5'-CCGGCCGCA-3'
gKCP-1+6aa_rev	5'-CCGGACACGATGTTGGCG-3'
gKCP-1+10aa_rev	5'-CCGGCGTACACGCGGTTGAT AGAGAACATG-3'
AgeI_YFP232_s	5'-GTGACCGGTATGGTGAGCAAGGGC-3'
BspEI_YFP232_rev	5'-GTATCCGGAAGTGATCCCGGCGGC-3'
BamHI-XaaPH_rev	5'-CACGGATCCTTCTTTCAGAATCACATC-3'
2BamHI-XaaPH2_rev	5'-CATGGATCCGTCTGGAAAGTAGTAG-3'
BspEI_neg_s	5'-GACTCCGGAATGGAACCAGAGGAGATC GAAGAGGGCTACCTTGTG-3'
BspEI_Neutr_s	5'-GACTCCGGAATGGAACCATTGCTGATCA GTGAGGGCTACCTTGTG-3'

S1_GFP2_BamHI	5'-GTAGGATCCATGGTGAGCAAGGGC-3'
R2_A206K_rev	5'-GGGGTCTTTGCTCAGTTTGGACTG-3'
mGFP_XbaI_rev	5'-TTGTCTAGATTACTTGGACAGCTCGT CC-3'
S2_A206K_sense	5'-CAGTCCAAACTGAGCAAAGACCCC-3'
mYFP_NheI_sense	5'-ACGGCTAGCATGGTGAGCAAGGGCG-3'
mYFP_BsrGI_rev	5'-ACTTGTACAGCTCGTCCATGCCGAG-3'
BamHI-AGT-GUT_sens	5'-ACGAAAGGATCCATGGACAAGGATT GTG-3'
AGT-TAA-XbaI_rev	5'-TTGATTCTAGATTAGTTTCGGCCAGCA GG-3'
S1_NheI-AGT	5'-TACCGCTAGCATGGACAAGGATTG-3'
S2_primer_AGT-BspEI	5'-GGAGGTCCCGAGCCCCTGA-3'
R1_AGT-BspEI	5'-GTTATCCGGAGTTTCGGCCAGCAG-3'
R2_primer_AGT-BspEI	5'-TCAGGGGCTCGGGACCTCC-3'
optFlAsH_sense	5'-GATCCTTCCTGAACTGCTGCCCCGGCT GCTGCATGGAGCCCTAAC-3'
optFlAsH_rev	5'-CCGAGTTAGGGCTCCATGCAGCAGCCGG GGCAGCAGTTCAGGAAG-3'
T66S_YFP_sense	5'-CACCTTCGGCTCCGGCCTGCAG-3'
T66S_YFP_rev	5'-CTGCAGGCCGGAGCCGAAGGTG-3'
T66S_GFP2_sense	5'-CCCTGAGCTCCGGCGTGCAGTG-3'
T66S_ GFP2_rev	5'-CACTGCACGCCGGAGCTCAGGG-3'

Table 6.8.8 List of primers used for cloning of all constructs used in this thesis

8.3 Abbreviations

AGT	human O^6-alkylguanine-DNA alkyltransferase
BG	O^6-benzylguanine
BGAF	O^6-benzylguanine-fluorescein-diacetate
BGFL	O^6-benzylguanine-fluorescein
BG-SNARF	O^6-benzylguanine-SNARF-1
BG-TMR	O^6-benzylguanine-tetramethylrhodamine
BSA	Bovine serum albumin
CaMKII	Calcium/calmodulin dependent kinase II
cAMP	Cyclic adenosine monophosphate
CCD	Charge coupled device
cGMP	Cyclic guanosinemonophosphate
DAB	3,3'-diaminobenzidine
DAG	Diacylglycerol
DEP	Dishevelled, Egl-10, Pleckstrin
dNTP	Deoxynucleotide triphosphate
EBFP	Enhanced blue fluorescent protein
ECFP	Enhanced cyan fluorescent protein
EDTA	Ethylendiaminetetraacetic acid
EGF	Epidermal growth factor
EGFP	Enhanced green fluorescent protein
EYFP	Enhanced yellow fluorescent protein
EYF-KCP-1-EYFP	KCP-1 with N-and C-terminal EYFP
EYF-KCP-2-EYFP	KCP-2 with N-and C-terminal EYFP
EYFPY66S KCP-1	KCP-1 with non-fluorescent EYFP (Y66S mutation)
EYFPY66S KCP-2	KCP-2 with non-fluorescent EYFP (Y66S mutation)
FlAsH	Fluorescein arsenical hairpin binder
FP	Fluorescent protein
FRET	Fluorescence resonance energy transfer
GFP	Green fluorescent protein
GFP^2	Green fluorescent protein square
GFP^2-KCP-1- GFP^2	KCP-1 with N-and C-terminal GFP^2
GFP^2-KCP-2- GFP^2	KCP-2 with N-and C-terminal GFP^2
GFP^2Y66S KCP-1	KCP-1 with non-fluorescent GFP^2 (Y66S mutation)
GFP^2Y66S KCP-2	KCP-2 with non-fluorescent GFP^2 (Y66S mutation)
GPCR	G-protein coupled receptor
Hepes	4-(2-Hydroxyethyl)-1-piperazineethanesulfonic acid
IP_3	Inositol 1,4,5-trisphosphate
KCP-1	Protein kinase C probe 1
KCP-2	Protein kinase C probe 2
m221YG^2KCP-1	KCP-1 with L221K mutation in EYFP and GFP^2
m221YG^2KCP-2	KCP-2 with L221K mutation in EYFP and GFP^2
mCFP	Monomeric enhanced cyan fluorescent protein
mCherry	Monomeric cherry (red fluorescent protein)
mCh-KCP-1-mOr	KCP-1 with mCherry as N-terminal fluorophore and mOrange as C-terminal fluorophore
mCh-KCP-2-mOr	KCP-2 with mCherry as N-terminal fluorophore and mOrange as C-terminal fluorophore

$mGFP^2$	Monomeric green fluorescent protein square
mOrange	Monomeric orange (orange fluorescent protein)
MOPS	Morpholinepropanesulfonic acid
mRFP	Monomeric red fluorescent protein
mYFP	Monomeric enhanced yellow fluorescent protein
mYG^2KCP-1	KCP-1 with monomeric EYFP (A206K)
mYG^2KCP-2	KCP-2 with monomeric EYFP (A206K)
$mYmG^2KCP$-1	KCP-1 with monomeric EYFP and monomeric GFP^2 (A206K in both)
$mYmG^2KCP$-2	KCP-2 with monomeric EYFP and monomeric GFP^2 (A206K in both)
NegKCP-1	KCP-1 with three negative amino acids in the PH domain
NegKCP-1-$RR^{227/228}$	KCP-1 with three negative amino acids in the PH domain and two basic ones in the acidic loop
NegKCP-1-$RRR^{232-234}$	KCP-1 with three negative amino acids in the PH domain and three basic ones in the acidic loop
NegKCP-2	KCP-2 with three negative amino acids in the PH domain
NeutKCP-1	KCP-1 with three neutral amino acids in the PH domain
NeutKCP-1-$RR^{227/228}$	KCP-1 with three neutral amino acids in the PH domain and two basic ones in the acidic loop
NeutKCP-1-$RRR^{232-234}$	KCP-1 with three neutral amino acids in the PH domain and three basic ones in the acidic loop
NeutKCP-2	KCP-2 with three neutral amino acids in the PH domain
PA	Phosphatidic acid
PAGE	Polyacrylamide gel electrophoresis
PAP	Phosphohydrolase
PC	Phosphatidylcholine
PCR	Polymerase chain reaction
PDK-1	Phosphoinositol dependent kinase 1
PH	Pleckstrin homology
PIP_2	Phosphatidylinositol 4,5-bisphosphate
PKA	cAMP-dependant protein kinase
PKB	Protein kinase B, also known as RAC (related to PKA and PKC) and Akt1
PKC	Ca^{2+} activated, phospholipids-dependent protein kinase
PKD	Protein kinase D
PKG	cGMP-dependant protein kinase
PKM	Catalytic subunit of protein kinase C
PLC	Phospholipase C
PLD	Phospholipase D
PMA	4-12-O-Tetradecanoylphorbol 13-acetate
PMT	Photo multiplier tube
PS	Phosphatidylserine
PTP1B	Phosphotyrosinephosphatase 1B
RACK	Receptor for activated C kinase

ROI	Region of interest
RTK	Receptor tyrosine kinase
T4-PNK	T4-polynucleotide kinase
TPA	4-12-O-Tetradecanoylphorbol 13-acetate
YGY66S KCP-1	Co-transfection of EYFPY66S KCP-1 and GFP^2Y66S KCP-1
YGY66S KCP-2	Co-transfection of EYFPY66S KCP-2 and GFP^2Y66S KCP-2
YYGG KCP-1	Co-transfection of EYF-KCP-1-EYFP and GFP^2-KCP-1- GFP^2
YYGG KCP-2	Co-transfection of EYF-KCP-2-EYFP and GFP^2-KCP-2- GFP^2
YmG^2KCP-1	KCP-1 with monomeric GFP^2 (A206K)
YmG^2KCP-2	KCP-2 with monomeric GFP^2 (A206K)

9 References

1. Schleifenbaum, A., Stier, G., Gasch, A., Sattler, M. & Schultz, C. Genetically encoded FRET probe for PKC activity based on pleckstrin. *J Am Chem Soc* **126**, 11786-7 (2004).
2. Brumbaugh, J., Schleifenbaum, A., Gasch, A., Sattler, M. & Schultz, C. A dual parameter FRET probe for measuring PKC and PKA activity in living cells. *J Am Chem Soc* **128**, 24-5 (2006).
3. Lipmann, F. A. & Levene, P. A. Serinephosphoric acid obtained on hydrolysis of vitellinic acid. *J. Biol. Chem* **98**, 109-114 (1932).
4. Fischer, E. H. & Krebs, E. G. Conversion of phosphorylase b to phosphorylase a in muscle extracts. *J Biol Chem* **216**, 121-32 (1955).
5. Krebs, E. G. & Fischer, E. H. Phosphorylase activity of skeletal muscle extracts. *J Biol Chem* **216**, 113-20 (1955).
6. Krebs, E. G. & Fischer, E. H. The phosphorylase b to a converting enzyme of rabbit skeletal muscle. *Biochim Biophys Acta* **20**, 150-7 (1956).
7. Walsh, D. A., Perkins, J. P. & Krebs, E. G. An adenosine 3',5'-monophosphate-dependant protein kinase from rabbit skeletal muscle. *J Biol Chem* **243**, 3763-5 (1968).
8. Inoue, M., Kishimoto, A., Takai, Y. & Nishizuka, Y. Guanosine 3':5'-monophosphate-dependent protein kinase from silkworm, properties of a catalytic fragment obtained by limited proteolysis. *J Biol Chem* **251**, 4476-8 (1976).
9. Yamamoto, M., Takai, Y., Hashimoto, E. & Nishizuka, Y. Intrinsic activity of guanosine 3',5'-monophosphate-dependent protein kinase similar to adenosine 3',5'-monophosphate-dependent protein kinase. I. Phosphorylation of histone fractions. *J Biochem (Tokyo)* **81**, 1857-62 (1977).
10. Inoue, M., Kishimoto, A., Takai, Y. & Nishizuka, Y. Studies on a cyclic nucleotide-independent protein kinase and its proenzyme in mammalian tissues. II. Proenzyme and its activation by calcium-dependent protease from rat brain. *J Biol Chem* **252**, 7610-6 (1977).
11. Kishimoto, A., Takai, Y. & Nishizuka, Y. Activation of glycogen phosphorylase kinase by a calcium-activated, cyclic nucleotide-independent protein kinase system. *J Biol Chem* **252**, 7449-52 (1977).
12. Takai, Y., Kishimoto, A., Inoue, M. & Nishizuka, Y. Studies on a cyclic nucleotide-independent protein kinase and its proenzyme in mammalian tissues. I. Purification and characterization of an active enzyme from bovine cerebellum. *J Biol Chem* **252**, 7603-9 (1977).
13. Nishizuka, Y. & Kikkawa, U. Early studies of protein kinase C: a historical perspective. *Methods Mol Biol* **233**, 9-18 (2003).
14. Takai, Y. et al. A role of membranes in the activation of a new multifunctional protein kinase system. *J Biochem (Tokyo)* **86**, 575-8 (1979).
15. Takai, Y. et al. Calcium-dependent activation of a multifunctional protein kinase by membrane phospholipids. *J Biol Chem* **254**, 3692-5 (1979).

16. Brooks, G. The role of 80K/MARCKS, a specific substrate of protein kinase C, in cell growth and tumour progression. *Pigment Cell Res* **7**, 451-7 (1994).
17. Oka, M. & Kikkawa, U. Protein kinase C in melanoma. *Cancer Metastasis Rev* **24**, 287-300 (2005).
18. Nakashima, S. Protein kinase C alpha (PKC alpha): regulation and biological function. *J Biochem (Tokyo)* **132**, 669-75 (2002).
19. Oliva, J. L., Griner, E. M. & Kazanietz, M. G. PKC isozymes and diacylglycerol-regulated proteins as effectors of growth factor receptors. *Growth Factors* **23**, 245-52 (2005).
20. Denning, M. F. Epidermal keratinocytes: regulation of multiple cell phenotypes by multiple protein kinase C isoforms. *Int J Biochem Cell Biol* **36**, 1141-6 (2004).
21. Clemens, M. J., Trayner, I. & Menaya, J. The role of protein kinase C isoenzymes in the regulation of cell proliferation and differentiation. *J Cell Sci* **103 (Pt 4)**, 881-7 (1992).
22. Johnson, G. L. & Vaillancourt, R. R. Sequential protein kinase reactions controlling cell growth and differentiation. *Curr Opin Cell Biol* **6**, 230-8 (1994).
23. Ventura, C. & Maioli, M. Protein kinase C control of gene expression. *Crit Rev Eukaryot Gene Expr* **11**, 243-67 (2001).
24. Gallicano, G. I., Yousef, M. C. & Capco, D. G. PKC--a pivotal regulator of early development. *Bioessays* **19**, 29-36 (1997).
25. Suzuki, A., Akimoto, K. & Ohno, S. Protein kinase C lambda/iota (PKClambda/iota): a PKC isotype essential for the development of multicellular organisms. *J Biochem (Tokyo)* **133**, 9-16 (2003).
26. Shieh, B. H., Parker, L. & Popescu, D. Protein kinase C (PKC) isoforms in Drosophila. *J Biochem (Tokyo)* **132**, 523-7 (2002).
27. Lucas, M. & Sanchez-Margalet, V. Protein kinase C involvement in apoptosis. *Gen Pharmacol* **26**, 881-7 (1995).
28. Brodie, C. & Blumberg, P. M. Regulation of cell apoptosis by protein kinase c delta. *Apoptosis* **8**, 19-27 (2003).
29. Deacon, E. M., Pongracz, J., Griffiths, G. & Lord, J. M. Isoenzymes of protein kinase C: differential involvement in apoptosis and pathogenesis. *Mol Pathol* **50**, 124-31 (1997).
30. Gutcher, I., Webb, P. R. & Anderson, N. G. The isoform-specific regulation of apoptosis by protein kinase C. *Cell Mol Life Sci* **60**, 1061-70 (2003).
31. Tigges, U., Koch, B., Wissing, J., Jockusch, B. M. & Ziegler, W. H. The F-actin cross-linking and focal adhesion protein filamin A is a ligand and in vivo substrate for protein kinase C alpha. *J Biol Chem* **278**, 23561-9 (2003).
32. Anilkumar, N., Parsons, M., Monk, R., Ng, T. & Adams, J. C. Interaction of fascin and protein kinase Calpha: a novel intersection in cell adhesion and motility. *Embo J* **22**, 5390-402 (2003).
33. Mackay, K. & Mochly-Rosen, D. Localization, anchoring, and functions of protein kinase C isozymes in the heart. *J Mol Cell Cardiol* **33**, 1301-7 (2001).

34. Murriel, C. L. & Mochly-Rosen, D. Opposing roles of delta and epsilonPKC in cardiac ischemia and reperfusion: targeting the apoptotic machinery. *Arch Biochem Biophys* **420**, 246-54 (2003).
35. Pass, J. M. et al. Enhanced PKC beta II translocation and PKC beta II-RACK1 interactions in PKC epsilon-induced heart failure: a role for RACK1. *Am J Physiol Heart Circ Physiol* **281**, H2500-10 (2001).
36. Ping, P., Zhang, J., Pierce, W. M., Jr. & Bolli, R. Functional proteomic analysis of protein kinase C epsilon signaling complexes in the normal heart and during cardioprotection. *Circ Res* **88**, 59-62 (2001).
37. Ping, P. et al. Formation of protein kinase C(epsilon)-Lck signaling modules confers cardioprotection. *J Clin Invest* **109**, 499-507 (2002).
38. Murphy, S. & Frishman, W. H. Protein kinase C in cardiac disease and as a potential therapeutic target. *Cardiol Rev* **13**, 3-12 (2005).
39. Bright, R. & Mochly-Rosen, D. The role of protein kinase C in cerebral ischemic and reperfusion injury. *Stroke* **36**, 2781-90 (2005).
40. Chou, W. H. & Messing, R. O. Protein kinase C isozymes in stroke. *Trends Cardiovasc Med* **15**, 47-51 (2005).
41. Battaini, F. & Pascale, A. Protein kinase C signal transduction regulation in physiological and pathological aging. *Ann N Y Acad Sci* **1057**, 177-92 (2005).
42. Sun, M. K. & Alkon, D. L. Protein kinase C isozymes: memory therapeutic potential. *Curr Drug Targets CNS Neurol Disord* **4**, 541-52 (2005).
43. Olive, M. F. & Messing, R. O. Protein kinase C isozymes and addiction. *Mol Neurobiol* **29**, 139-54 (2004).
44. Salamanca, D. A. & Khalil, R. A. Protein kinase C isoforms as specific targets for modulation of vascular smooth muscle function in hypertension. *Biochem Pharmacol* **70**, 1537-47 (2005).
45. Farhadi, A., Keshavarzian, A., Ranjbaran, Z., Fields, J. Z. & Banan, A. The role of protein kinase C isoforms in modulating injury and repair of the intestinal barrier. *J Pharmacol Exp Ther* **316**, 1-7 (2006).
46. Farese, R. V., Sajan, M. P. & Standaert, M. L. Atypical protein kinase C in insulin action and insulin resistance. *Biochem Soc Trans* **33**, 350-3 (2005).
47. Rask-Madsen, C. & King, G. L. Proatherosclerotic mechanisms involving protein kinase C in diabetes and insulin resistance. *Arterioscler Thromb Vasc Biol* **25**, 487-96 (2005).
48. Koivunen, J., Aaltonen, V. & Peltonen, J. Protein kinase C (PKC) family in cancer progression. *Cancer Lett* **235**, 1-10 (2006).
49. Lahn, M., Paterson, B. M., Sundell, K. & Ma, D. The role of protein kinase C-alpha (PKC-alpha) in malignancies of the gastrointestinal tract. *Eur J Cancer* **40**, 10-20 (2004).
50. Dempsey, E. C. et al. Protein kinase C isozymes and the regulation of diverse cell responses. *Am J Physiol Lung Cell Mol Physiol* **279**, L429-38 (2000).
51. Coussens, L. et al. Multiple, distinct forms of bovine and human protein kinase C suggest diversity in cellular signaling pathways. *Science* **233**, 859-66 (1986).
52. Parker, P. J. et al. The complete primary structure of protein kinase C--the major phorbol ester receptor. *Science* **233**, 853-9 (1986).

53. Coussens, L., Rhee, L., Parker, P. J. & Ullrich, A. Alternative splicing increases the diversity of the human protein kinase C family. *DNA* **6**, 389-94 (1987).
54. Ono, Y. et al. Identification of three additional members of rat protein kinase C family: delta-, epsilon- and zeta-subspecies. *FEBS Lett* **226**, 125-8 (1987).
55. Osada, S. et al. A phorbol ester receptor/protein kinase, nPKC eta, a new member of the protein kinase C family predominantly expressed in lung and skin. *J Biol Chem* **265**, 22434-40 (1990).
56. Osada, S. et al. A new member of the protein kinase C family, nPKC theta, predominantly expressed in skeletal muscle. *Mol Cell Biol* **12**, 3930-8 (1992).
57. Selbie, L. A., Schmitz-Peiffer, C., Sheng, Y. & Biden, T. J. Molecular cloning and characterization of PKC iota, an atypical isoform of protein kinase C derived from insulin-secreting cells. *J Biol Chem* **268**, 24296-302 (1993).
58. Corbalan-Garcia, S. & Gomez-Fernandez, J. C. Protein kinase C regulatory domains: The art of decoding many different signals in membranes. *Biochim Biophys Acta* (2006).
59. Newton, A. C. The ins and outs of protein kinase C. *Methods Mol Biol* **233**, 3-7 (2003).
60. House, C. & Kemp, B. E. Protein kinase C contains a pseudosubstrate prototope in its regulatory domain. *Science* **238**, 1726-8 (1987).
61. Becker, K. P. & Hannun, Y. A. Protein kinase C and phospholipase D: intimate interactions in intracellular signaling. *Cell Mol Life Sci* **62**, 1448-61 (2005).
62. House, C., Wettenhall, R. E. & Kemp, B. E. The influence of basic residues on the substrate specificity of protein kinase C. *J Biol Chem* **262**, 772-7 (1987).
63. Craig, K. L. & Harley, C. B. Phosphorylation of human pleckstrin on Ser-113 and Ser-117 by protein kinase C. *Biochem J* **314 (Pt 3)**, 937-42 (1996).
64. Orr, J. W. & Newton, A. C. Intrapeptide regulation of protein kinase C. *J Biol Chem* **269**, 8383-7 (1994).
65. Orr, J. W., Keranen, L. M. & Newton, A. C. Reversible exposure of the pseudosubstrate domain of protein kinase C by phosphatidylserine and diacylglycerol. *J Biol Chem* **267**, 15263-6 (1992).
66. Burns, D. J. & Bell, R. M. Protein kinase C contains two phorbol ester binding domains. *J Biol Chem* **266**, 18330-8 (1991).
67. Bell, R. M. & Burns, D. J. Lipid activation of protein kinase C. *J Biol Chem* **266**, 4661-4 (1991).
68. Castagna, M. et al. Direct activation of calcium-activated, phospholipid-dependent protein kinase by tumor-promoting phorbol esters. *J Biol Chem* **257**, 7847-51 (1982).
69. Asaoka, Y., Nakamura, S., Yoshida, K. & Nishizuka, Y. Protein kinase C, calcium and phospholipid degradation. *Trends Biochem Sci* **17**, 414-7 (1992).
70. Nishizuka, Y. Intracellular signaling by hydrolysis of phospholipids and activation of protein kinase C. *Science* **258**, 607-14 (1992).

71. Newton, A. C. Protein kinase C. Seeing two domains. *Curr Biol* **5**, 973-6 (1995).
72. Benes, C. H. et al. The C2 domain of PKCdelta is a phosphotyrosine binding domain. *Cell* **121**, 271-80 (2005).
73. Corbalan-Garcia, S., Sanchez-Carrillo, S., Garcia-Garcia, J. & Gomez-Fernandez, J. C. Characterization of the membrane binding mode of the C2 domain of PKC epsilon. *Biochemistry* **42**, 11661-8 (2003).
74. Garcia-Garcia, J., Gomez-Fernandez, J. C. & Corbalan-Garcia, S. Structural characterization of the C2 domain of novel protein kinase Cepsilon. *Eur J Biochem* **268**, 1107-17 (2001).
75. Brose, N. & Rosenmund, C. Move over protein kinase C, you've got company: alternative cellular effectors of diacylglycerol and phorbol esters. *J Cell Sci* **115**, 4399-411 (2002).
76. Orita, S. et al. Doc2 enhances Ca2+-dependent exocytosis from PC12 cells. *J Biol Chem* **271**, 7257-60 (1996).
77. Ponting, C. P. & Parker, P. J. Extending the C2 domain family: C2s in PKCs delta, epsilon, eta, theta, phospholipases, GAPs, and perforin. *Protein Sci* **5**, 162-6 (1996).
78. Ahmed, S. et al. A novel functional target for tumor-promoting phorbol esters and lysophosphatidic acid. The p21rac-GTPase activating protein n-chimaerin. *J Biol Chem* **268**, 10709-12 (1993).
79. Orita, S. et al. Physical and functional interactions of Doc2 and Munc13 in Ca2+-dependent exocytotic machinery. *J Biol Chem* **272**, 16081-4 (1997).
80. Taylor, S. S. & Radzio-Andzelm, E. Three protein kinase structures define a common motif. *Structure* **2**, 345-55 (1994).
81. Kennelly, P. J. & Krebs, E. G. Consensus sequences as substrate specificity determinants for protein kinases and protein phosphatases. *J Biol Chem* **266**, 15555-8 (1991).
82. Newton, A. C. Interaction of proteins with lipid headgroups: lessons from protein kinase C. *Annu Rev Biophys Biomol Struct* **22**, 1-25 (1993).
83. Nishizuka, Y. The role of protein kinase C in cell surface signal transduction and tumour promotion. *Nature* **308**, 693-8 (1984).
84. Harden, T. K. & Sondek, J. Regulation of phospholipase C isozymes by ras superfamily GTPases. *Annu Rev Pharmacol Toxicol* **46**, 355-79 (2006).
85. Billah, M. M. & Anthes, J. C. The regulation and cellular functions of phosphatidylcholine hydrolysis. *Biochem J* **269**, 281-91 (1990).
86. Jenkins, G. M. & Frohman, M. A. Phospholipase D: a lipid centric review. *Cell Mol Life Sci* **62**, 2305-16 (2005).
87. Nishizuka, Y. Protein kinase C and lipid signaling for sustained cellular responses. *Faseb J* **9**, 484-96 (1995).
88. Hodgkin, M. N. et al. Diacylglycerols and phosphatidates: which molecular species are intracellular messengers? *Trends Biochem Sci* **23**, 200-4 (1998).
89. Mora, A., Komander, D., van Aalten, D. M. & Alessi, D. R. PDK1, the master regulator of AGC kinase signal transduction. *Semin Cell Dev Biol* **15**, 161-70 (2004).

90. Le Good, J. A. et al. Protein kinase C isotypes controlled by phosphoinositide 3-kinase through the protein kinase PDK1. *Science* **281**, 2042-5 (1998).
91. Toker, A. & Newton, A. C. Cellular signaling: pivoting around PDK-1. *Cell* **103**, 185-8 (2000).
92. Newton, A. C. Regulation of the ABC kinases by phosphorylation: protein kinase C as a paradigm. *Biochem J* **370**, 361-71 (2003).
93. Williams, M. R. et al. The role of 3-phosphoinositide-dependent protein kinase 1 in activating AGC kinases defined in embryonic stem cells. *Curr Biol* **10**, 439-48 (2000).
94. Vanhaesebroeck, B. & Alessi, D. R. The PI3K-PDK1 connection: more than just a road to PKB. *Biochem J* **346 Pt 3**, 561-76 (2000).
95. Alessi, D. R. et al. 3-Phosphoinositide-dependent protein kinase-1 (PDK1): structural and functional homology with the Drosophila DSTPK61 kinase. *Curr Biol* **7**, 776-89 (1997).
96. Stephens, L. et al. Protein kinase B kinases that mediate phosphatidylinositol 3,4,5-trisphosphate-dependent activation of protein kinase B. *Science* **279**, 710-4 (1998).
97. Knighton, D. R. et al. Crystal structure of the catalytic subunit of cyclic adenosine monophosphate-dependent protein kinase. *Science* **253**, 407-14 (1991).
98. Srinivasan, N., Bax, B., Blundell, T. L. & Parker, P. J. Structural aspects of the functional modules in human protein kinase-C alpha deduced from comparative analyses. *Proteins* **26**, 217-35 (1996).
99. Bornancin, F. & Parker, P. J. Phosphorylation of threonine 638 critically controls the dephosphorylation and inactivation of protein kinase Calpha. *Curr Biol* **6**, 1114-23 (1996).
100. Edwards, A. S., Faux, M. C., Scott, J. D. & Newton, A. C. Carboxyl-terminal phosphorylation regulates the function and subcellular localization of protein kinase C betaII. *J Biol Chem* **274**, 6461-8 (1999).
101. Messerschmidt, A. et al. Crystal structure of the catalytic domain of human atypical protein kinase C-iota reveals interaction mode of phosphorylation site in turn motif. *J Mol Biol* **352**, 918-31 (2005).
102. Cenni, V. et al. Regulation of novel protein kinase C epsilon by phosphorylation. *Biochem J* **363**, 537-45 (2002).
103. Parker, P. J. & Murray-Rust, J. PKC at a glance. *J Cell Sci* **117**, 131-2 (2004).
104. Nalefski, E. A. & Newton, A. C. Membrane binding kinetics of protein kinase C betaII mediated by the C2 domain. *Biochemistry* **40**, 13216-29 (2001).
105. Ochoa, W. F. et al. Structure of the C2 domain from novel protein kinase Cepsilon. A membrane binding model for Ca(2+)-independent C2 domains. *J Mol Biol* **311**, 837-49 (2001).
106. Verdaguer, N., Corbalan-Garcia, S., Ochoa, W. F., Fita, I. & Gomez-Fernandez, J. C. Ca(2+) bridges the C2 membrane-binding domain of protein kinase Calpha directly to phosphatidylserine. *Embo J* **18**, 6329-38 (1999).
107. Sutton, R. B. & Sprang, S. R. Structure of the protein kinase Cbeta phospholipid-binding C2 domain complexed with Ca2+. *Structure* **6**, 1395-405 (1998).

108. Sutton, R. B., Davletov, B. A., Berghuis, A. M., Sudhof, T. C. & Sprang, S. R. Structure of the first C2 domain of synaptotagmin I: a novel Ca2+/phospholipid-binding fold. *Cell* **80**, 929-38 (1995).
109. Poole, A. W., Pula, G., Hers, I., Crosby, D. & Jones, M. L. PKC-interacting proteins: from function to pharmacology. *Trends Pharmacol Sci* **25**, 528-35 (2004).
110. Jaken, S. Protein kinase C isozymes and substrates. *Curr Opin Cell Biol* **8**, 168-73 (1996).
111. Chapline, C. et al. A major, transformation-sensitive PKC-binding protein is also a PKC substrate involved in cytoskeletal remodeling. *J Biol Chem* **273**, 19482-9 (1998).
112. Sim, A. T. & Scott, J. D. Targeting of PKA, PKC and protein phosphatases to cellular microdomains. *Cell Calcium* **26**, 209-17 (1999).
113. Mochly-Rosen, D., Khaner, H., Lopez, J. & Smith, B. L. Intracellular receptors for activated protein kinase C. Identification of a binding site for the enzyme. *J Biol Chem* **266**, 14866-8 (1991).
114. Mochly-Rosen, D., Khaner, H. & Lopez, J. Identification of intracellular receptor proteins for activated protein kinase C. *Proc Natl Acad Sci U S A* **88**, 3997-4000 (1991).
115. Mochly-Rosen, D. Localization of protein kinases by anchoring proteins: a theme in signal transduction. *Science* **268**, 247-51 (1995).
116. Mochly-Rosen, D. & Gordon, A. S. Anchoring proteins for protein kinase C: a means for isozyme selectivity. *Faseb J* **12**, 35-42 (1998).
117. Schechtman, D. & Mochly-Rosen, D. Isozyme-specific inhibitors and activators of protein kinase C. *Methods Enzymol* **345**, 470-89 (2002).
118. Zhang, J., Ma, Y., Taylor, S. S. & Tsien, R. Y. Genetically encoded reporters of protein kinase A activity reveal impact of substrate tethering. *Proc Natl Acad Sci U S A* **98**, 14997-5002 (2001).
119. Violin, J. D., Zhang, J., Tsien, R. Y. & Newton, A. C. A genetically encoded fluorescent reporter reveals oscillatory phosphorylation by protein kinase C. *J Cell Biol* **161**, 899-909 (2003).
120. Ting, A. Y., Kain, K. H., Klemke, R. L. & Tsien, R. Y. Genetically encoded fluorescent reporters of protein tyrosine kinase activities in living cells. *Proc Natl Acad Sci U S A* **98**, 15003-8 (2001).
121. Sato, M., Ozawa, T., Inukai, K., Asano, T. & Umezawa, Y. Fluorescent indicators for imaging protein phosphorylation in single living cells. *Nat Biotechnol* **20**, 287-94 (2002).
122. Lyons, R. M. & Atherton, R. M. Characterization of a platelet protein phosphorylated during the thrombin-induced release reaction. *Biochemistry* **18**, 544-52 (1979).
123. Haslam, R. J. & Lynham, J. A. Increased phosphorylation of specific blood platelet proteins in association with the release reaction. *Biochem Soc Trans* **4**, 694-7 (1976).
124. Haslam, R. J. & Lynham, J. A. Relationship between phosphorylation of blood platelet proteins and secretion of platelet granule constituents. I. Effects of different aggregating agents. *Biochem Biophys Res Commun* **77**, 714-22 (1977).
125. Haslam, R. J., Davidson, M. M., Fox, J. E. & Lynham, J. A. Cyclic nucleotides in platelet function. *Thromb Haemost* **40**, 232-40 (1978).

126. Haslam, R. J., Lynham, J. A. & Fox, J. E. Effects of collagen, ionophore A23187 and prostaglandin E1 on the phosphorylation of specific proteins in blood platelets. *Biochem J* **178**, 397-406 (1979).
127. Imaoka, T., Lynham, J. A. & Haslam, R. J. Purification and characterization of the 47,000-dalton protein phosphorylated during degranulation of human platelets. *J Biol Chem* **258**, 11404-14 (1983).
128. Tyers, M., Rachubinski, R. A., Sartori, C. S., Harley, C. B. & Haslam, R. J. Induction of the 47 kDa platelet substrate of protein kinase C during differentiation of HL-60 cells. *Biochem J* **243**, 249-53 (1987).
129. Gerrard, J. M., Friesen, L. L., McCrea, J. M., Israels, S. J. & Robinson, P. Platelet protein phosphorylation. *Adv Exp Med Biol* **192**, 235-48 (1985).
130. Abrams, C. S., Zhao, W., Belmonte, E. & Brass, L. F. Protein kinase C regulates pleckstrin by phosphorylation of sites adjacent to the N-terminal pleckstrin homology domain. *J Biol Chem* **270**, 23317-21 (1995).
131. Brumell, J. H., Craig, K. L., Ferguson, D., Tyers, M. & Grinstein, S. Phosphorylation and subcellular redistribution of pleckstrin in human neutrophils. *J Immunol* **158**, 4862-71 (1997).
132. Sano, K., Takai, Y., Yamanishi, J. & Nishizuka, Y. A role of calcium-activated phospholipid-dependent protein kinase in human platelet activation. Comparison of thrombin and collagen actions. *J Biol Chem* **258**, 2010-3 (1983).
133. Zhang, J. et al. Phosphatidylinositol (3,4,5)-trisphosphate stimulates phosphorylation of pleckstrin in human platelets. *J Biol Chem* **270**, 22807-10 (1995).
134. Sloan, D. C., Wang, P., Bao, X. & Haslam, R. J. Translocation of pleckstrin requires its phosphorylation and newly formed ligands. *Biochem Biophys Res Commun* **293**, 640-6 (2002).
135. Auethavekiat, V., Abrams, C. S. & Majerus, P. W. Phosphorylation of platelet pleckstrin activates inositol polyphosphate 5-phosphatase I. *J Biol Chem* **272**, 1786-90 (1997).
136. al-Aoukaty, A., Rolstad, B. & Maghazachi, A. A. Recruitment of pleckstrin and phosphoinositide 3-kinase gamma into the cell membranes, and their association with G beta gamma after activation of NK cells with chemokines. *J Immunol* **162**, 3249-55 (1999).
137. Lemmon, M. A. & Ferguson, K. M. Signal-dependent membrane targeting by pleckstrin homology (PH) domains. *Biochem J* **350 Pt 1**, 1-18 (2000).
138. Mayer, B. J., Ren, R., Clark, K. L. & Baltimore, D. A putative modular domain present in diverse signaling proteins. *Cell* **73**, 629-30 (1993).
139. Haslam, R. J., Koide, H. B. & Hemmings, B. A. Pleckstrin domain homology. *Nature* **363**, 309-10 (1993).
140. Edlich, C., Stier, G., Simon, B., Sattler, M. & Muhle-Goll, C. Structure and phosphatidylinositol-(3,4)-bisphosphate binding of the C-terminal PH domain of human pleckstrin. *Structure* **13**, 277-86 (2005).
141. Yoon, H. S. et al. Solution structure of a pleckstrin-homology domain. *Nature* **369**, 672-5 (1994).
142. Harlan, J. E., Yoon, H. S., Hajduk, P. J. & Fesik, S. W. Structural characterization of the interaction between a pleckstrin homology

domain and phosphatidylinositol 4,5-bisphosphate. *Biochemistry* **34**, 9859-64 (1995).
143. Harlan, J. E., Hajduk, P. J., Yoon, H. S. & Fesik, S. W. Pleckstrin homology domains bind to phosphatidylinositol-4,5-bisphosphate. *Nature* **371**, 168-70 (1994).
144. Gibson, T. J., Hyvonen, M., Musacchio, A., Saraste, M. & Birney, E. PH domain: the first anniversary. *Trends Biochem Sci* **19**, 349-53 (1994).
145. Lemmon, M. A., Ferguson, K. M., O'Brien, R., Sigler, P. B. & Schlessinger, J. Specific and high-affinity binding of inositol phosphates to an isolated pleckstrin homology domain. *Proc Natl Acad Sci U S A* **92**, 10472-6 (1995).
146. Garcia, P. et al. The pleckstrin homology domain of phospholipase C-delta 1 binds with high affinity to phosphatidylinositol 4,5-bisphosphate in bilayer membranes. *Biochemistry* **34**, 16228-34 (1995).
147. Franke, T. F., Kaplan, D. R., Cantley, L. C. & Toker, A. Direct regulation of the Akt proto-oncogene product by phosphatidylinositol-3,4-bisphosphate. *Science* **275**, 665-8 (1997).
148. Rao, V. R. et al. Expression cloning of protein targets for 3-phosphorylated phosphoinositides. *J Biol Chem* **274**, 37893-900 (1999).
149. Kavran, J. M. et al. Specificity and promiscuity in phosphoinositide binding by pleckstrin homology domains. *J Biol Chem* **273**, 30497-508 (1998).
150. Abrams, C. S., Zhao, W. & Brass, L. F. A site of interaction between pleckstrin's PH domains and G beta gamma. *Biochim Biophys Acta* **1314**, 233-8 (1996).
151. Ponting, C. P. & Bork, P. Pleckstrin's repeat performance: a novel domain in G-protein signaling? *Trends Biochem Sci* **21**, 245-6 (1996).
152. Schultz, J., Milpetz, F., Bork, P. & Ponting, C. P. SMART, a simple modular architecture research tool: identification of signaling domains. *Proc Natl Acad Sci U S A* **95**, 5857-64 (1998).
153. Burchett, S. A. et al. Regulation of stress response signaling by the N-terminal dishevelled/EGL-10/pleckstrin domain of Sst2, a regulator of G protein signaling in Saccharomyces cerevisiae. *J Biol Chem* **277**, 22156-67 (2002).
154. Hu, G., Zhang, Z. & Wensel, T. G. Activation of RGS9-1GTPase acceleration by its membrane anchor, R9AP. *J Biol Chem* **278**, 14550-4 (2003).
155. Martemyanov, K. A. et al. The DEP domain determines subcellular targeting of the GTPase activating protein RGS9 in vivo. *J Neurosci* **23**, 10175-81 (2003).
156. Atkins, P. W. *Physical Chemistry* (ed. Press, O. U.) (Oxford, 1998).
157. Wolf, D. E. Fundamentals of fluorescence and fluorescence microscopy. *Methods Cell Biol* **72**, 157-84 (2003).
158. Förster, V. T. Zwischenmolekulare Energiewanderung und Fluoreszenz. *Ann. Phys.*, 54-75 (1948).
159. Cardullo, R. A. & Parpura, V. Fluorescence resonance energy transfer microscopy: theory and instrumentation. *Methods Cell Biol* **72**, 415-30 (2003).

160. Wouters, F. S., Verveer, P. J. & Bastiaens, P. I. Imaging biochemistry inside cells. *Trends Cell Biol* **11**, 203-11 (2001).
161. Majoul, I., Straub, M., Duden, R., Hell, S. W. & Soling, H. D. Fluorescence resonance energy transfer analysis of protein-protein interactions in single living cells by multifocal multiphoton microscopy. *J Biotechnol* **82**, 267-77 (2002).
162. Kenworthy, A. K. Imaging protein-protein interactions using fluorescence resonance energy transfer microscopy. *Methods* **24**, 289-96 (2001).
163. van Munster, E. B. & Gadella, T. W. Fluorescence lifetime imaging microscopy (FLIM). *Adv Biochem Eng Biotechnol* **95**, 143-75 (2005).
164. Breusegem, S. Y., Levi, M. & Barry, N. P. Fluorescence correlation spectroscopy and fluorescence lifetime imaging microscopy. *Nephron Exp Nephrol* **103**, e41-9 (2006).
165. Miyawaki, A., Griesbeck, O., Heim, R. & Tsien, R. Y. Dynamic and quantitative Ca2+ measurements using improved cameleons. *Proc Natl Acad Sci U S A* **96**, 2135-40 (1999).
166. Miyawaki, A. et al. Fluorescent indicators for Ca2+ based on green fluorescent proteins and calmodulin. *Nature* **388**, 882-7 (1997).
167. Tyas, L., Brophy, V. A., Pope, A., Rivett, A. J. & Tavare, J. M. Rapid caspase-3 activation during apoptosis revealed using fluorescence-resonance energy transfer. *EMBO Rep* **1**, 266-70 (2000).
168. Nagai, Y. et al. A fluorescent indicator for visualizing cAMP-induced phosphorylation in vivo. *Nat Biotechnol* **18**, 313-6 (2000).
169. Adams, S. R., Harootunian, A. T., Buechler, Y. J., Taylor, S. S. & Tsien, R. Y. Fluorescence ratio imaging of cyclic AMP in single cells. *Nature* **349**, 694-7 (1991).
170. Damelin, M. & Silver, P. A. Mapping interactions between nuclear transport factors in living cells reveals pathways through the nuclear pore complex. *Mol Cell* **5**, 133-40 (2000).
171. Jares-Erijman, E. A. & Jovin, T. M. FRET imaging. *Nat Biotechnol* **21**, 1387-95 (2003).
172. Majoul, I., Straub, M., Hell, S. W., Duden, R. & Soling, H. D. KDEL-cargo regulates interactions between proteins involved in COPI vesicle traffic: measurements in living cells using FRET. *Dev Cell* **1**, 139-53 (2001).
173. Giraudo, C. G., Daniotti, J. L. & Maccioni, H. J. Physical and functional association of glycolipid N-acetyl-galactosaminyl and galactosyl transferases in the Golgi apparatus. *Proc Natl Acad Sci U S A* **98**, 1625-30 (2001).
174. Wirz, S. A., Davis, C. N., Lu, X., Zal, T. & Bartfai, T. Homodimerization and internalization of galanin type 1 receptor in living CHO cells. *Neuropeptides* **39**, 535-46 (2005).
175. Gadella, T. W., Jr. & Jovin, T. M. Oligomerization of epidermal growth factor receptors on A431 cells studied by time-resolved fluorescence imaging microscopy. A stereochemical model for tyrosine kinase receptor activation. *J Cell Biol* **129**, 1543-58 (1995).
176. Bastiaens, P. I., Majoul, I. V., Verveer, P. J., Soling, H. D. & Jovin, T. M. Imaging the intracellular trafficking and state of the AB5 quaternary structure of cholera toxin. *Embo J* **15**, 4246-53 (1996).

177. Mahajan, N. P., Harrison-Shostak, D. C., Michaux, J. & Herman, B. Novel mutant green fluorescent protein protease substrates reveal the activation of specific caspases during apoptosis. *Chem Biol* **6**, 401-9 (1999).
178. Hoffmann, C. et al. A FlAsH-based FRET approach to determine G protein-coupled receptor activation in living cells. *Nat Methods* **2**, 171-6 (2005).
179. Palmer, A. E., Jin, C., Reed, J. C. & Tsien, R. Y. Bcl-2-mediated alterations in endoplasmic reticulum Ca2+ analyzed with an improved genetically encoded fluorescent sensor. *Proc Natl Acad Sci U S A* **101**, 17404-9 (2004).
180. Demaurex, N. & Frieden, M. Measurements of the free luminal ER Ca(2+) concentration with targeted "cameleon" fluorescent proteins. *Cell Calcium* **34**, 109-19 (2003).
181. Truong, K. et al. FRET-based in vivo Ca2+ imaging by a new calmodulin-GFP fusion molecule. *Nat Struct Biol* **8**, 1069-73 (2001).
182. Meldolesi, J. The development of Ca2+ indicators: a breakthrough in pharmacological research. *Trends Pharmacol Sci* **25**, 172-4 (2004).
183. Berridge, M. J., Bootman, M. D. & Roderick, H. L. Calcium signalling: dynamics, homeostasis and remodelling. *Nat Rev Mol Cell Biol* **4**, 517-29 (2003).
184. Simpson, A. W. Fluorescent measurement of [Ca2+]c: basic practical considerations. *Methods Mol Biol* **312**, 3-36 (2006).
185. Demaurex, N. Calcium measurements in organelles with Ca2+-sensitive fluorescent proteins. *Cell Calcium* **38**, 213-22 (2005).
186. Michalet, X. et al. Quantum dots for live cells, in vivo imaging, and diagnostics. *Science* **307**, 538-44 (2005).
187. Alivisatos, A. P., Gu, W. & Larabell, C. Quantum dots as cellular probes. *Annu Rev Biomed Eng* **7**, 55-76 (2005).
188. Fu, A., Gu, W., Larabell, C. & Alivisatos, A. P. Semiconductor nanocrystals for biological imaging. *Curr Opin Neurobiol* **15**, 568-75 (2005).
189. Krokhin, O. V. et al. Mass spectrometric based mapping of the disulfide bonding patterns of integrin alpha chains. *Biochemistry* **42**, 12950-9 (2003).
190. Ge, P. & Selvin, P. R. Thiol-reactive luminescent lanthanide chelates: part 2. *Bioconjug Chem* **14**, 870-6 (2003).
191. Shimomura, O., Johnson, F. H. & Saiga, Y. Extraction, purification and properties of aequorin, a bioluminescent protein from the luminous hydromedusan, Aequorea. *J Cell Comp Physiol* **59**, 223-39 (1962).
192. Prasher, D. C., Eckenrode, V. K., Ward, W. W., Prendergast, F. G. & Cormier, M. J. Primary structure of the Aequorea victoria green-fluorescent protein. *Gene* **111**, 229-33 (1992).
193. Chalfie, M., Tu, Y., Euskirchen, G., Ward, W. W. & Prasher, D. C. Green fluorescent protein as a marker for gene expression. *Science* **263**, 802-5 (1994).
194. Inouye, S. & Tsuji, F. I. Aequorea green fluorescent protein. Expression of the gene and fluorescence characteristics of the recombinant protein. *FEBS Lett* **341**, 277-80 (1994).

195. Ormo, M. et al. Crystal structure of the Aequorea victoria green fluorescent protein. *Science* **273**, 1392-5 (1996).
196. Yang, F., Moss, L. G. & Phillips, G. N., Jr. The molecular structure of green fluorescent protein. *Nat Biotechnol* **14**, 1246-51 (1996).
197. Reid, B. G. & Flynn, G. C. Chromophore formation in green fluorescent protein. *Biochemistry* **36**, 6786-91 (1997).
198. Heim, R., Prasher, D. C. & Tsien, R. Y. Wavelength mutations and posttranslational autoxidation of green fluorescent protein. *Proc Natl Acad Sci U S A* **91**, 12501-4 (1994).
199. Heim, R., Cubitt, A. B. & Tsien, R. Y. Improved green fluorescence. *Nature* **373**, 663-4 (1995).
200. Cormack, B. P., Valdivia, R. H. & Falkow, S. FACS-optimized mutants of the green fluorescent protein (GFP). *Gene* **173**, 33-8 (1996).
201. Zhang, G., Gurtu, V. & Kain, S. R. An enhanced green fluorescent protein allows sensitive detection of gene transfer in mammalian cells. *Biochem Biophys Res Commun* **227**, 707-11 (1996).
202. Griesbeck, O., Baird, G. S., Campbell, R. E., Zacharias, D. A. & Tsien, R. Y. Reducing the environmental sensitivity of yellow fluorescent protein. Mechanism and applications. *J Biol Chem* **276**, 29188-94 (2001).
203. Heim, R. & Tsien, R. Y. Engineering green fluorescent protein for improved brightness, longer wavelengths and fluorescence resonance energy transfer. *Curr Biol* **6**, 178-82 (1996).
204. Kremers, G. J., Goedhart, J., van Munster, E. B. & Gadella, T. W., Jr. Cyan and yellow super fluorescent proteins with improved brightness, protein folding, and FRET Forster radius. *Biochemistry* **45**, 6570-80 (2006).
205. Zapata-Hommer, O. & Griesbeck, O. Efficiently folding and circularly permuted variants of the Sapphire mutant of GFP. *BMC Biotechnol* **3**, 5 (2003).
206. Zimmermann, T., Rietdorf, J., Girod, A., Georget, V. & Pepperkok, R. Spectral imaging and linear un-mixing enables improved FRET efficiency with a novel GFP2-YFP FRET pair. *FEBS Lett* **531**, 245-9 (2002).
207. Matz, M. V. et al. Fluorescent proteins from nonbioluminescent Anthozoa species. *Nat Biotechnol* **17**, 969-73 (1999).
208. Baird, G. S., Zacharias, D. A. & Tsien, R. Y. Biochemistry, mutagenesis, and oligomerization of DsRed, a red fluorescent protein from coral. *Proc Natl Acad Sci U S A* **97**, 11984-9 (2000).
209. Campbell, R. E. et al. A monomeric red fluorescent protein. *Proc Natl Acad Sci U S A* **99**, 7877-82 (2002).
210. Shaner, N. C. et al. Improved monomeric red, orange and yellow fluorescent proteins derived from Discosoma sp. red fluorescent protein. *Nat Biotechnol* **22**, 1567-72 (2004).
211. Wang, L., Jackson, W. C., Steinbach, P. A. & Tsien, R. Y. Evolution of new nonantibody proteins via iterative somatic hypermutation. *Proc Natl Acad Sci U S A* **101**, 16745-9 (2004).
212. Karasawa, S., Araki, T., Nagai, T., Mizuno, H. & Miyawaki, A. Cyan-emitting and orange-emitting fluorescent proteins as a donor/acceptor

pair for fluorescence resonance energy transfer. *Biochem J* **381**, 307-12 (2004).
213. Verkhusha, V. V. & Lukyanov, K. A. The molecular properties and applications of Anthozoa fluorescent proteins and chromoproteins. *Nat Biotechnol* **22**, 289-96 (2004).
214. Patterson, G. H. & Lippincott-Schwartz, J. A photoactivatable GFP for selective photolabeling of proteins and cells. *Science* **297**, 1873-7 (2002).
215. Patterson, G. H. & Lippincott-Schwartz, J. Selective photolabeling of proteins using photoactivatable GFP. *Methods* **32**, 445-50 (2004).
216. Chudakov, D. M. et al. Photoswitchable cyan fluorescent protein for protein tracking. *Nat Biotechnol* **22**, 1435-9 (2004).
217. Lukyanov, K. A., Chudakov, D. M., Lukyanov, S. & Verkhusha, V. V. Innovation: Photoactivatable fluorescent proteins. *Nat Rev Mol Cell Biol* **6**, 885-91 (2005).
218. Ando, R., Mizuno, H. & Miyawaki, A. Regulated fast nucleocytoplasmic shuttling observed by reversible protein highlighting. *Science* **306**, 1370-3 (2004).
219. Ando, R., Hama, H., Yamamoto-Hino, M., Mizuno, H. & Miyawaki, A. An optical marker based on the UV-induced green-to-red photoconversion of a fluorescent protein. *Proc Natl Acad Sci U S A* **99**, 12651-6 (2002).
220. Wiedenmann, J. et al. EosFP, a fluorescent marker protein with UV-inducible green-to-red fluorescence conversion. *Proc Natl Acad Sci U S A* **101**, 15905-10 (2004).
221. Nguyen, A. W. & Daugherty, P. S. Evolutionary optimization of fluorescent proteins for intracellular FRET. *Nat Biotechnol* **23**, 355-60 (2005).
222. Erickson, M. G., Moon, D. L. & Yue, D. T. DsRed as a potential FRET partner with CFP and GFP. *Biophys J* **85**, 599-611 (2003).
223. Patterson, G. H., Piston, D. W. & Barisas, B. G. Forster distances between green fluorescent protein pairs. *Anal Biochem* **284**, 438-40 (2000).
224. Shaner, N. C., Steinbach, P. A. & Tsien, R. Y. A guide to choosing fluorescent proteins. *Nat Methods* **2**, 905-9 (2005).
225. Tsien, R. Y. The green fluorescent protein. *Annu Rev Biochem* **67**, 509-44 (1998).
226. Chalfie, M. & Kain, S. R. *Green Fluorescent Protein* (Wiley & Sons, Inc., Hoboken, New Jersey, USA, 2005).
227. Keppler, A. et al. A general method for the covalent labeling of fusion proteins with small molecules in vivo. *Nat Biotechnol* **21**, 86-9 (2003).
228. Keppler, A., Pick, H., Arrivoli, C., Vogel, H. & Johnsson, K. Labeling of fusion proteins with synthetic fluorophores in live cells. *Proc Natl Acad Sci U S A* **101**, 9955-9 (2004).
229. Kyrtopoulos, S. A. et al. DNA adducts and the mechanism of carcinogenesis and cytotoxicity of methylating agents of environmental and clinical significance. *Cancer Detect Prev* **21**, 391-405 (1997).
230. Kindermann, M., George, N., Johnsson, N. & Johnsson, K. Covalent and selective immobilization of fusion proteins. *J Am Chem Soc* **125**, 7810-1 (2003).

231. Gendreizig, S., Kindermann, M. & Johnsson, K. Induced protein dimerization in vivo through covalent labeling. *J Am Chem Soc* **125**, 14970-1 (2003).
232. Regoes, A. & Hehl, A. B. SNAP-tag mediated live cell labeling as an alternative to GFP in anaerobic organisms. *Biotechniques* **39**, 809-10, 812 (2005).
233. Griffin, B. A., Adams, S. R. & Tsien, R. Y. Specific covalent labeling of recombinant protein molecules inside live cells. *Science* **281**, 269-72 (1998).
234. Martin, B. R., Giepmans, B. N., Adams, S. R. & Tsien, R. Y. Mammalian cell-based optimization of the biarsenical-binding tetracysteine motif for improved fluorescence and affinity. *Nat Biotechnol* **23**, 1308-14 (2005).
235. Stroffekova, K., Proenza, C. & Beam, K. G. The protein-labeling reagent FLASH-EDT2 binds not only to CCXXCC motifs but also non-specifically to endogenous cysteine-rich proteins. *Pflugers Arch* **442**, 859-66 (2001).
236. Adams, S. R. et al. New biarsenical ligands and tetracysteine motifs for protein labeling in vitro and in vivo: synthesis and biological applications. *J Am Chem Soc* **124**, 6063-76 (2002).
237. Gaietta, G. et al. Multicolor and electron microscopic imaging of connexin trafficking. *Science* **296**, 503-7 (2002).
238. Ju, W. et al. Activity-dependent regulation of dendritic synthesis and trafficking of AMPA receptors. *Nat Neurosci* **7**, 244-53 (2004).
239. Tour, O., Meijer, R. M., Zacharias, D. A., Adams, S. R. & Tsien, R. Y. Genetically targeted chromophore-assisted light inactivation. *Nat Biotechnol* **21**, 1505-8 (2003).
240. Marek, K. W. & Davis, G. W. Transgenically encoded protein photoinactivation (FlAsH-FALI): acute inactivation of synaptotagmin I. *Neuron* **36**, 805-13 (2002).
241. Andresen, M., Schmitz-Salue, R. & Jakobs, S. Short tetracysteine tags to beta-tubulin demonstrate the significance of small labels for live cell imaging. *Molecular Biology of the Cell* **15**, 5616-5622 (2004).
242. Zhang, J., Campbell, R. E., Ting, A. Y. & Tsien, R. Y. Creating new fluorescent probes for cell biology. *Nat Rev Mol Cell Biol* **3**, 906-18 (2002).
243. Lippincott-Schwartz, J., Snapp, E. & Kenworthy, A. Studying protein dynamics in living cells. *Nat Rev Mol Cell Biol* **2**, 444-56 (2001).
244. van Roessel, P. & Brand, A. H. Imaging into the future: visualizing gene expression and protein interactions with fluorescent proteins. *Nat Cell Biol* **4**, E15-20 (2002).
245. Hakansson, A., Bentley, C. C., Shakhnovic, E. A. & Wessels, M. R. Cytolysin-dependent evasion of lysosomal killing *PNAS* **102**, 5192-5197 (2005).
246. Kneen, M., Farinas, J., Li, Y. & Verkman, A. S. Green fluorescent protein as a noninvasive intracellular pH indicator. *Biophys J* **74**, 1591-9 (1998).
247. Llopis, J., McCaffery, J. M., Miyawaki, A., Farquhar, M. G. & Tsien, R. Y. Measurement of cytosolic, mitochondrial, and Golgi pH in single

living cells with green fluorescent proteins. *Proc Natl Acad Sci U S A* **95**, 6803-8 (1998).
248. Miesenbock, G., De Angelis, D. A. & Rothman, J. E. Visualizing secretion and synaptic transmission with pH-sensitive green fluorescent proteins. *Nature* **394**, 192-5 (1998).
249. Jayaraman, S., Haggie, P., Wachter, R. M., Remington, S. J. & Verkman, A. S. Mechanism and cellular applications of a green fluorescent protein-based halide sensor. *J Biol Chem* **275**, 6047-50 (2000).
250. Oancea, E., Teruel, M. N., Quest, A. F. & Meyer, T. Green fluorescent protein (GFP)-tagged cysteine-rich domains from protein kinase C as fluorescent indicators for diacylglycerol signaling in living cells. *J Cell Biol* **140**, 485-98 (1998).
251. Rizzo, M. A., Shome, K., Watkins, S. C. & Romero, G. The recruitment of Raf-1 to membranes is mediated by direct interaction with phosphatidic acid and is independent of association with Ras. *J Biol Chem* **275**, 23911-8 (2000).
252. Teruel, M. N. & Meyer, T. Translocation and reversible localization of signaling proteins: a dynamic future for signal transduction. *Cell* **103**, 181-4 (2000).
253. Haugh, J. M., Codazzi, F., Teruel, M. & Meyer, T. Spatial sensing in fibroblasts mediated by 3' phosphoinositides. *J Cell Biol* **151**, 1269-80 (2000).
254. Oatey, P. B. et al. Confocal imaging of the subcellular distribution of phosphatidylinositol 3,4,5-trisphosphate in insulin- and PDGF-stimulated 3T3-L1 adipocytes. *Biochem J* **344 Pt 2**, 511-8 (1999).
255. Honda, A. et al. Spatiotemporal dynamics of guanosine 3',5'-cyclic monophosphate revealed by a genetically encoded, fluorescent indicator. *Proc Natl Acad Sci U S A* **98**, 2437-42 (2001).
256. Sato, M., Hida, N., Ozawa, T. & Umezawa, Y. Fluorescent indicators for cyclic GMP based on cyclic GMP-dependent protein kinase Ialpha and green fluorescent proteins. *Anal Chem* **72**, 5918-24 (2000).
257. Llopis, J. et al. Ligand-dependent interactions of coactivators steroid receptor coactivator-1 and peroxisome proliferator-activated receptor binding protein with nuclear hormone receptors can be imaged in live cells and are required for transcription. *Proc Natl Acad Sci U S A* **97**, 4363-8 (2000).
258. Janetopoulos, C., Jin, T. & Devreotes, P. Receptor-mediated activation of heterotrimeric G-proteins in living cells. *Science* **291**, 2408-11 (2001).
259. Ruehr, M. L., Zakhary, D. R., Damron, D. S. & Bond, M. Cyclic AMP-dependent protein kinase binding to A-kinase anchoring proteins in living cells by fluorescence resonance energy transfer of green fluorescent protein fusion proteins. *J Biol Chem* **274**, 33092-6 (1999).
260. Siegel, R. M. et al. Fas preassociation required for apoptosis signaling and dominant inhibition by pathogenic mutations. *Science* **288**, 2354-7 (2000).
261. Xia, Z., Zhou, Q., Lin, J. & Liu, Y. Stable SNARE complex prior to evoked synaptic vesicle fusion revealed by fluorescence resonance energy transfer. *J Biol Chem* **276**, 1766-71 (2001).

262. Li, H. Y. et al. Protein-protein interaction of FHL3 with FHL2 and visualization of their interaction by green fluorescent proteins (GFP) two-fusion fluorescence resonance energy transfer (FRET). *J Cell Biochem* **80**, 293-303 (2001).
263. Mas, P., Devlin, P. F., Panda, S. & Kay, S. A. Functional interaction of phytochrome B and cryptochrome 2. *Nature* **408**, 207-11 (2000).
264. Tertoolen, L. G. et al. Dimerization of receptor protein-tyrosine phosphatase alpha in living cells. *BMC Cell Biol* **2**, 8 (2001).
265. Kurokawa, K. et al. A pair of fluorescent resonance energy transfer-based probes for tyrosine phosphorylation of the CrkII adaptor protein in vivo. *J Biol Chem* **276**, 31305-10 (2001).
266. Sambrook, J. & Russell, D. W. *Molecular Cloning: A Laboratory Manual* (Cold Spring Harbor Laboratory Press, 2001).
267. Mülhardt, C. *Der Experimentator: Molekularbiologie/Genomics* (Spektrum Akademischer Verlag, 2003).
268. Rasband, W. (National Institute of Health, USA).
269. OriginLabCorporation. *Origin v6.1* (Northampton, USA).
270. Zacharias, D. A., Violin, J. D., Newton, A. C. & Tsien, R. Y. Partitioning of lipid-modified monomeric GFPs into membrane microdomains of live cells. *Science* **296**, 913-6 (2002).
271. Zacharias, D. A. Sticky caveats in an otherwise glowing report: oligomerizing fluorescent proteins and their use in cell biology. *Sci STKE* **2002**, PE23 (2002).
272. Tyers, M., Haslam, R. J., Rachubinski, R. A. & Harley, C. B. Molecular analysis of pleckstrin: the major protein kinase C substrate of platelets. *J Cell Biochem* **40**, 133-45 (1989).
273. Blumberg, P. M. Protein kinase C as the receptor for the phorbol ester tumor promoters: sixth Rhoads memorial award lecture. *Cancer Res* **48**, 1-8 (1988).
274. Plevin, R. & Boarder, M. R. Stimulation of formation of inositol phosphates in primary cultures of bovine adrenal chromaffin cells by angiotensin II, histamine, bradykinin, and carbachol. *J Neurochem* **51**, 634-41 (1988).
275. Challis, R. A., Jones, J. A., Owen, P. J. & Boarder, M. R. Changes in inositol 1,4,5-trisphosphate and inositol 1,3,4,5- tetrakisphosphate mass accumulations in cultured adrenal chromaffin cells in response to bradykinin and histamine. *J Neurochem* **56**, 1083-6 (1991).
276. Regoli, D. & Barabe, J. Pharmacology of bradykinin and related kinins. *Pharmacol Rev* **32**, 1-46 (1980).
277. Fu, T., Okano, Y., Hagiwara, M., Hidaka, H. & Nozawa, Y. Bradykinin-induced translocation of protein kinases C in neuroblastoma NCB-20 cell: dependence on 1,2-diacylglycerol content and free calcium. *Biochem Biophys Res Commun* **162**, 1279-86 (1989).
278. Stempka, L. et al. Phosphorylation of protein kinase Cdelta (PKCdelta) at threonine 505 is not a prerequisite for enzymatic activity. Expression of rat PKCdelta and an alanine 505 mutant in bacteria in a functional form. *J Biol Chem* **272**, 6805-11 (1997).
279. Wachter, R. M., Elsliger, M. A., Kallio, K., Hanson, G. T. & Remington, S. J. Structural basis of spectral shifts in the yellow-emission variants of green fluorescent protein. *Structure* **6**, 1267-77 (1998).

280. Nikolaev, V. O., Bunemann, M., Hein, L., Hannawacker, A. & Lohse, M. J. Novel single chain cAMP sensors for receptor-induced signal propagation. *J Biol Chem* **279**, 37215-8 (2004).
281. Piljic, A. & Schultz, C. Annexin a4 self-association modulates general membrane protein mobility in living cells. *Mol Biol Cell* **17**, 3318-28 (2006).
282. Schleifenbaum, A. (University of Heidelberg/ EMBL, Heidelberg, 2005).
283. MolecularProbes. in *Molecular Probes Handbook* (USA, 2003).
284. Song, L., Hennink, E. J., Young, I. T. & Tanke, H. J. Photobleaching kinetics of fluorescein in quantitative fluorescence microscopy. *Biophys J* **68**, 2588-600 (1995).
285. Bender, K., Federwisch, M., Loggen, U., Nehls, P. & Rajewsky, M. F. Binding and repair of O6-ethylguanine in double-stranded oligodeoxynucleotides by recombinant human O6-alkylguanine-DNA alkyltransferase do not exhibit significant dependence on sequence context. *Nucleic Acids Res* **24**, 2087-94 (1996).
286. Crone, T. M., Goodtzova, K., Edara, S. & Pegg, A. E. Mutations in human O6-alkylguanine-DNA alkyltransferase imparting resistance to O6-benzylguanine. *Cancer Res* **54**, 6221-7 (1994).
287. Griffin, B. A., Adams, S. R., Jones, J. & Tsien, R. Y. Fluorescent labeling of recombinant proteins in living cells with FlAsH. *Methods Enzymol* **327**, 565-78 (2000).
288. Liu, L. & Makowske, M. Phosphotyrosine protein of molecular mass 30 kDa binds specifically to the positively charged region of the pleckstrin N-terminal pleckstrin homology domain. *Biochem J* **342 (Pt 2)**, 423-30 (1999).
289. Jackson, S. G. et al. Structure of the carboxy-terminal PH domain of pleckstrin at 2.1 Angstroms. *Acta Crystallogr D Biol Crystallogr* **62**, 324-30 (2006).
290. Ma, A. D. & Abrams, C. S. Pleckstrin Induces Cytoskeletal Reorganization via a Rac-dependent Pathway *J. Biol. Chem.* **274**, 28730-28735 (1999).
291. Andresen, M., Schmitz-Salue, R. & Jakobs, S. Short tetracysteine tags to beta-tubulin demonstrate the significance of small labels for live cell imaging. *Mol Biol Cell* **15**, 5616-22 (2004).